

Figure 1.1. Schematics of the heart showing the path of blood flow.

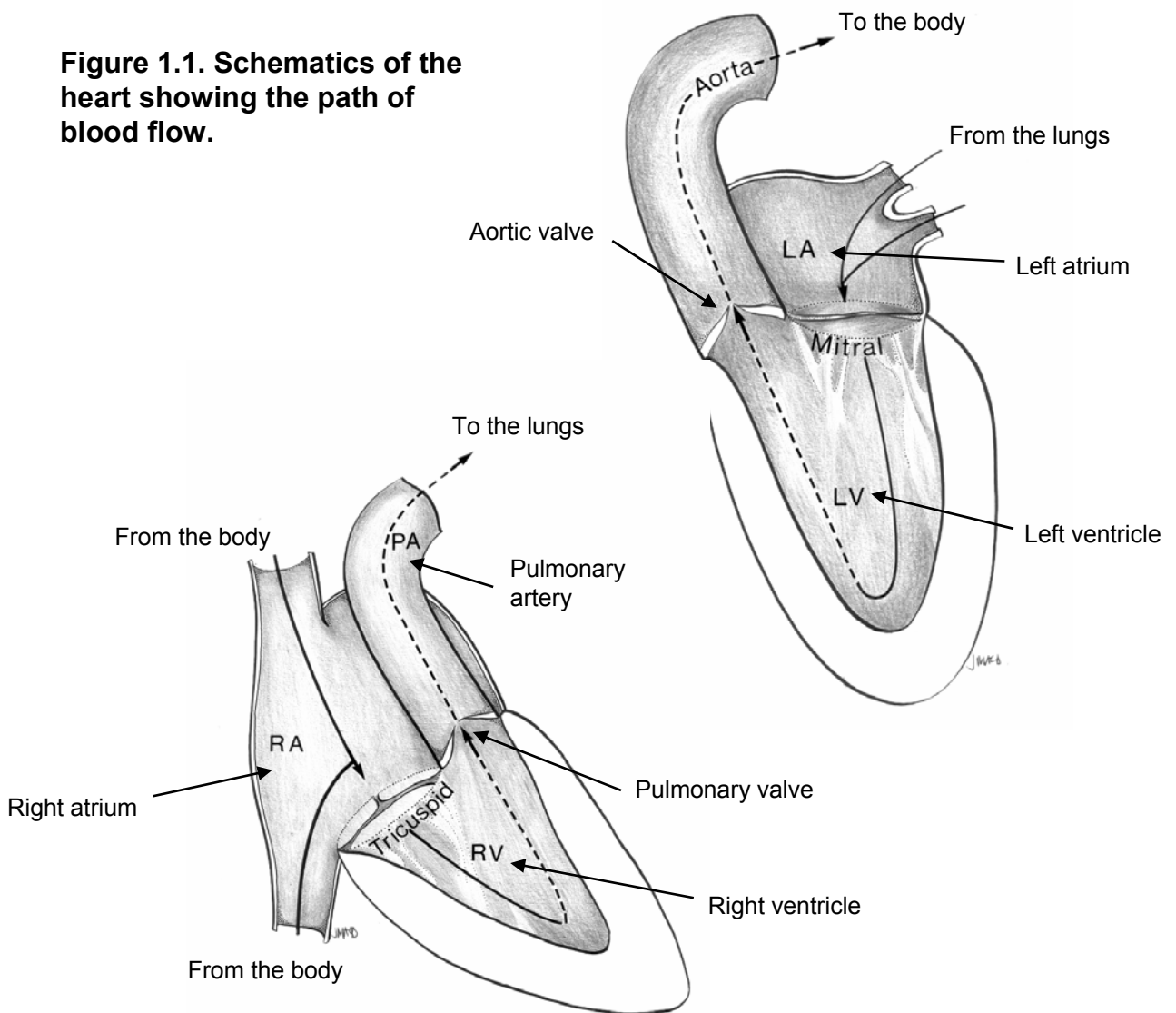


Figure 1.2. Left heart pumping cycle (2 - 540).

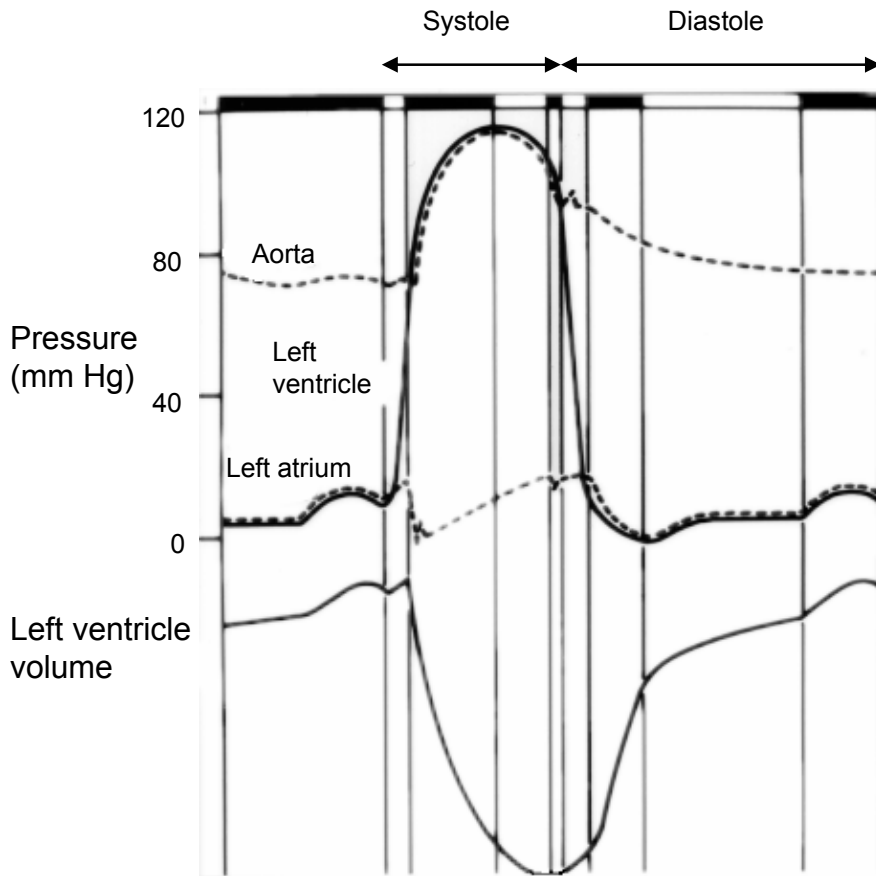


Figure 1.3. The twitch and tetanus mechanical responses of a muscle (12 - 557).

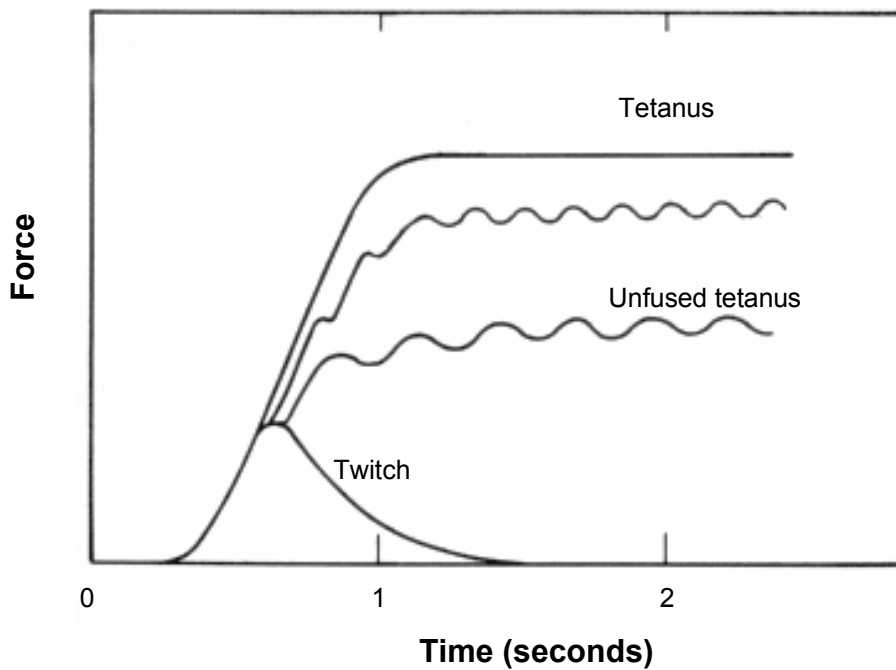


Figure 1.4. Shear Induced Damage of Erythrocytes (64 - 500).

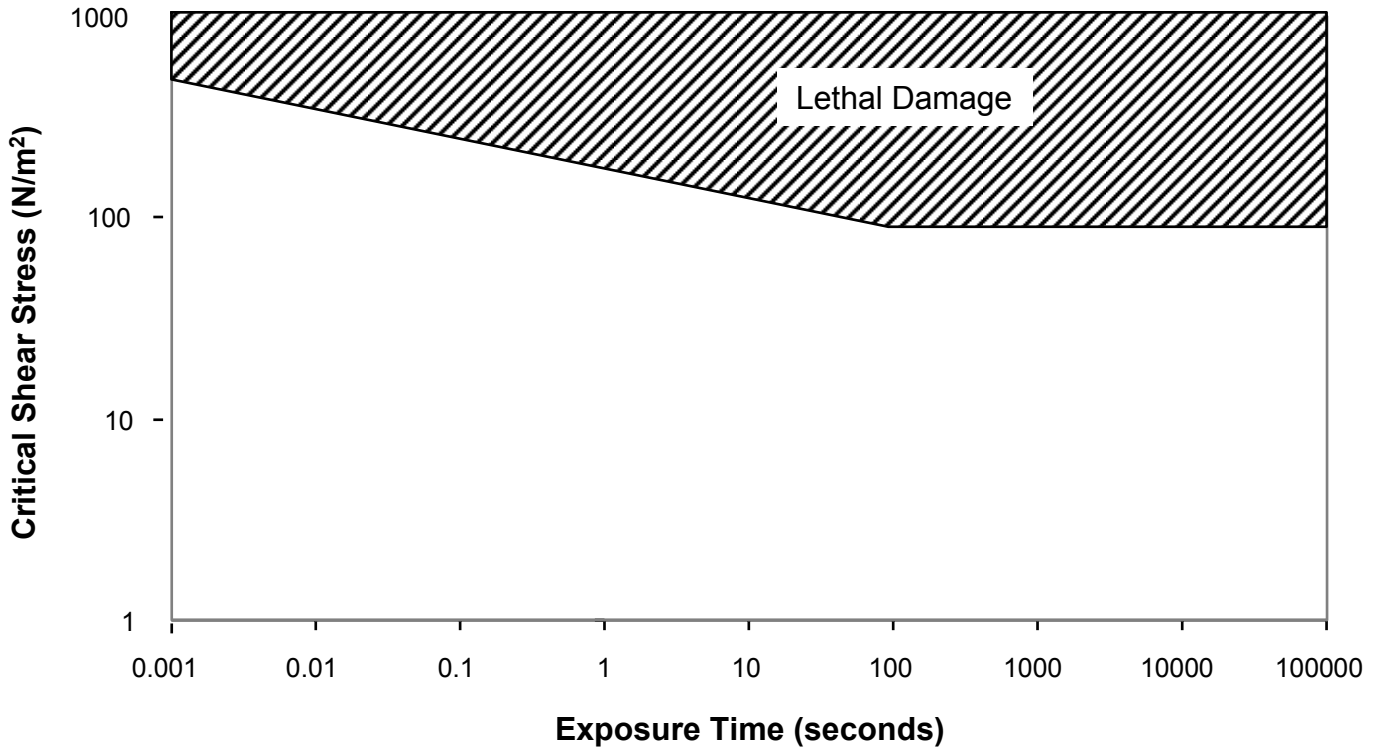


Figure 1.5. Shear Induced Damage of Platelets (the studies that provided the data for this graph were conducted at room temperature, nominally 24°C) (64 - 500).

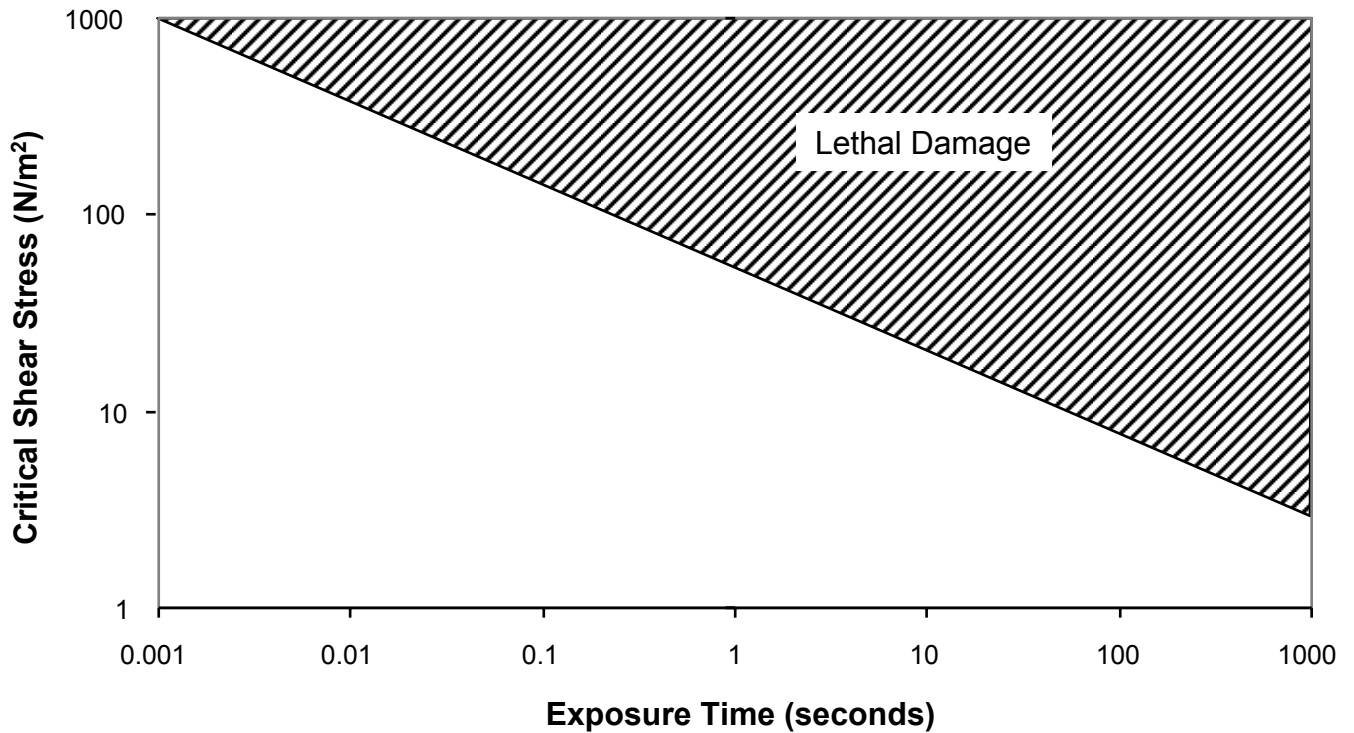
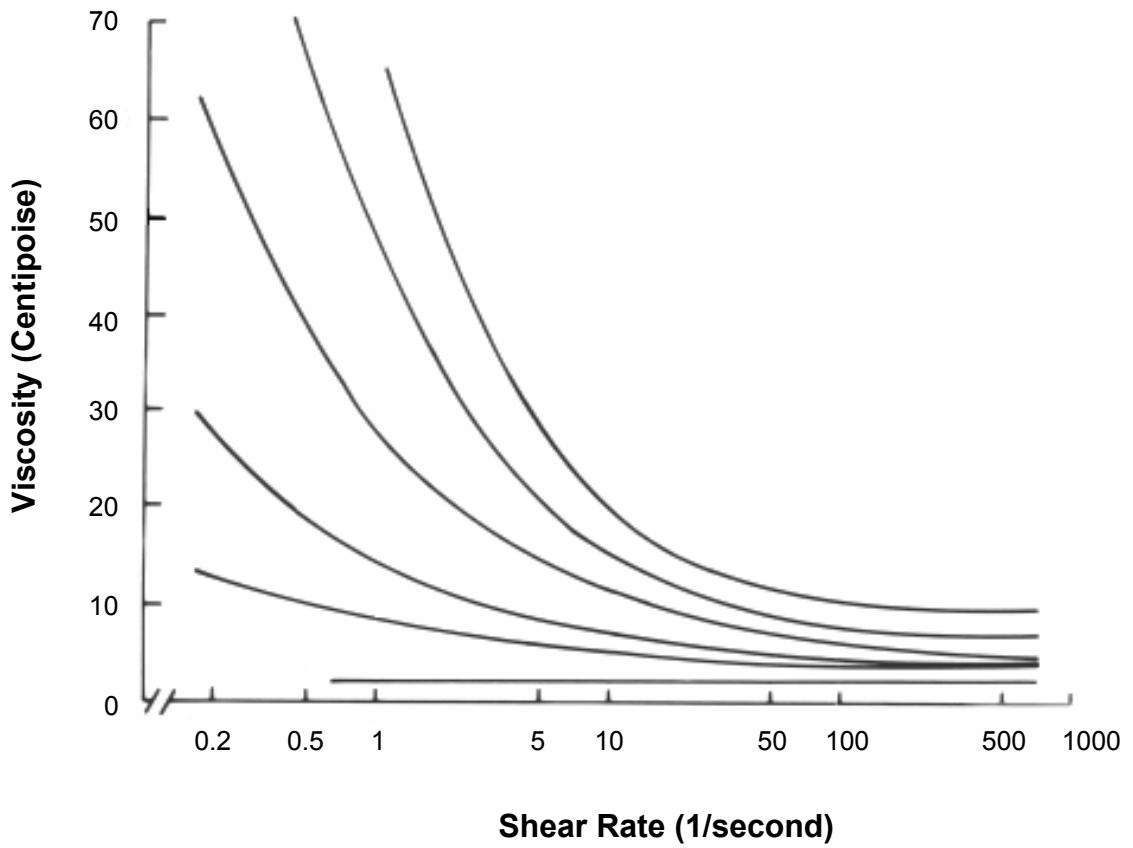


Figure 1.6. Relationship between viscosity and rate of shear at different hematocrits, H_n . For human red blood cell suspensions in plasma at 25°C. H_n =volume of erythrocytes multiplied by 0.96 put in (74 - 494).



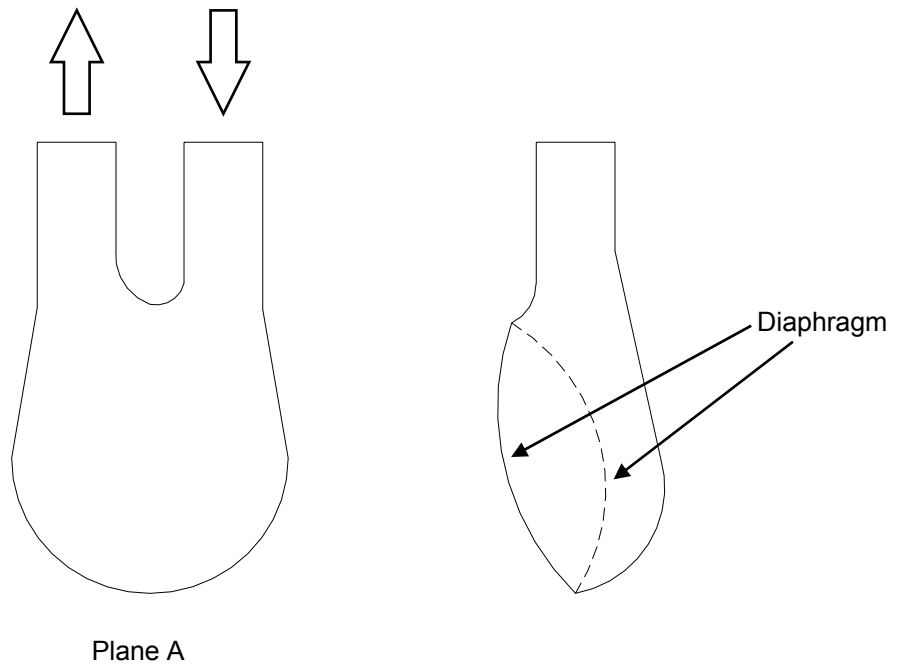


Figure 1.7. Schematic of a sac-type blood pump. The direction of fluid flow is indicated with arrows.

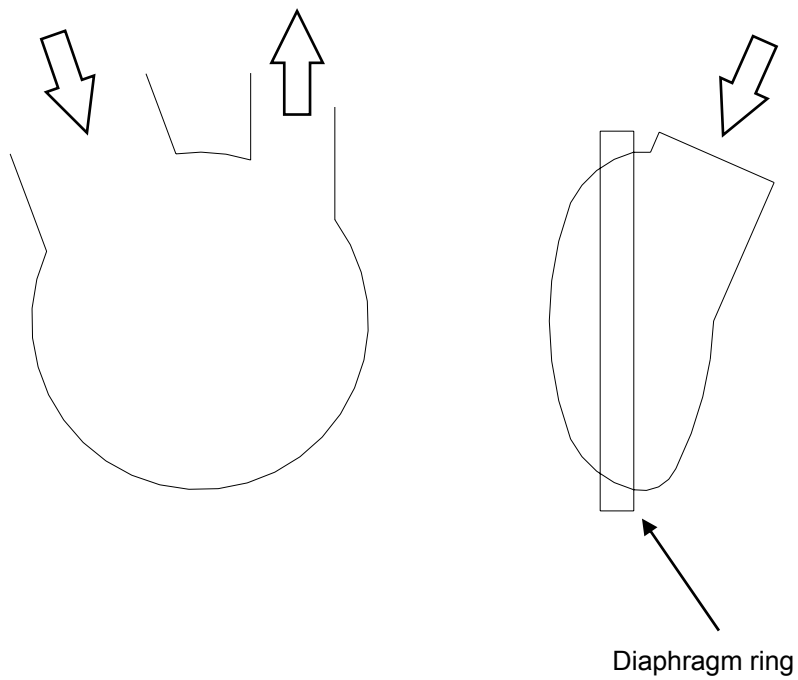


Figure 1.8. Schematic of the Penn State University sac-type blood pump.

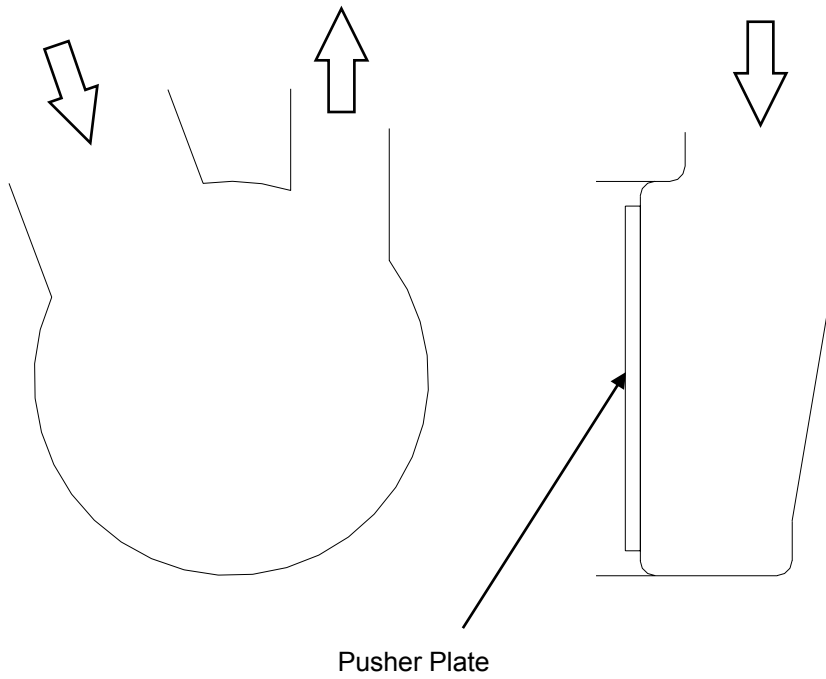


Figure 1.9. Schematic of the Penn State University electric blood pump.

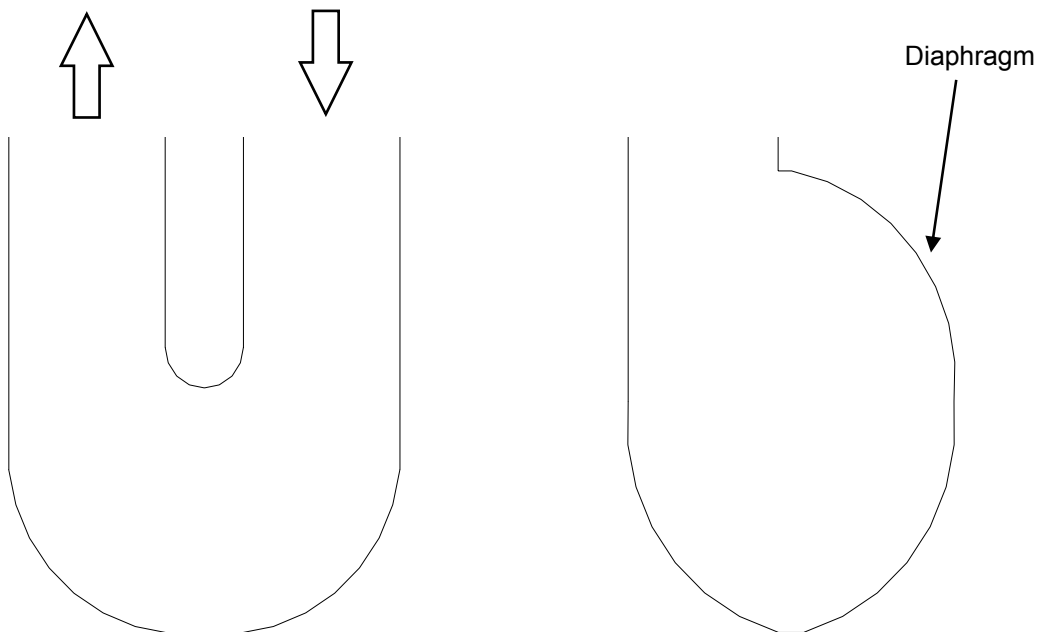


Figure 1.10. Schematic a pneumatic blood pump used for tracer residence time studies.

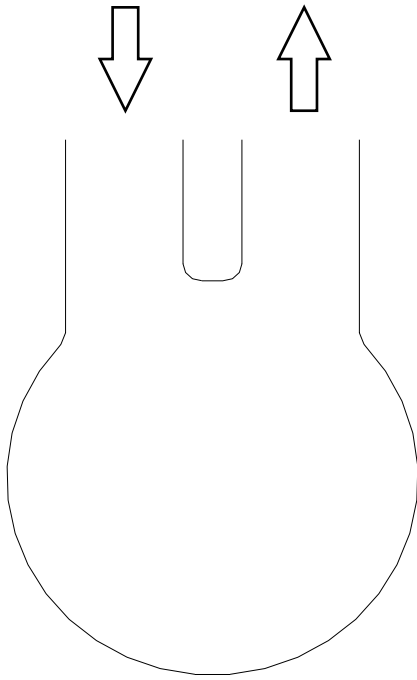
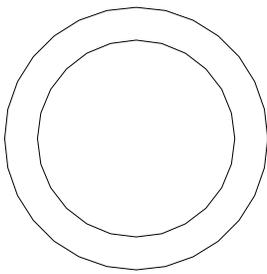
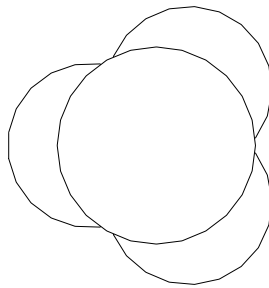


Figure 1.11. Schematic of a transparent sac-type blood pump, in which fluid flow was studied by tracer particle visualization.

Concentric sinus



Triple sinus



Modified triple sinus

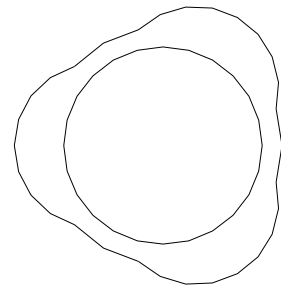


Figure 1.12. Three cross-section schematics of blood pump outflow housing designs.

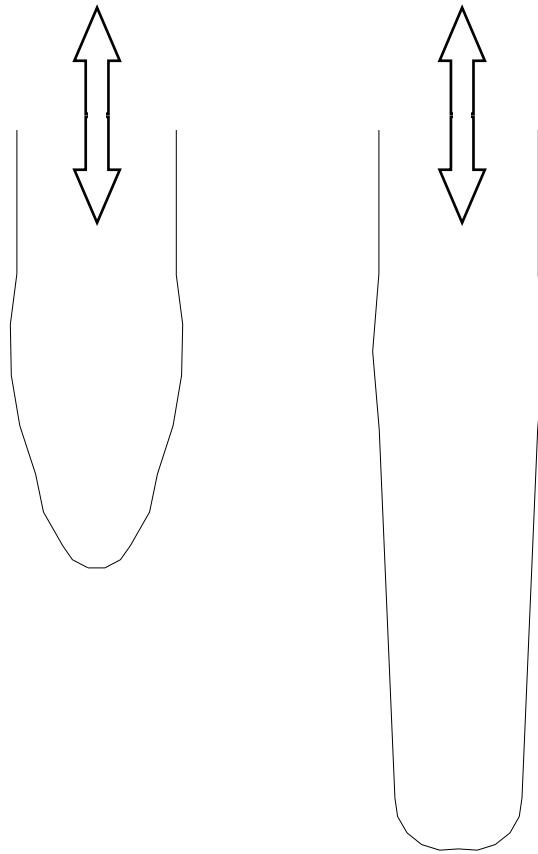


Figure 1.13. Two axisymmetric, valveless, skeletal muscle ventricles.

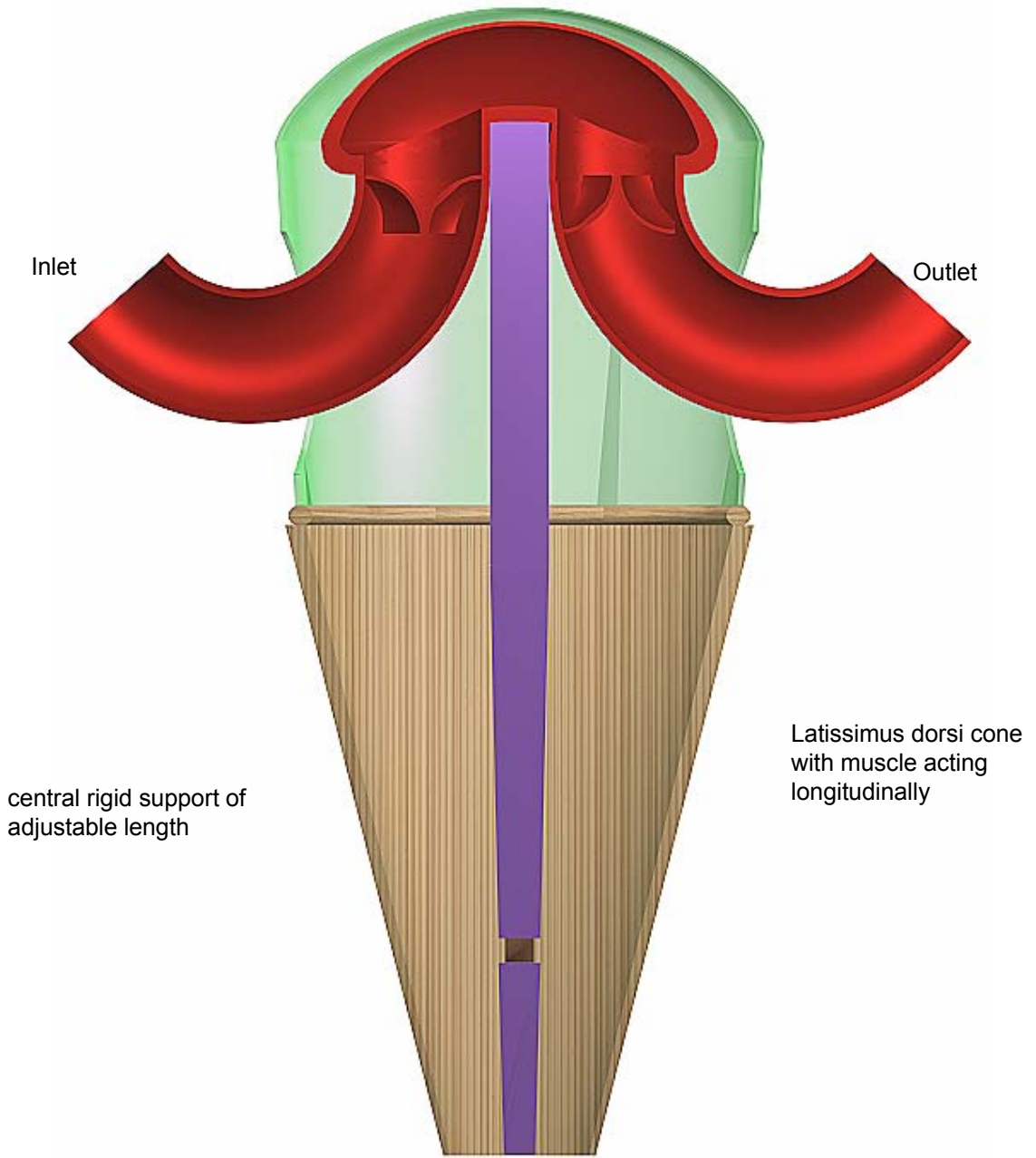


Figure . Proposed method of harnessing skeletal muscle to form the SMV.

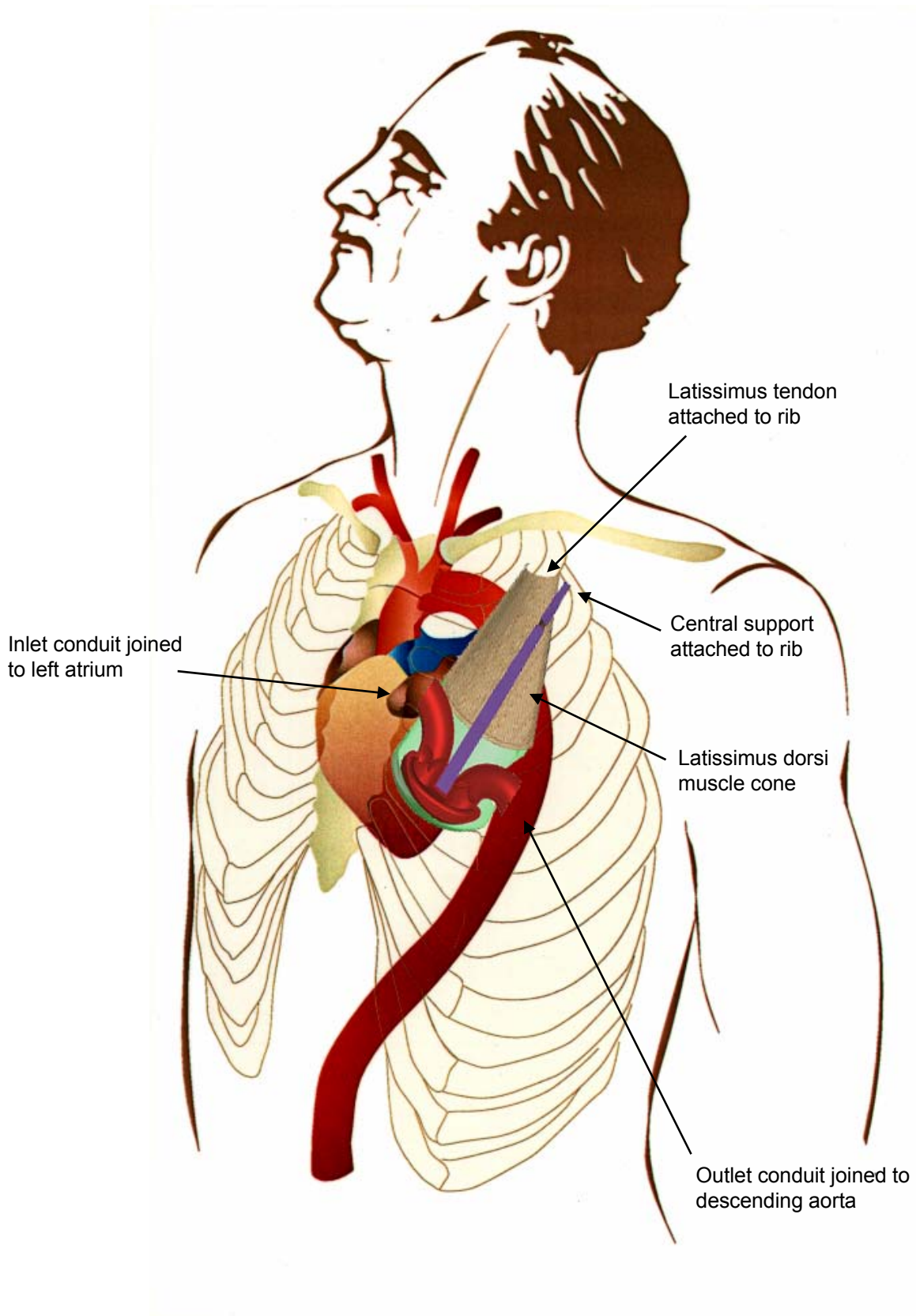
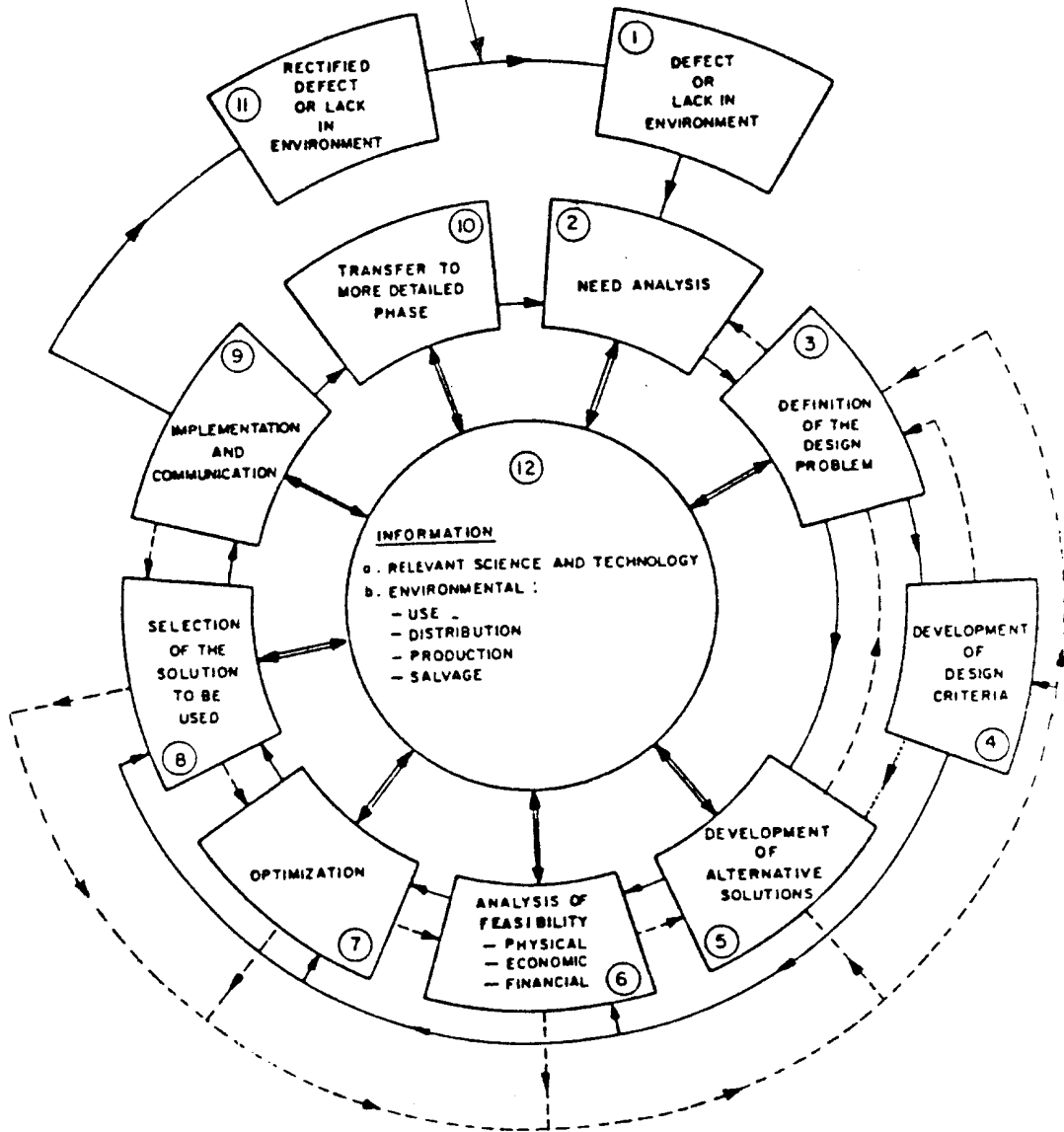
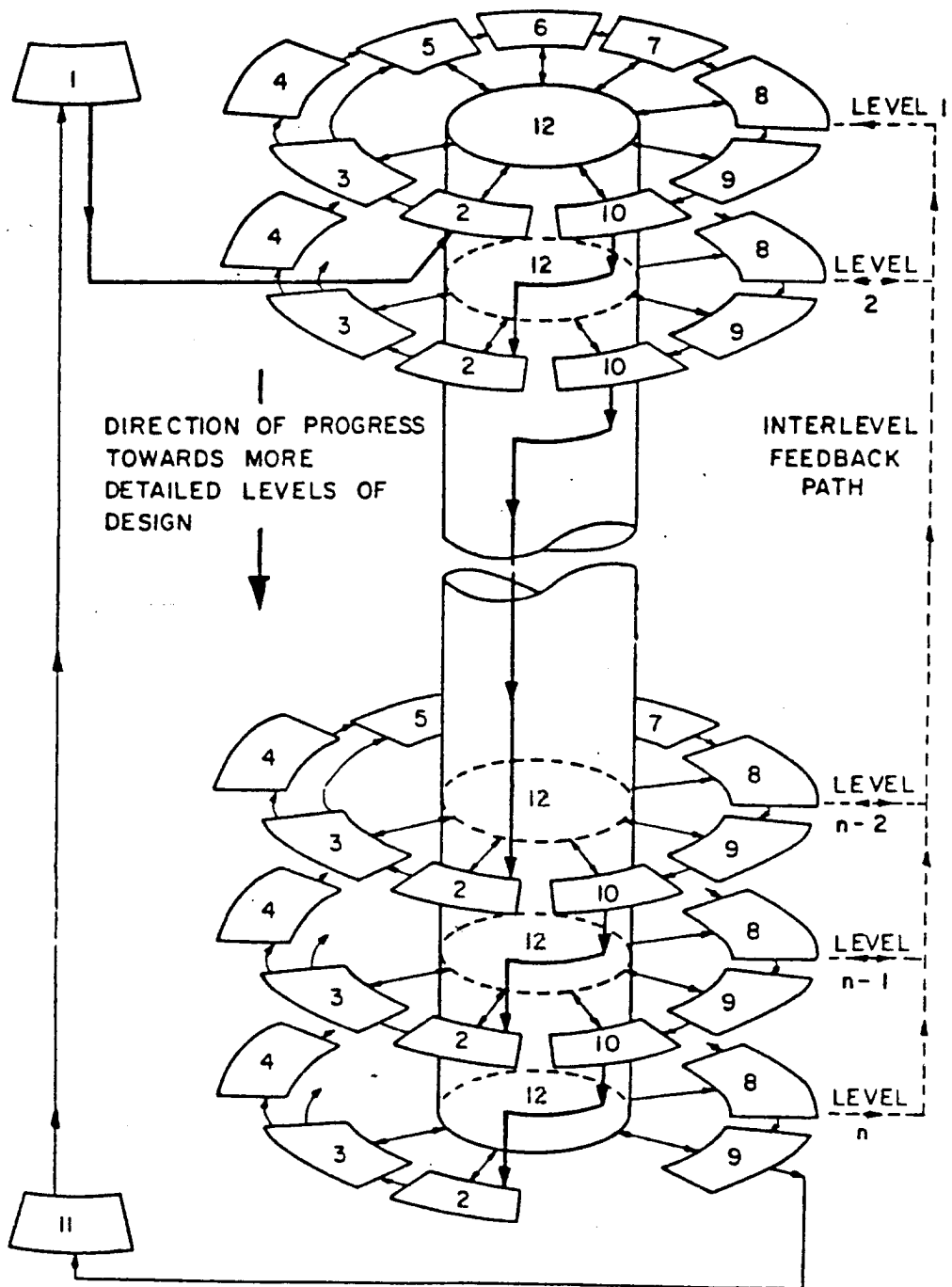


Figure . Proposed placement of SMV.

- ① solution may not provide long term solution
- ② solution of one design problem may lead to formation of new design problems





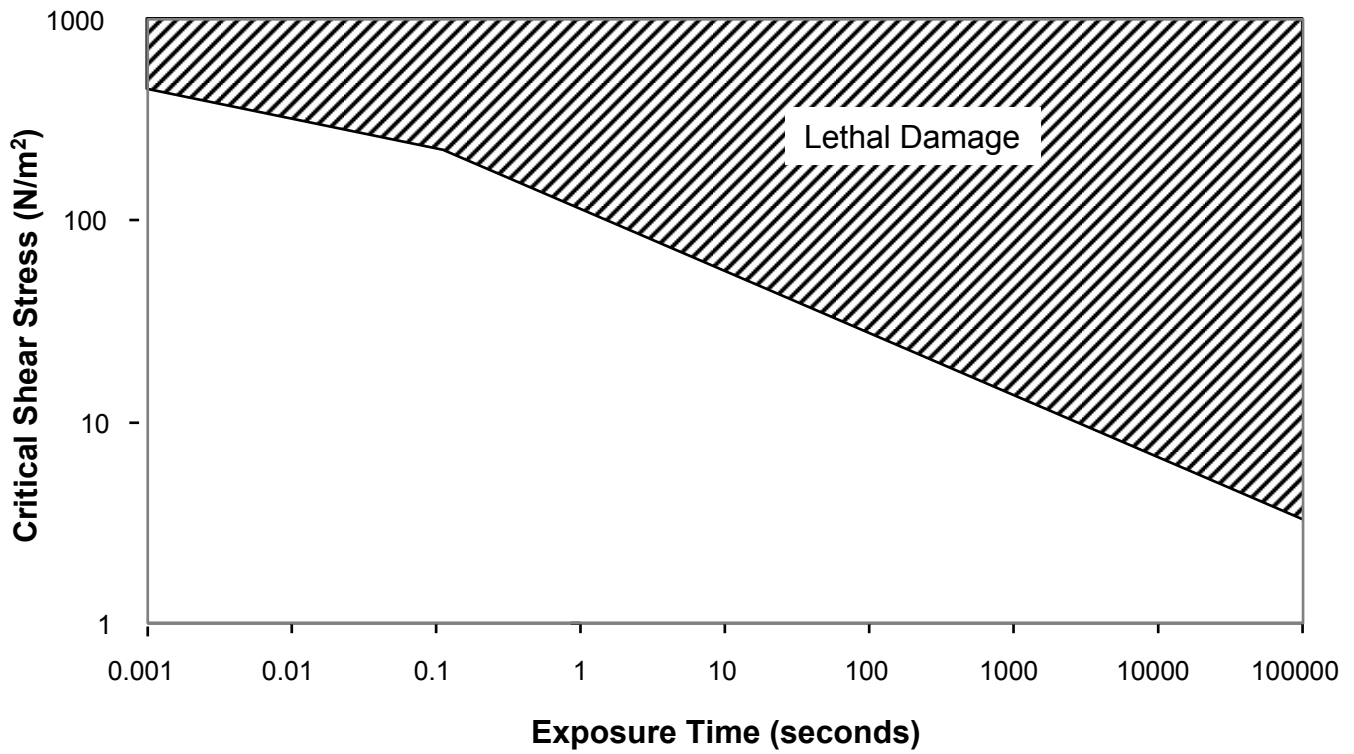


Figure 2.10. Combination of figures 1.3 and 1.4 showing the levels of shear stress and exposure time that are likely to damage blood elements.

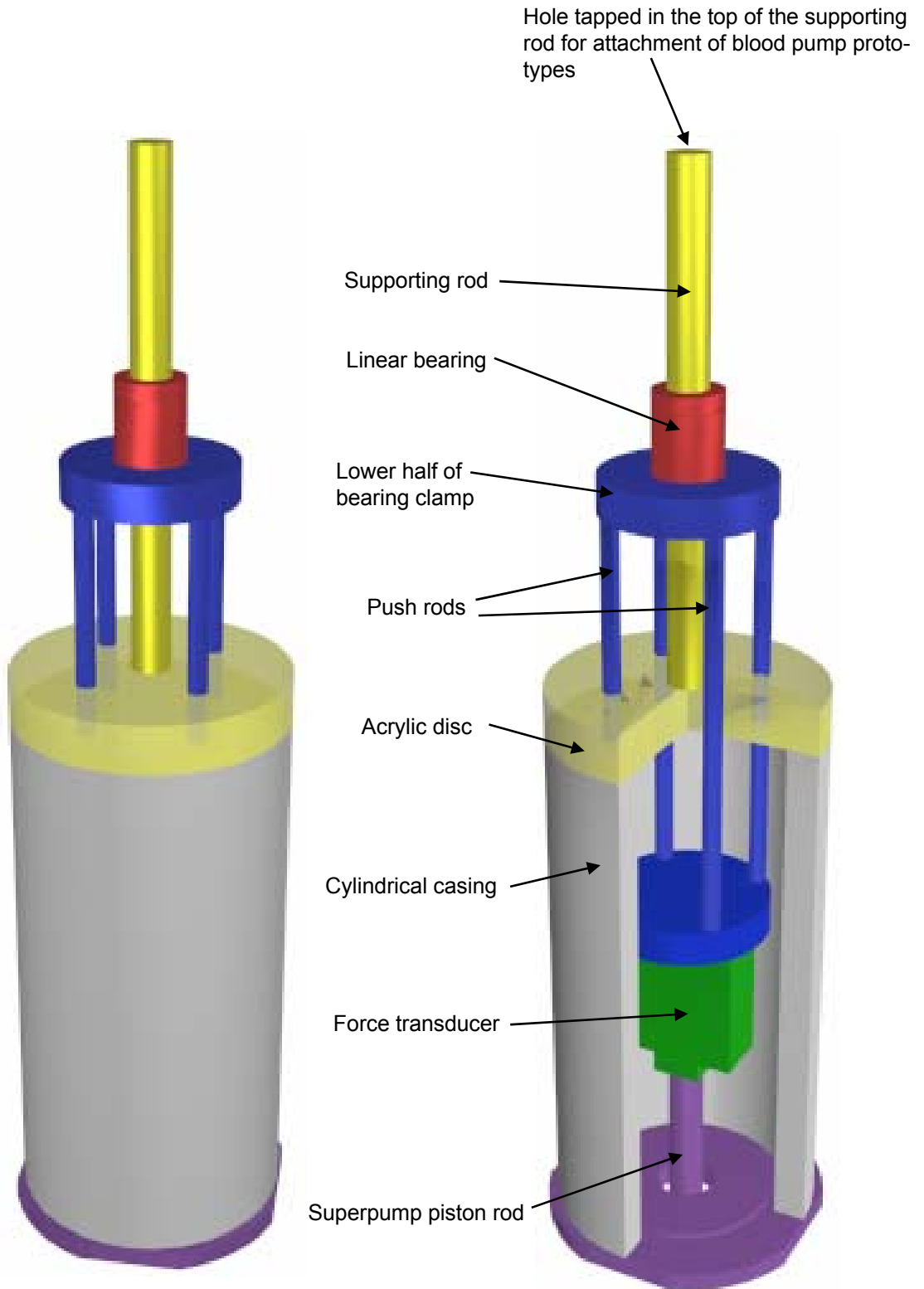


Figure 3.1. The mechanical system for harnessing a servo-controlled linear actuator to pump proto-type ventricles, as a complete solid model and with a section cut-away.

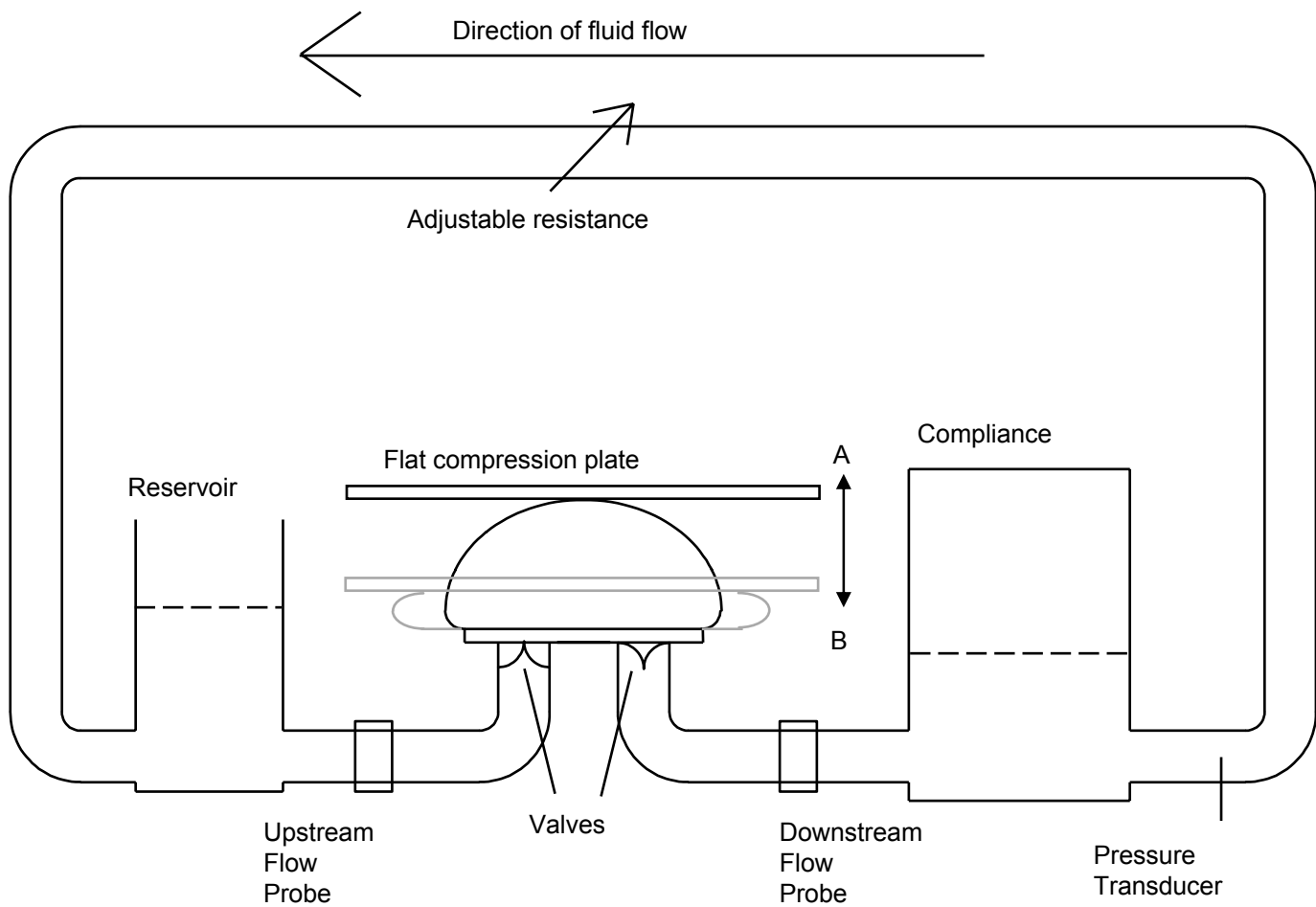


Figure 3.2. Schematic of the mock, closed, circulatory loop showing a ventricle in its uncompressed and compressed states at positions A and B, respectively.

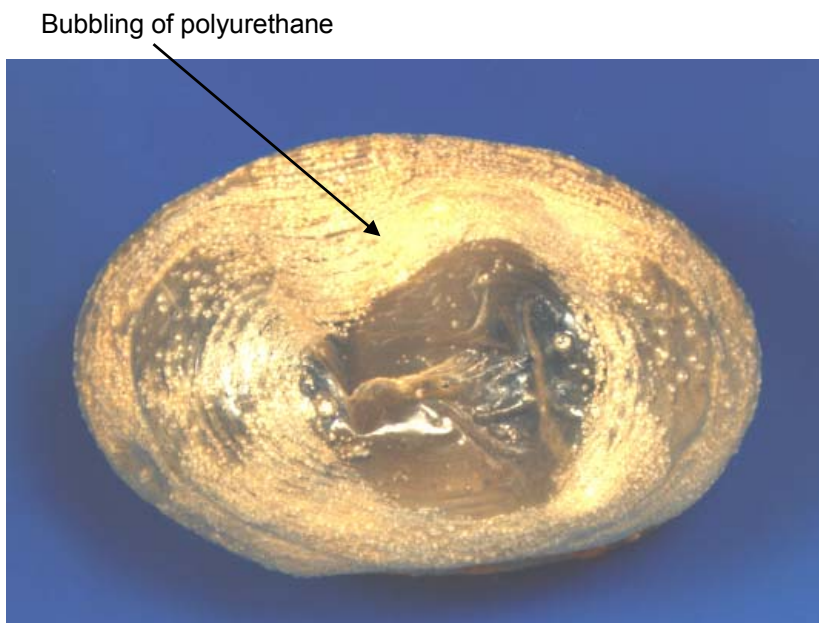


Figure 3.3. A polyurethane ventricle made by covering a wax mould with polyurethane, dissolved in DMAC.

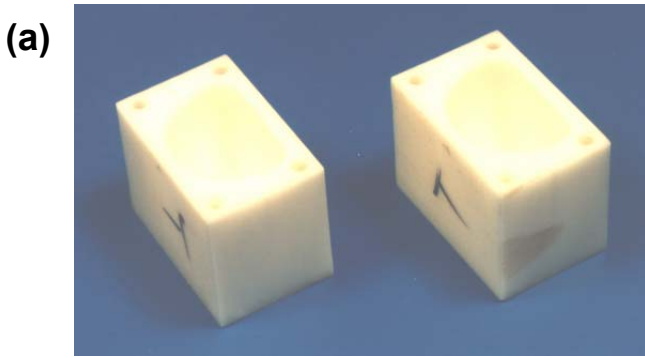


Figure 3.4. (a) Silicone rubber ventricle manufactured by rotating silicone rubber as it cures inside a mould (b) in an oven.

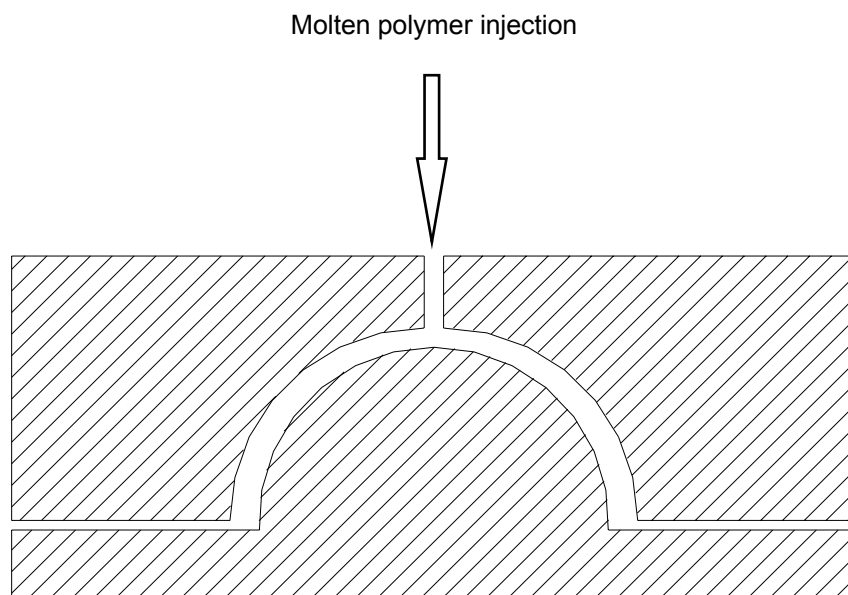
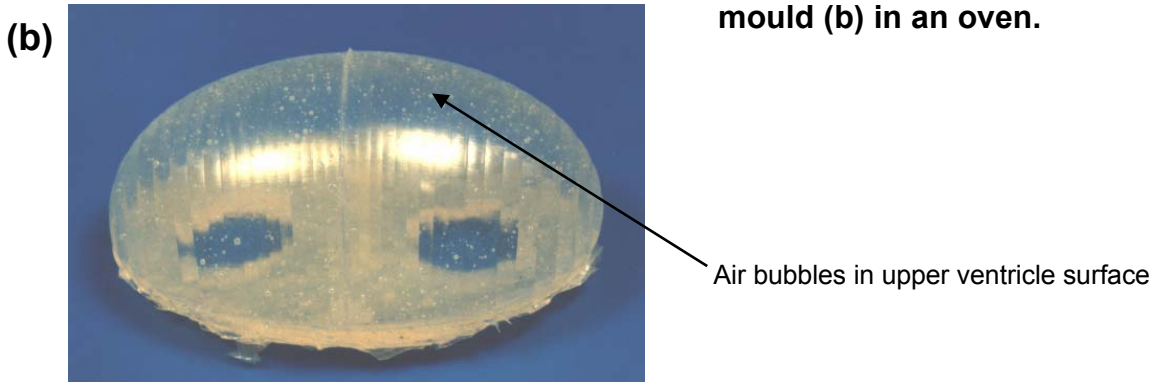


Figure 3.6. Section taken through an injection mould intended for manufacturing hemispherical pumping chambers.



Figure 3.6. Teflon dipping bowl with a screw top lid for storing polyurethane dissolved in DMAC. The large width of the bowl allows artificial ventricle sized geometries to be dipped in the solution.

(a)



Figure 3.7. (a) A polyurethane ventricle made by gluing two half ventricle forms together with a solution of DMAC and polyurethane. **(b)** The male resin former and the female mould it was cast from.

(b)

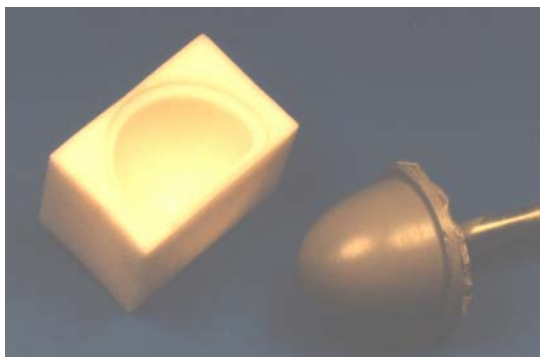
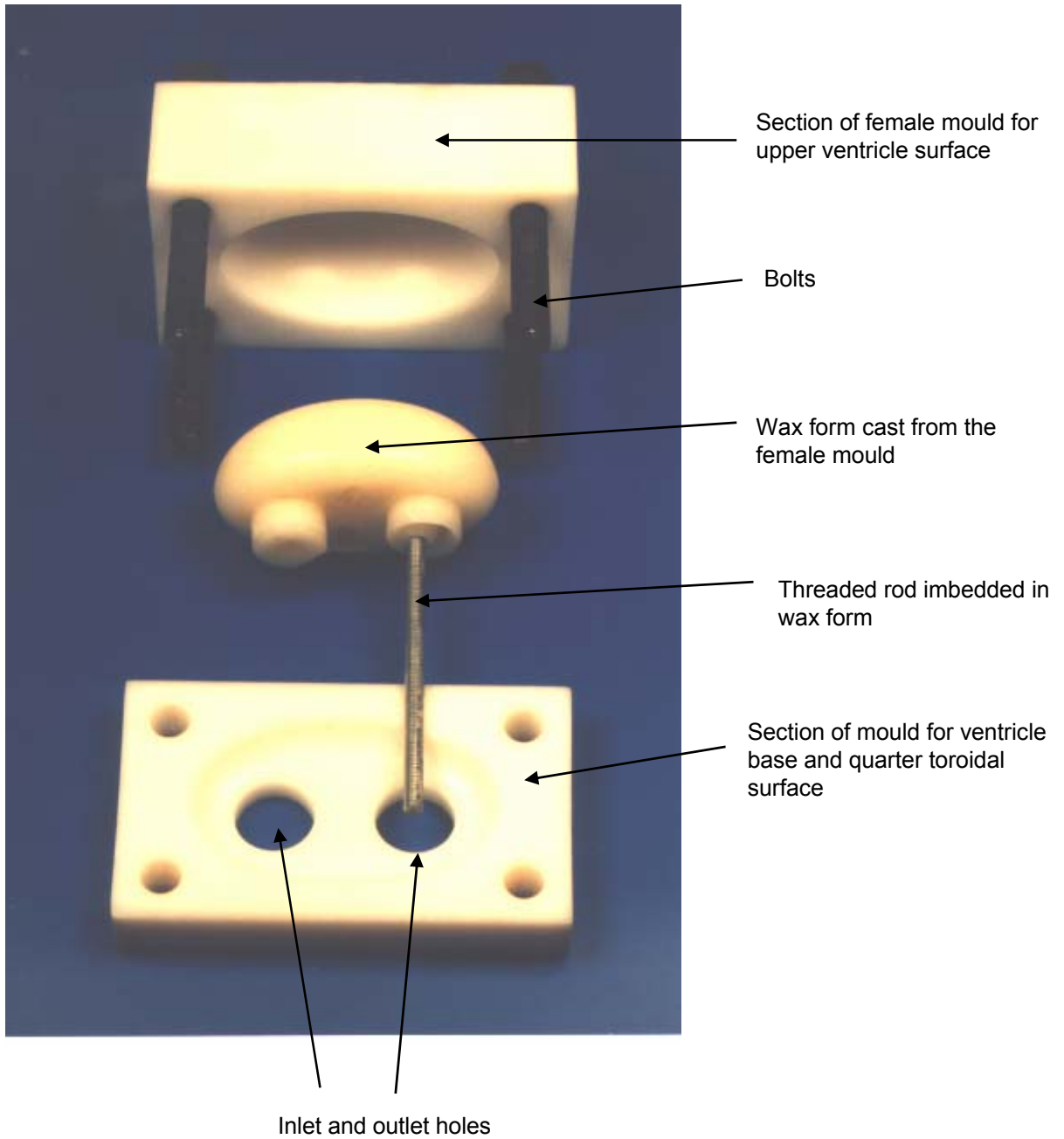


Figure 3.8. The smooth female mould, in two sections, made from acetal copolymer, and a wax mould cast from it.

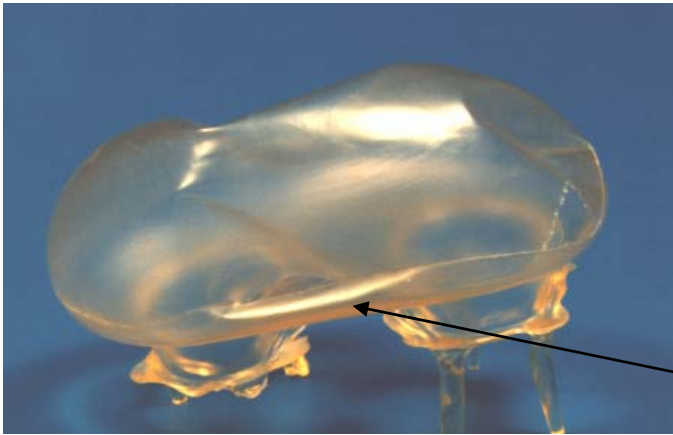


(a)

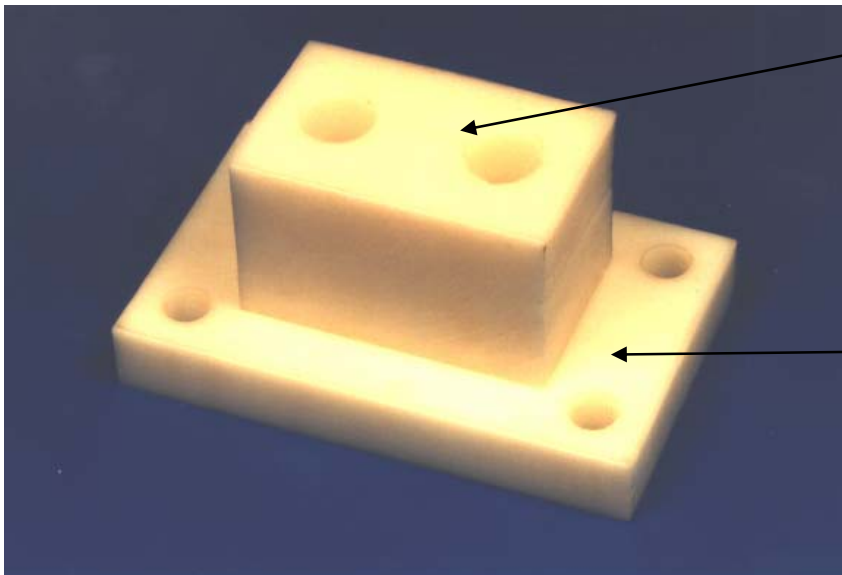


Figure 3.9. (a) The base of a polyurethane ventricle produced by coating the inside walls of a female mould with polyurethane solution. (b) A view of the ventricle showing the tear along the seam.

(b)



Tear along seam.



Extension piece

Thin section of the two part female mould

Figure 3.10. Extension for the smooth female mould inlet and outlet holes.

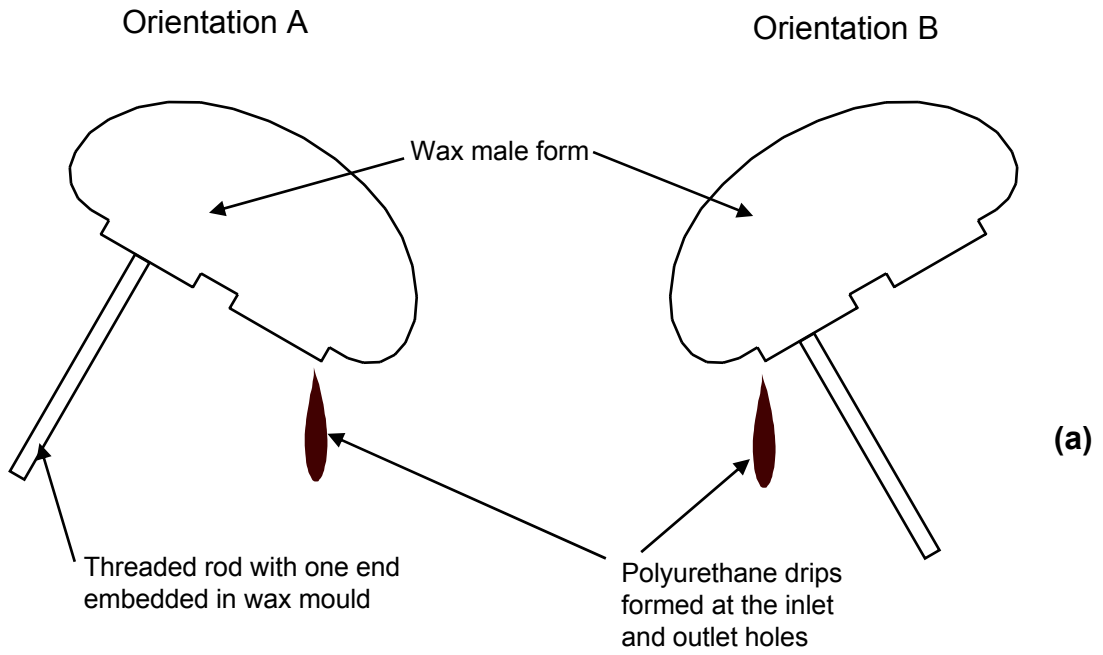


Figure 3.11. (a) Two orientations in which dipped wax moulds are dried. (b) Supporting method for melting wax out of a polyurethane ventricle.

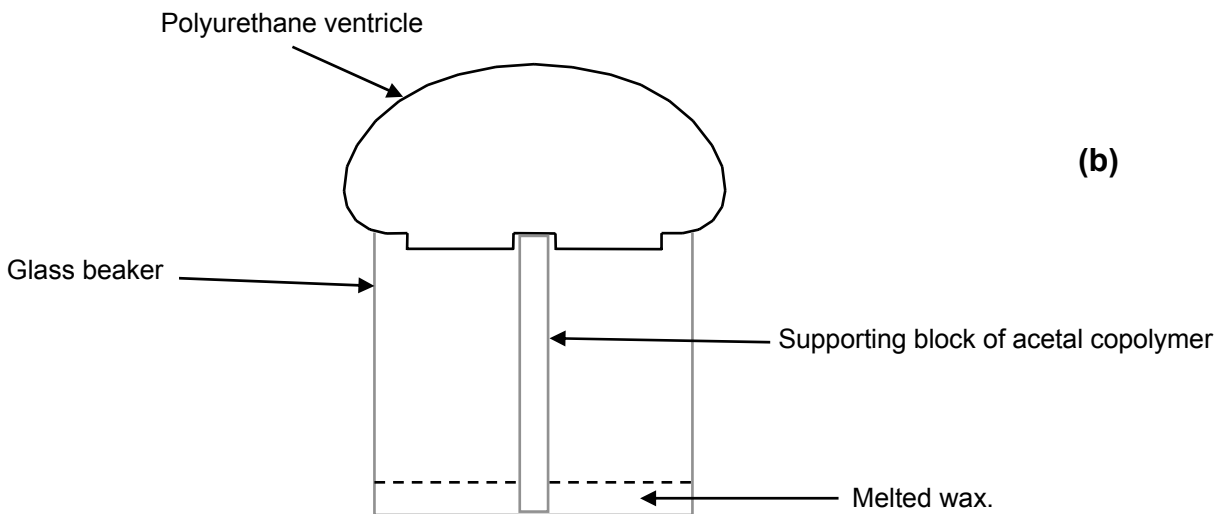
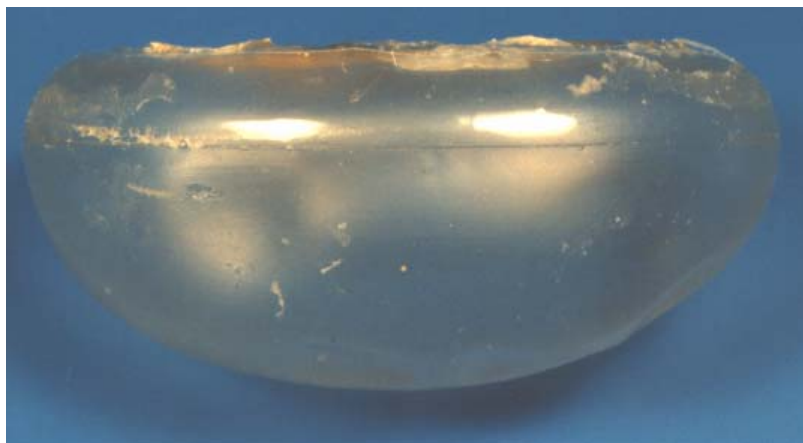
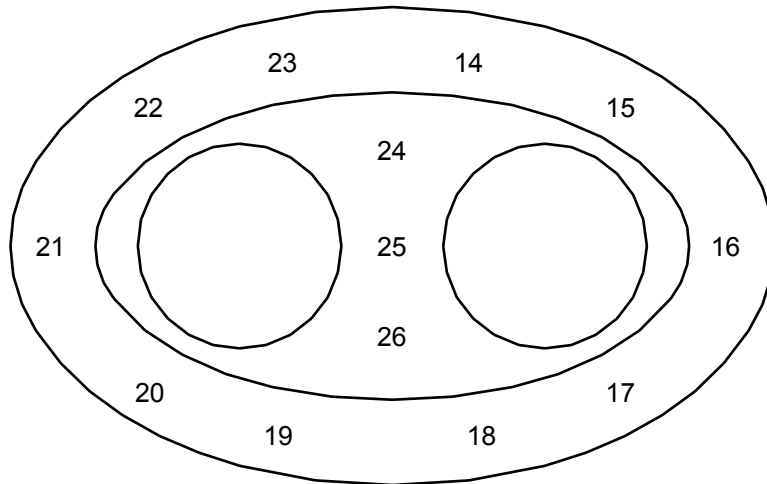


Figure 3.12. A polyurethane ventricle made by dipping a high melting point wax mould into polyurethane solution. The holes in the base are trimmed by hand.



Plan view of ventricle base



Plan view of ventricle upper surface

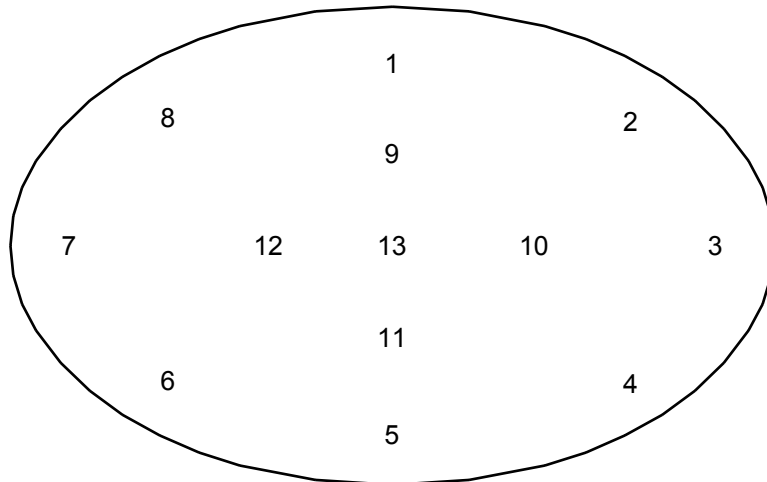


Figure 3.13. Thickness measurement positions made on each manufactured polyurethane ventricle. The measurements are numerically labeled, by order of measurement.

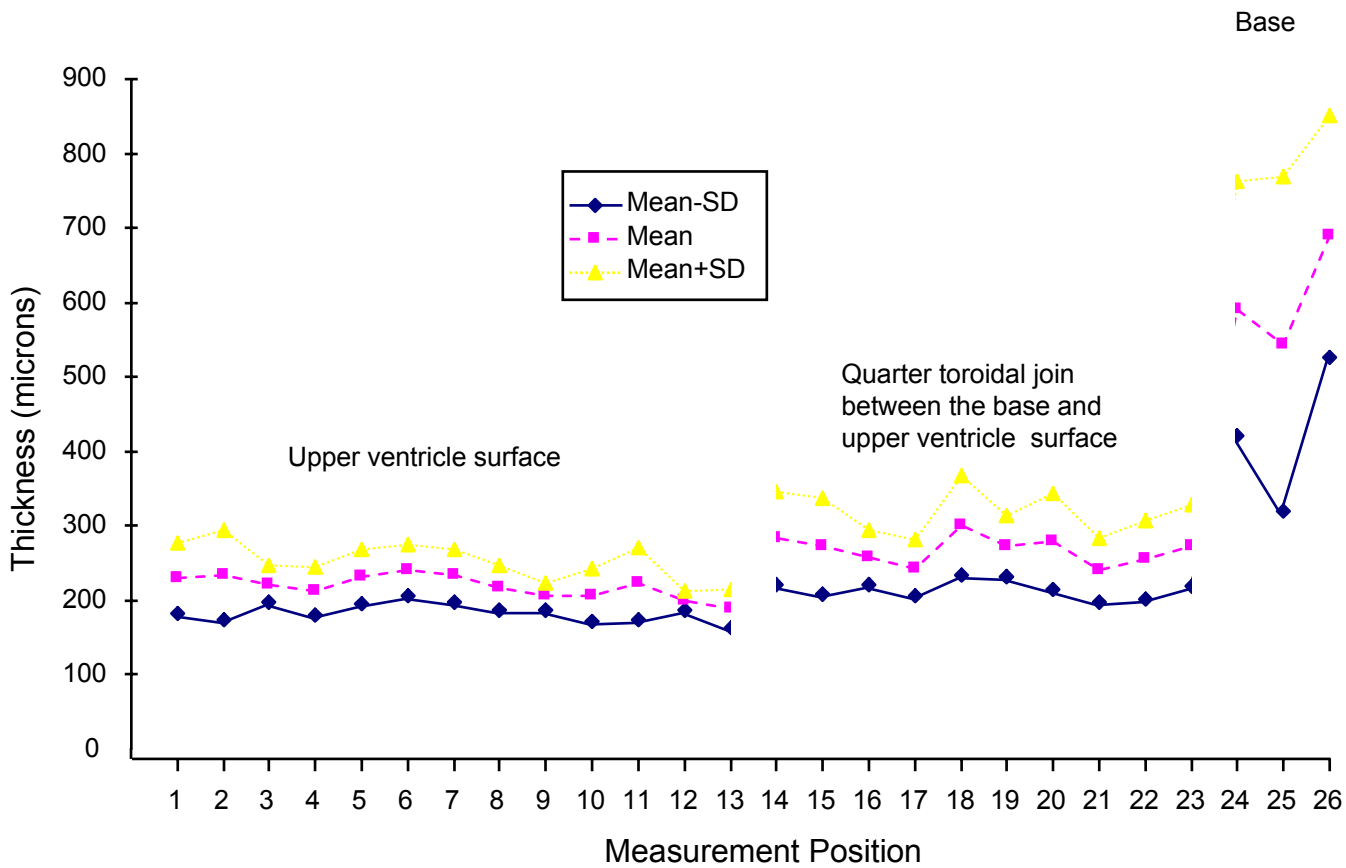


Figure 3.14. Mean thickness measurements of six 4 dip polyurethane ventricles.

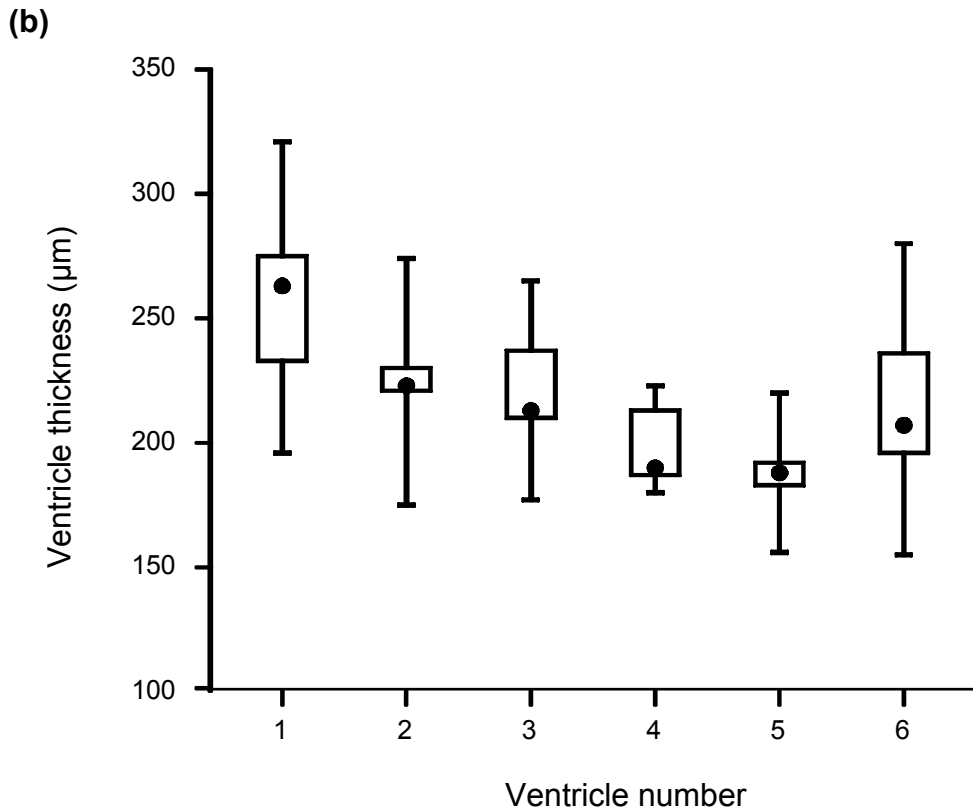
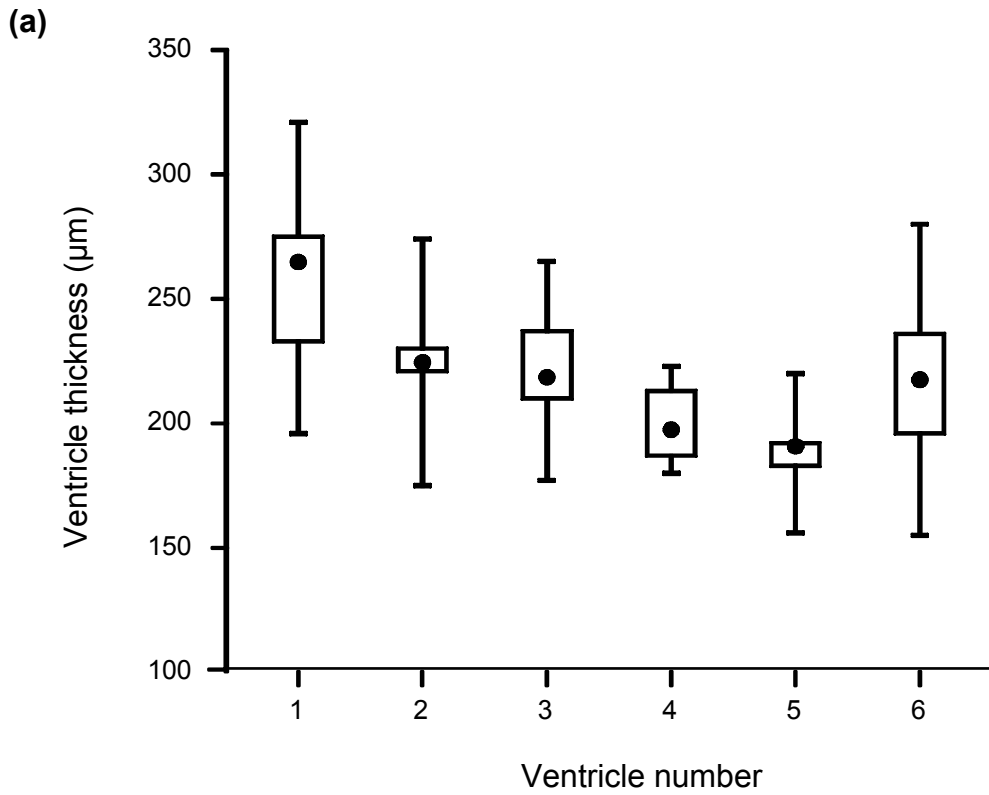
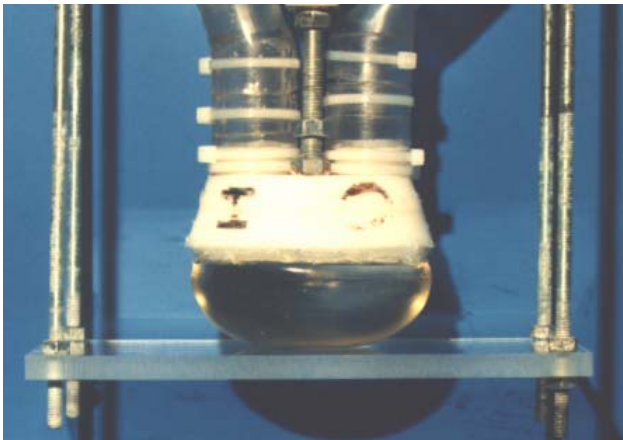
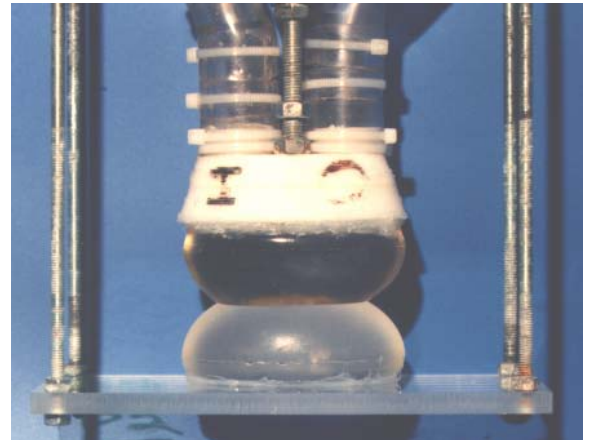


Figure 3.15. Box plots of the upper surface thickness measurements for the six 4 dip ventricles. The range is plotted together with the 25th and 75th percentiles. The filled circle represents the mean in (a) and the median in (b).

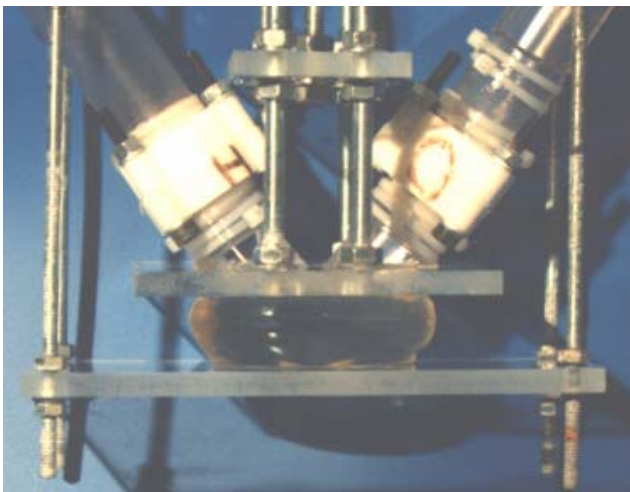
B1P1



B1P2



B2P1



B2P2

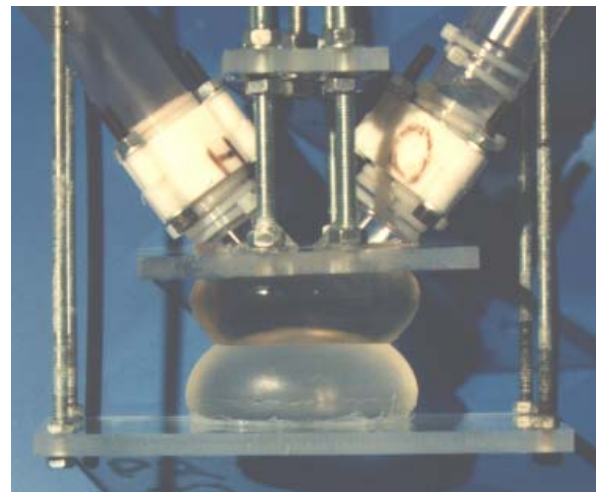


Figure 3.16. The four geometrical variations of proto-type blood pump made from combinations of B1 (base with straight pipes) and B2 (base with angled pipes) with P1 (flat compression plate) and P2 (domed compression plate).

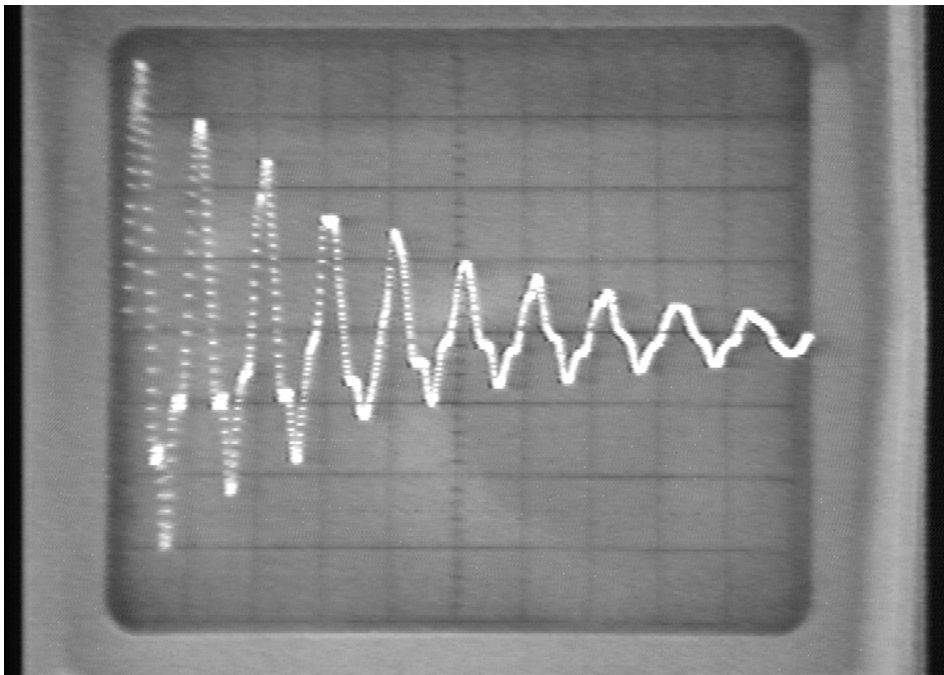


Figure 4.1. Signal from the force transducer and meter, on an oscilloscope, after delivering an impulse of short duration to the compression plate.

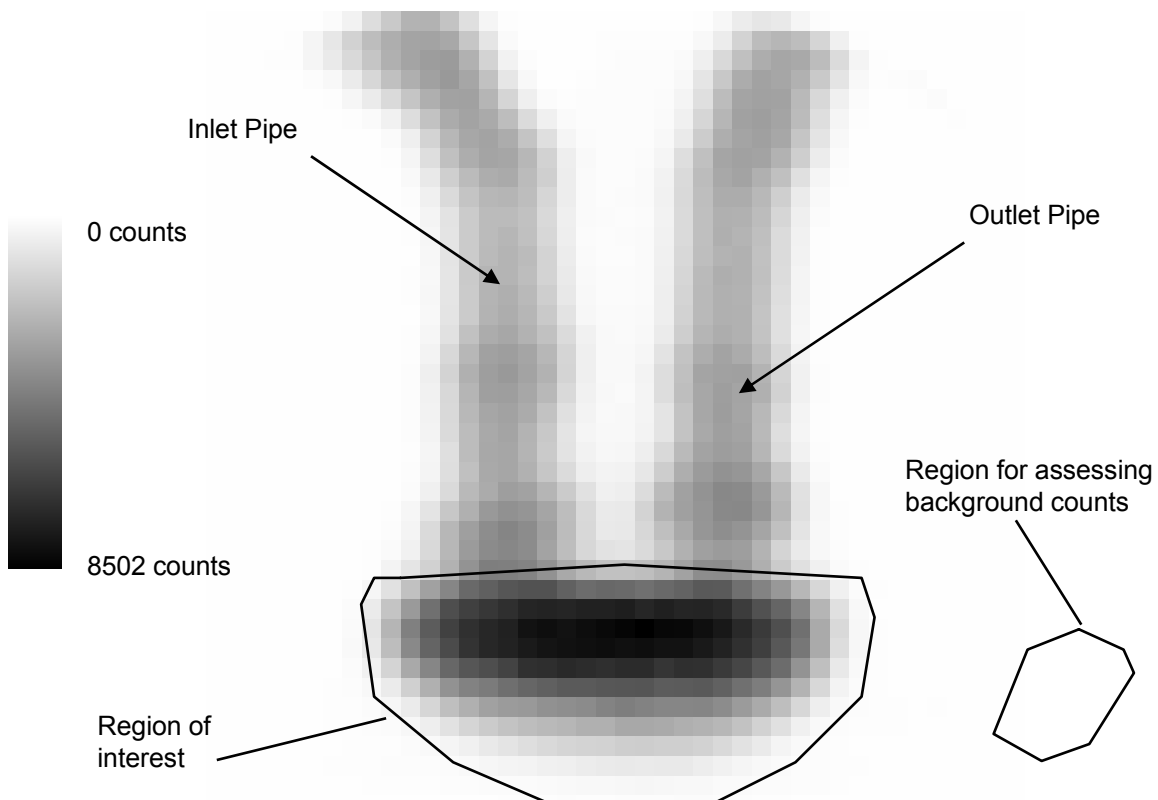


Figure 4.2. Totalised image of counts from within an artificial ventricle. The region of interest defines the area within which counts are summed for the calculation of ejection fraction. The relationship between grey scale and gamma ray counts is linear.

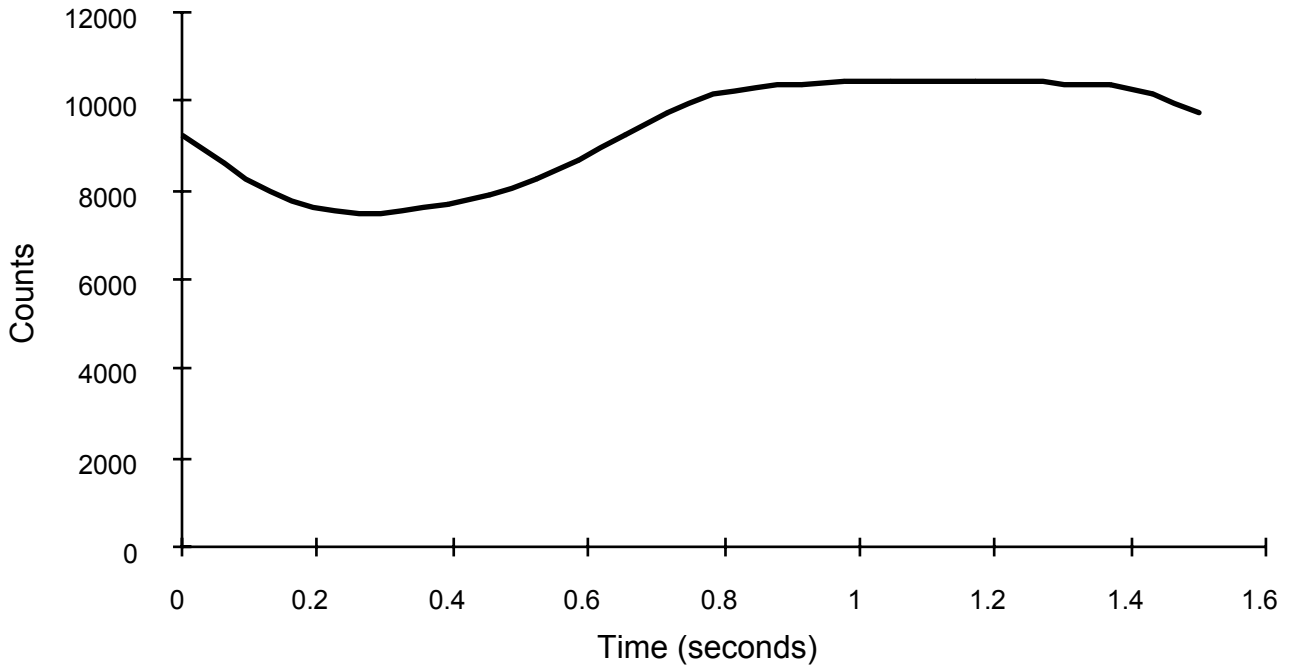


Figure 4.3. Gamma ray counts during one cycle inside a region of interest, for a 19.6mm stroke length at 40bpm.

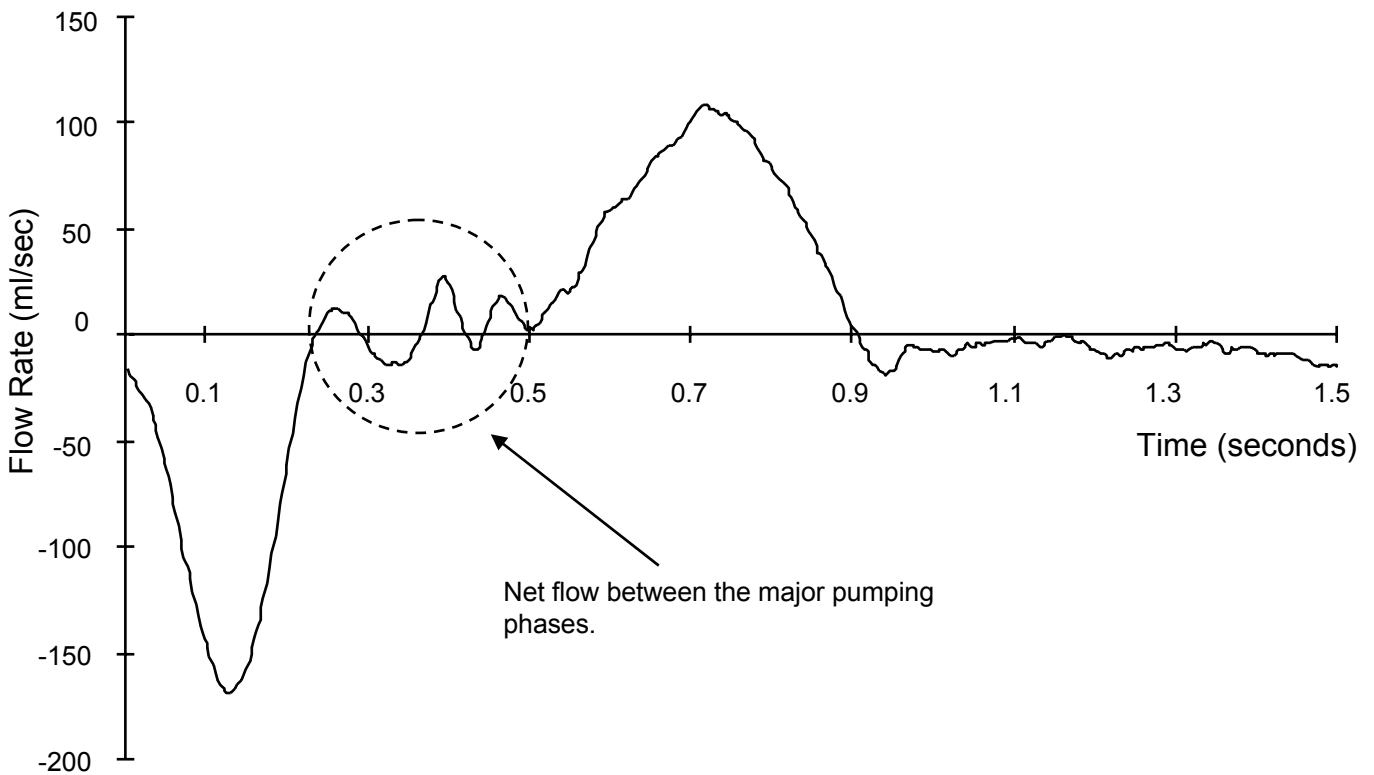


Figure 4.4 Net fluid flow rate through a ventricle. (Flow out of the ventricle is positive.)

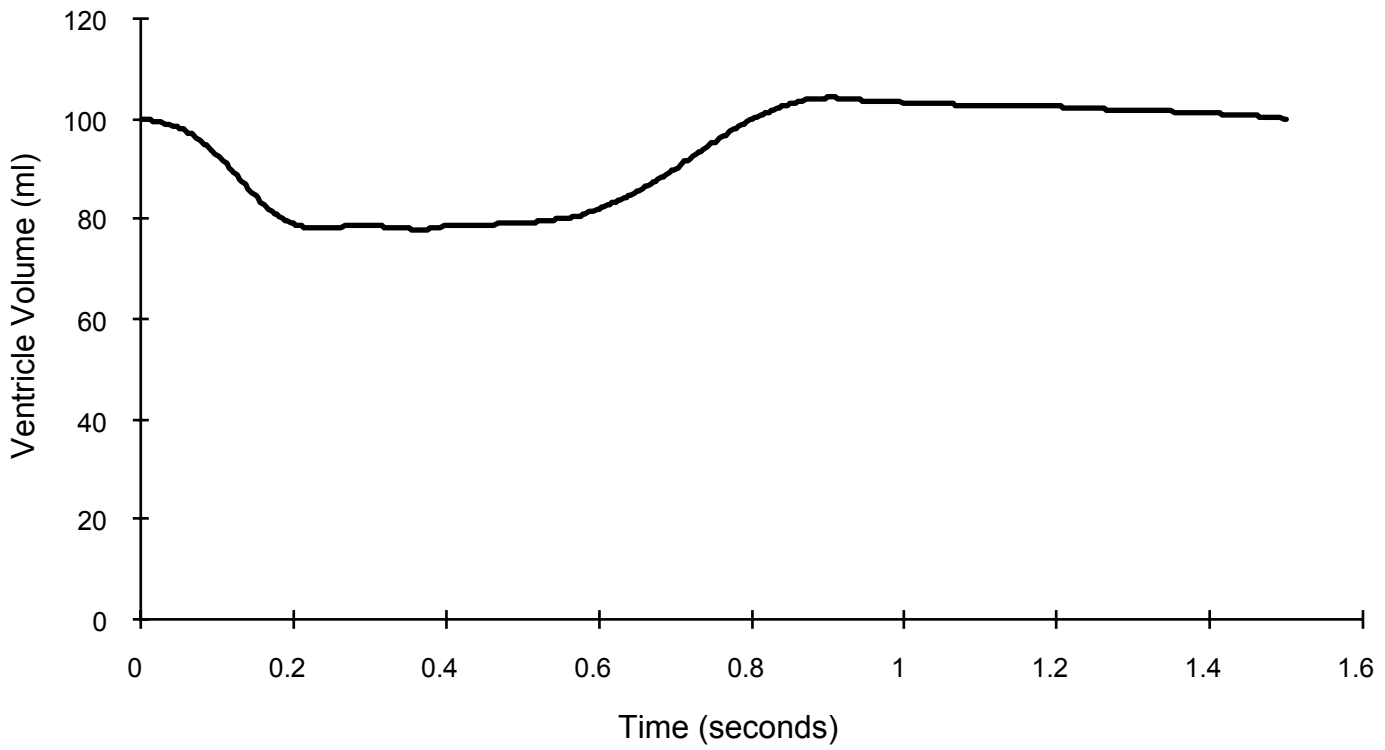


Figure 4.5. Ventricle volume during one cycle derived from flow measurements up and down stream of a ventricle (19.6mm stroke length at 40bpm).

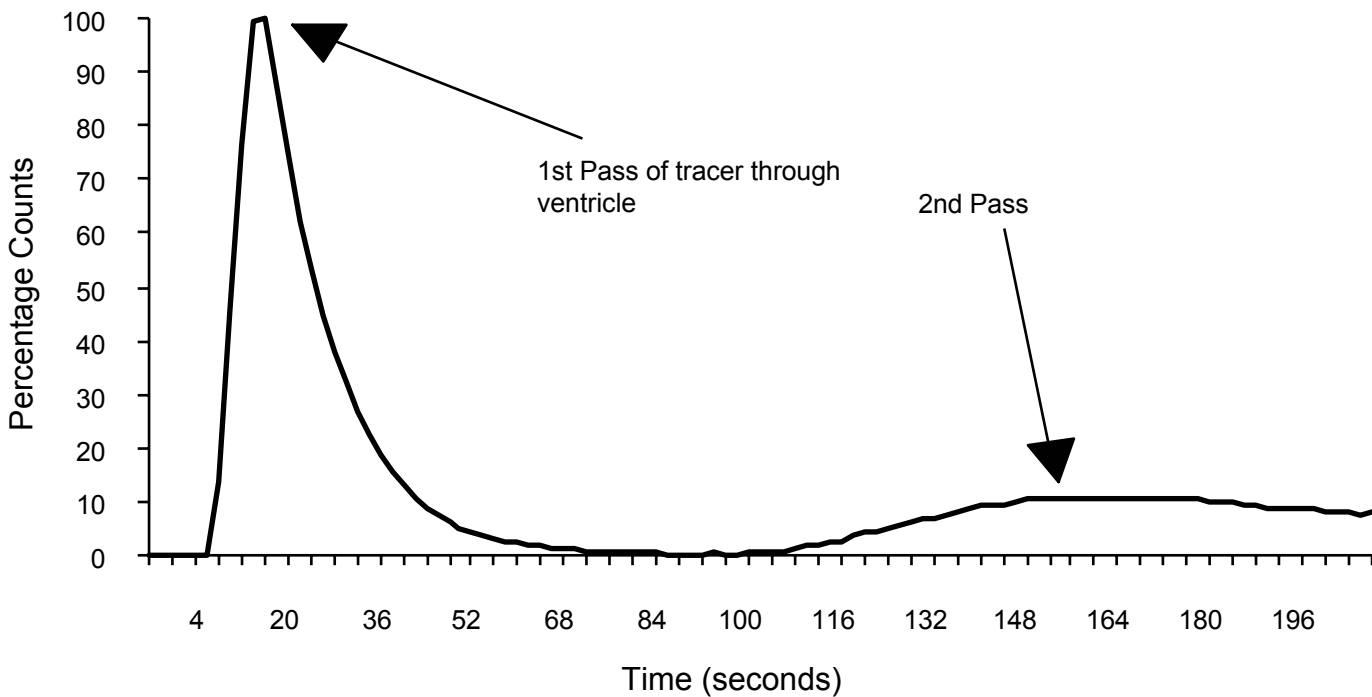


Figure 4.6. Clearance curve derived from gamma ray counts, within a region of interest, after the introduction of a Tc-99m bolus upstream of a ventricle (20.9mm stroke length at 30bpm).

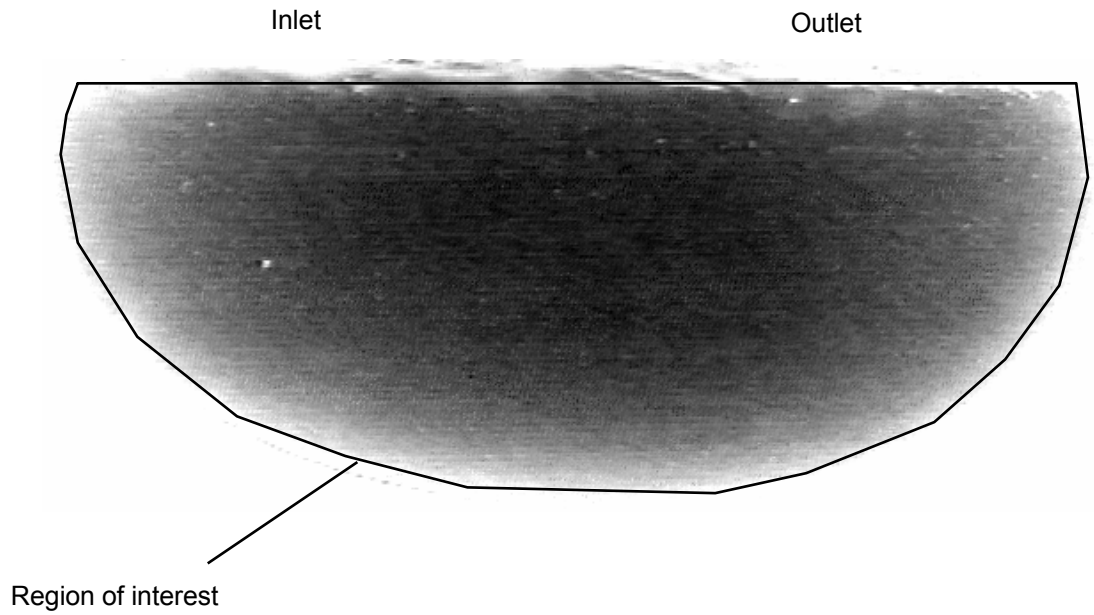


Figure 4.7. Captured image of dye inside the polyurethane ventricle at maximum ventricle volume, during a pumping cycle.

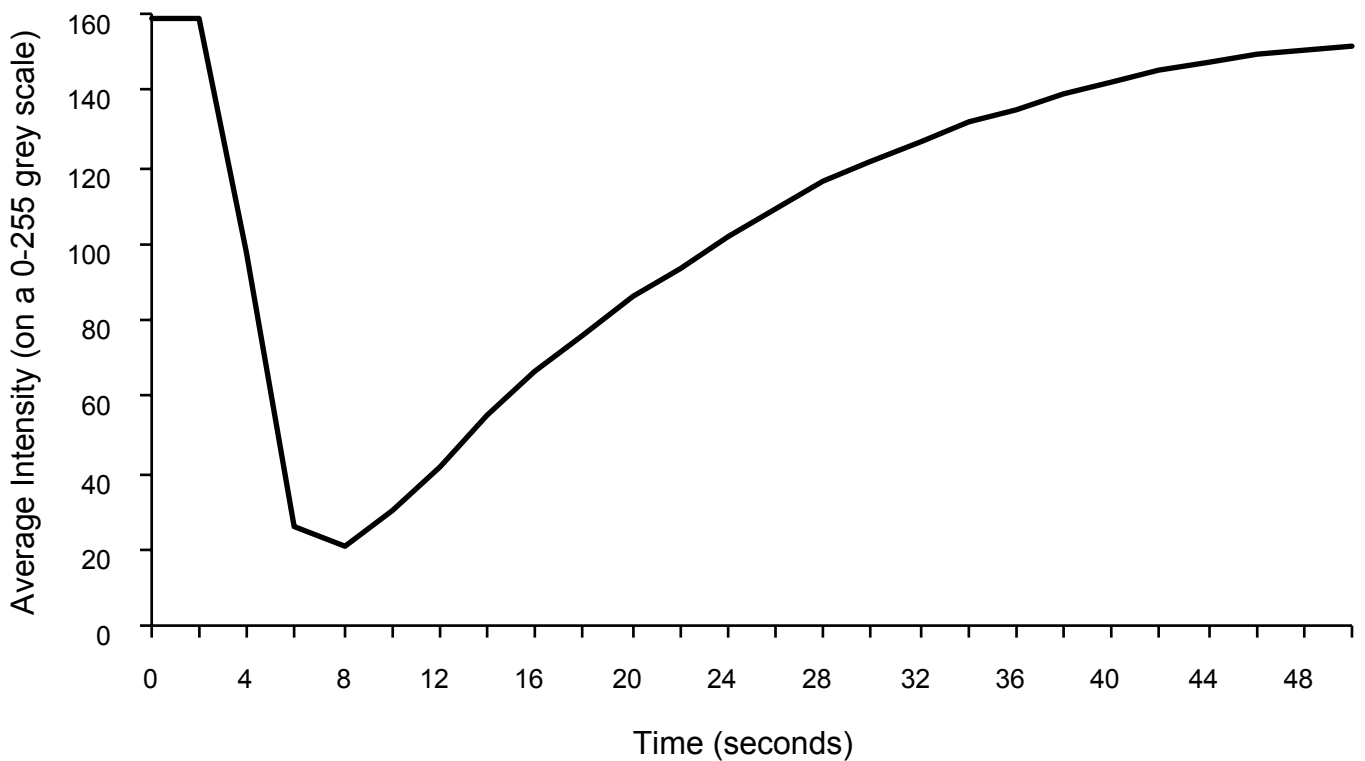


Figure 4.8. Average intensity, within a region of interest, after the introduction of an upstream dye bolus (20.9mm stroke length at 30bpm) plotted against time.

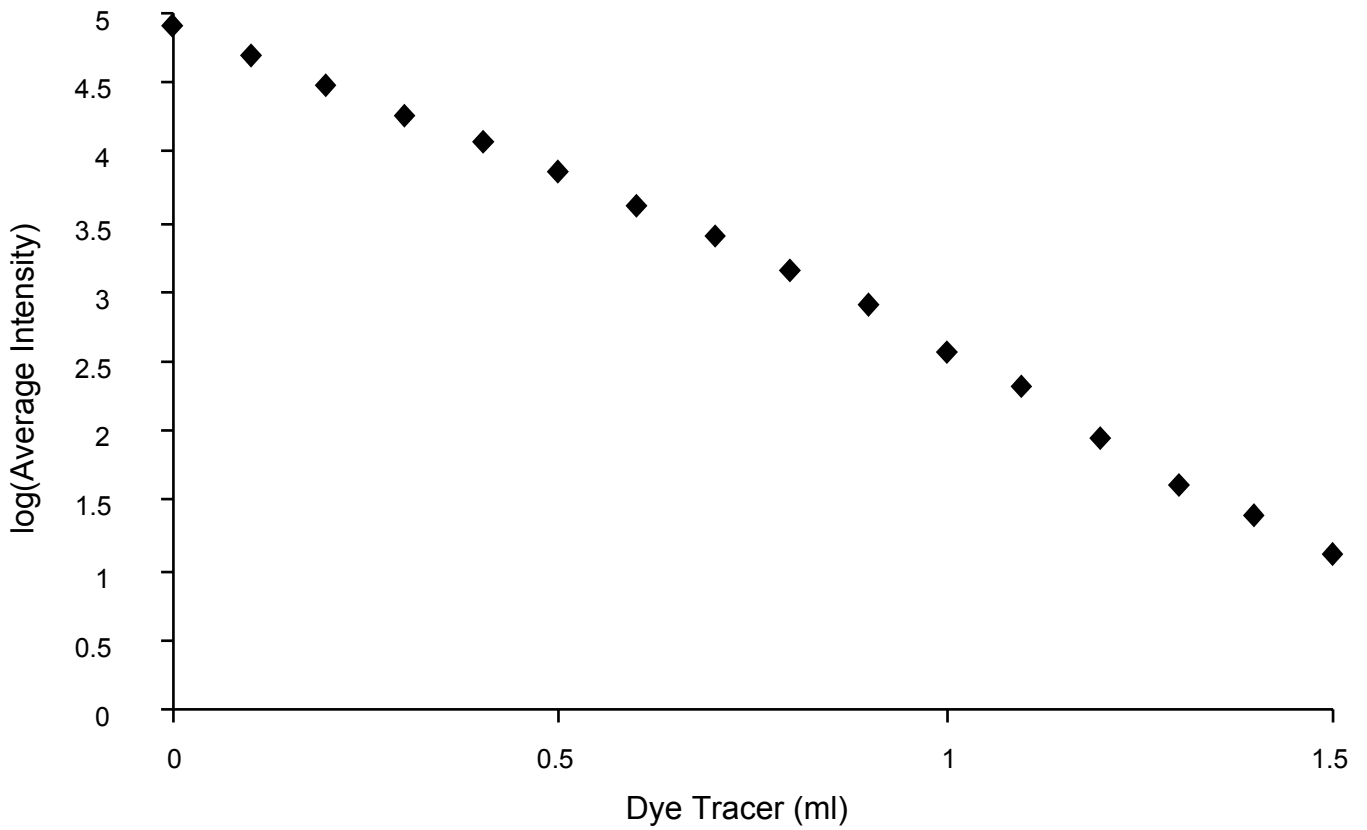


Figure 4.9. Logarithm of the average intensity plotted against incremental changes of, uniformly mixed, dye within the ventricle.

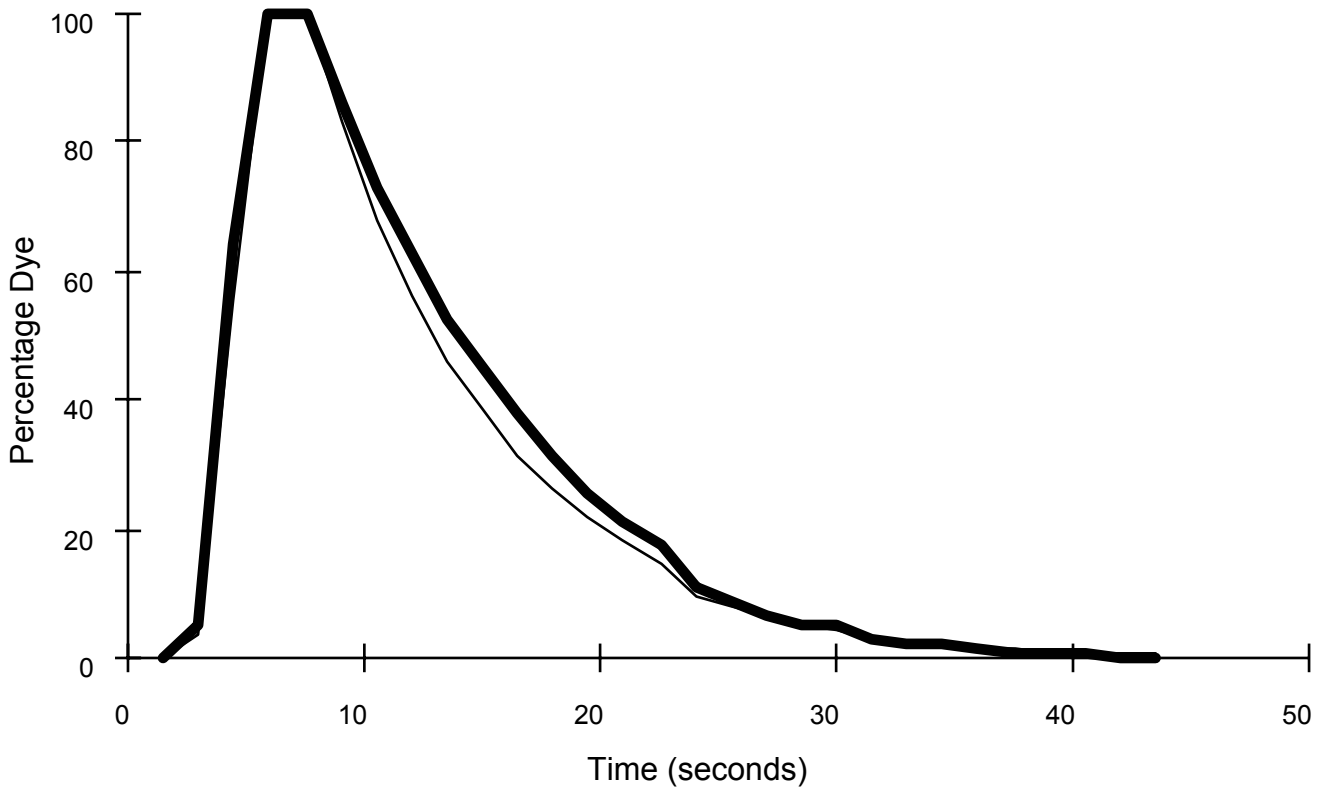


Figure 4.10. Comparison of clearance curves produced by the pixel method , that takes account of ventricle geometry, and the average intensity method , (20.9mm stroke length at 30bpm).

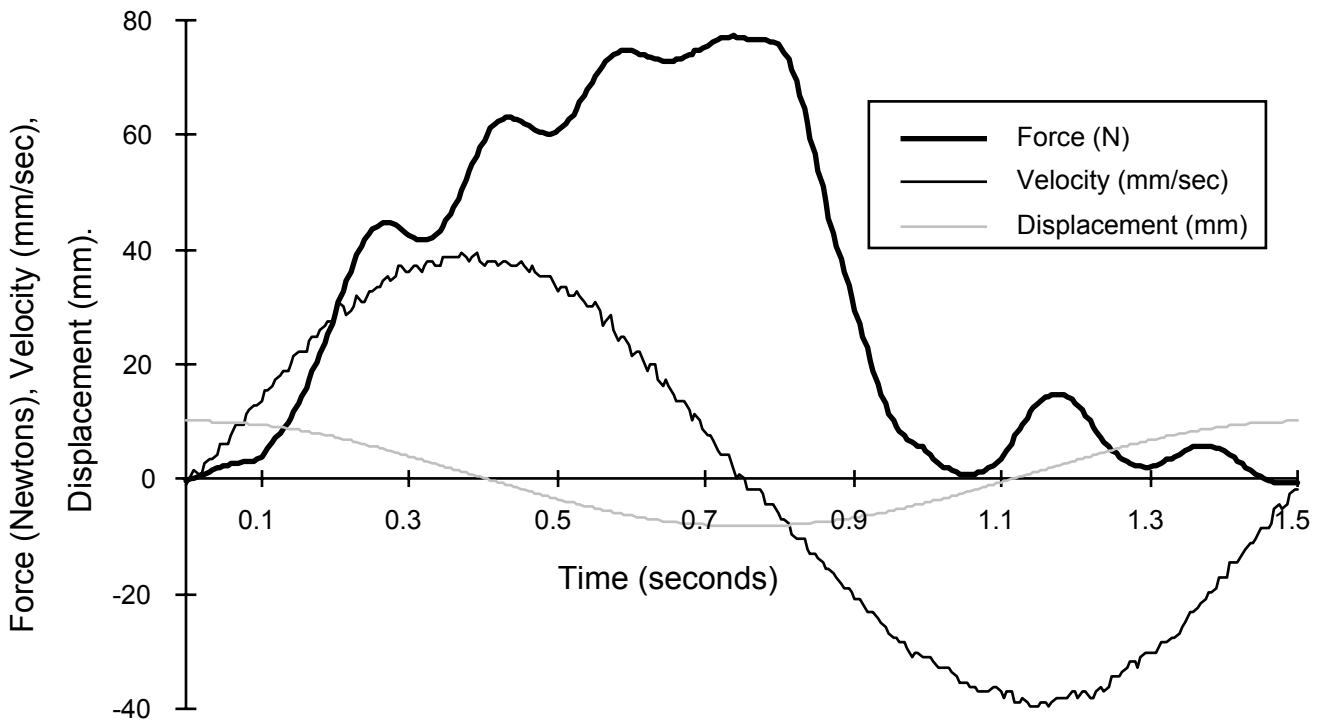


Figure 4.11. Displacement of the linear actuator during one pumping cycle of the polyurethane ventricle, 18.3mm stroke length at 40bpm, at a flow rate of 1.98 litres/minute . Positive displacement values are measured when the compression plate moves away from the ventricle, i.e. during filling. The velocity of the compression plate is derived from the displacement data. The force data is captured from a force transducer placed in series with the linear actuator piston.

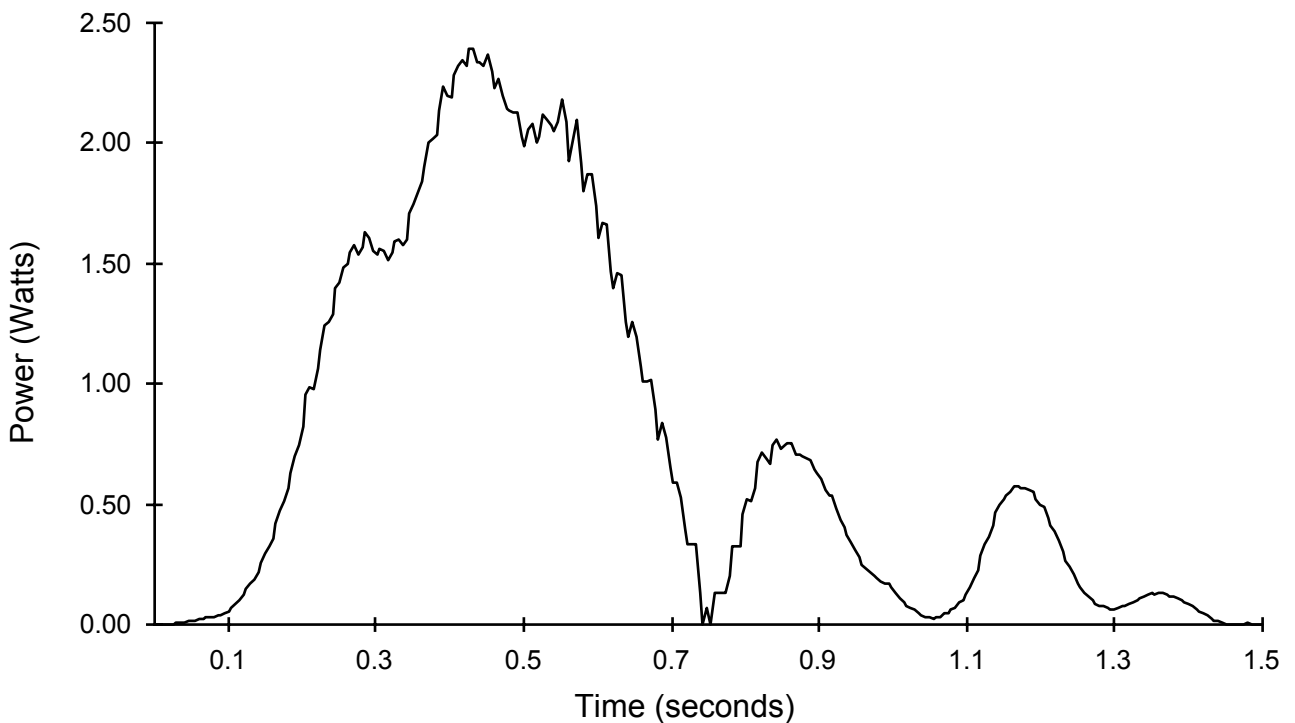


Figure 4.12. Graph of power necessary to actuate the compression plate while pumping at a flow rate of 1.98 litres/minute (18.3mm stroke length at 40bpm). This graph is in phase with the plot in figure 4.11. The power curve from 0 to 0.75 seconds corresponds to compression of the ventricle during ejection. 0.75 to 1.5 seconds corresponds to ventricle filling.

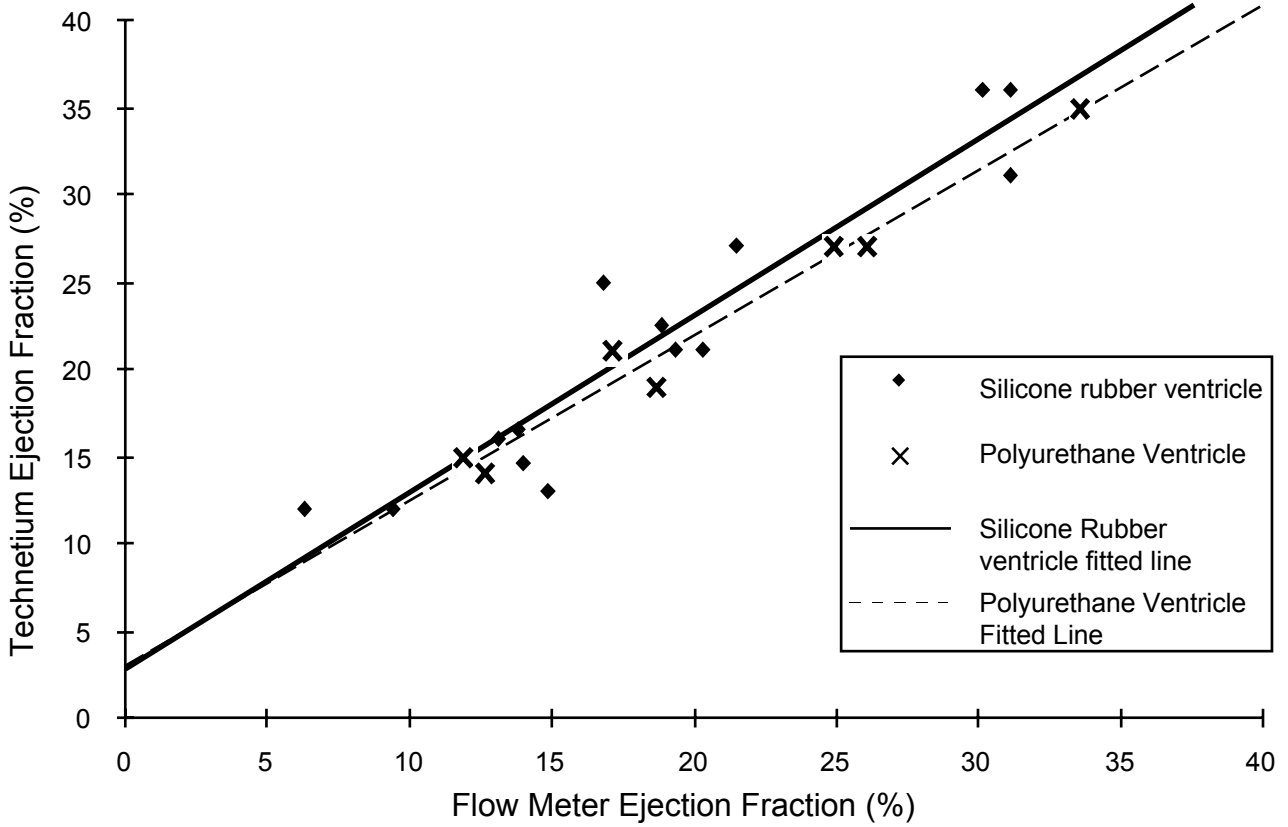


Figure 4.13. Comparison of ejection fractions measured with Tc-99m and EM flow meters at different flow rates in silicone rubber ($r = 0.94$, gradient = 1.02) and polyurethane ventricles ($r = 0.99$, gradient = 0.94).

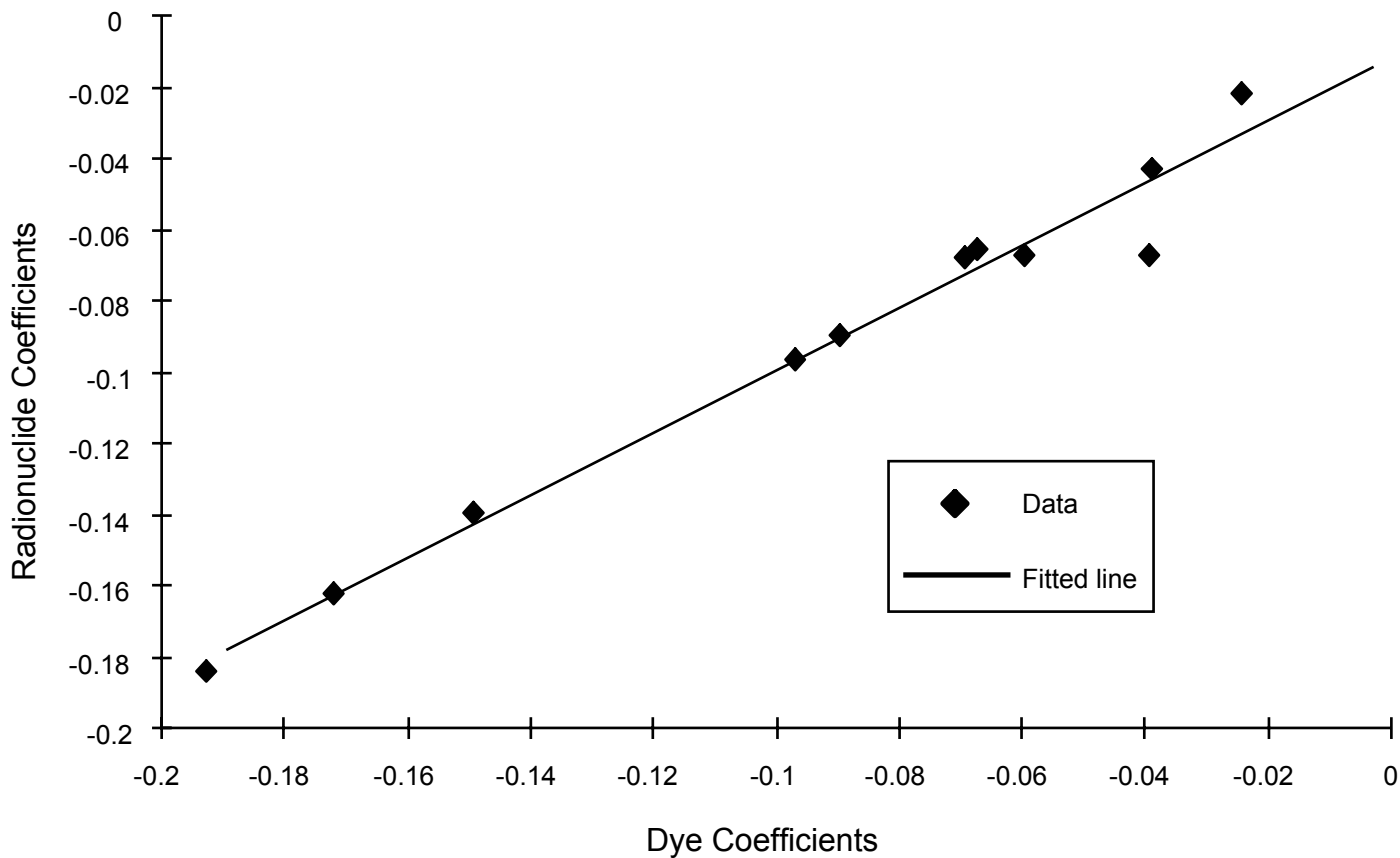


Figure 4.14. Comparison of exponential curves, $y = ae^{bx}$, fitted to the Tc-99m and dye clearance curves (fitted line: $r = 0.997$, gradient = 0.91).

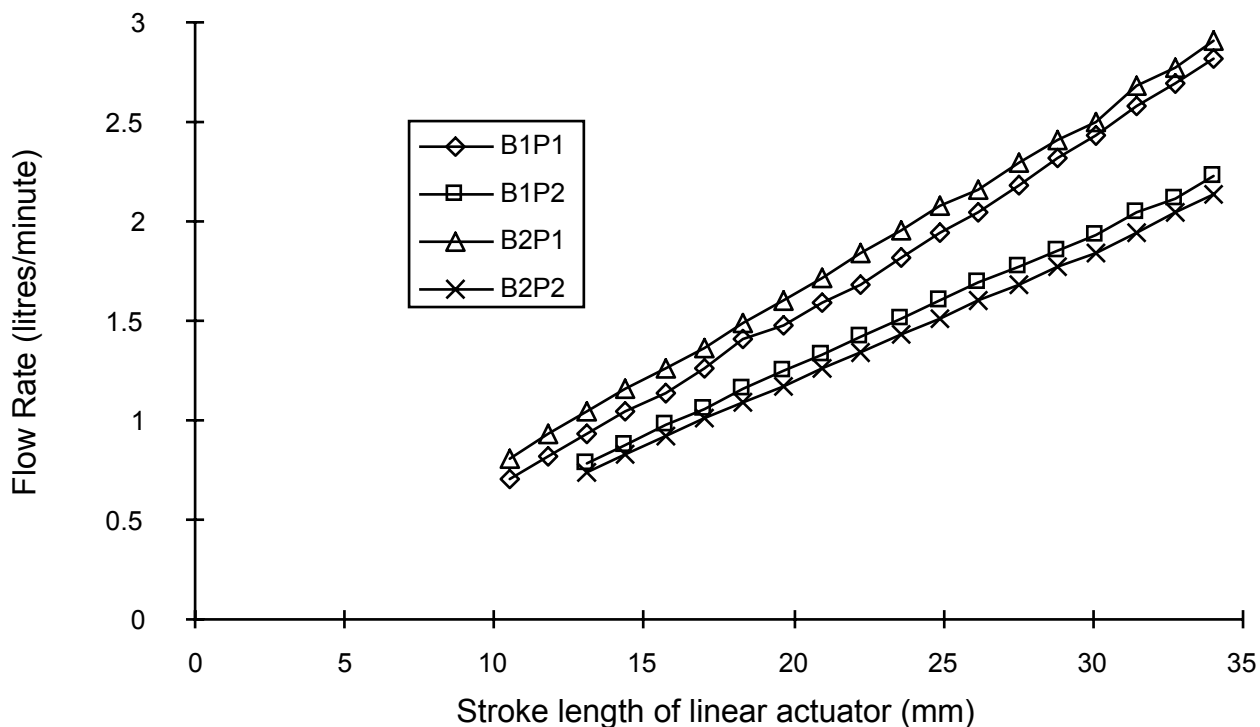


Figure 5.1. Calibration of the four designs for flow rate against superpump stroke length. The r values for the least squares linear fitted lines are all above 0.999.

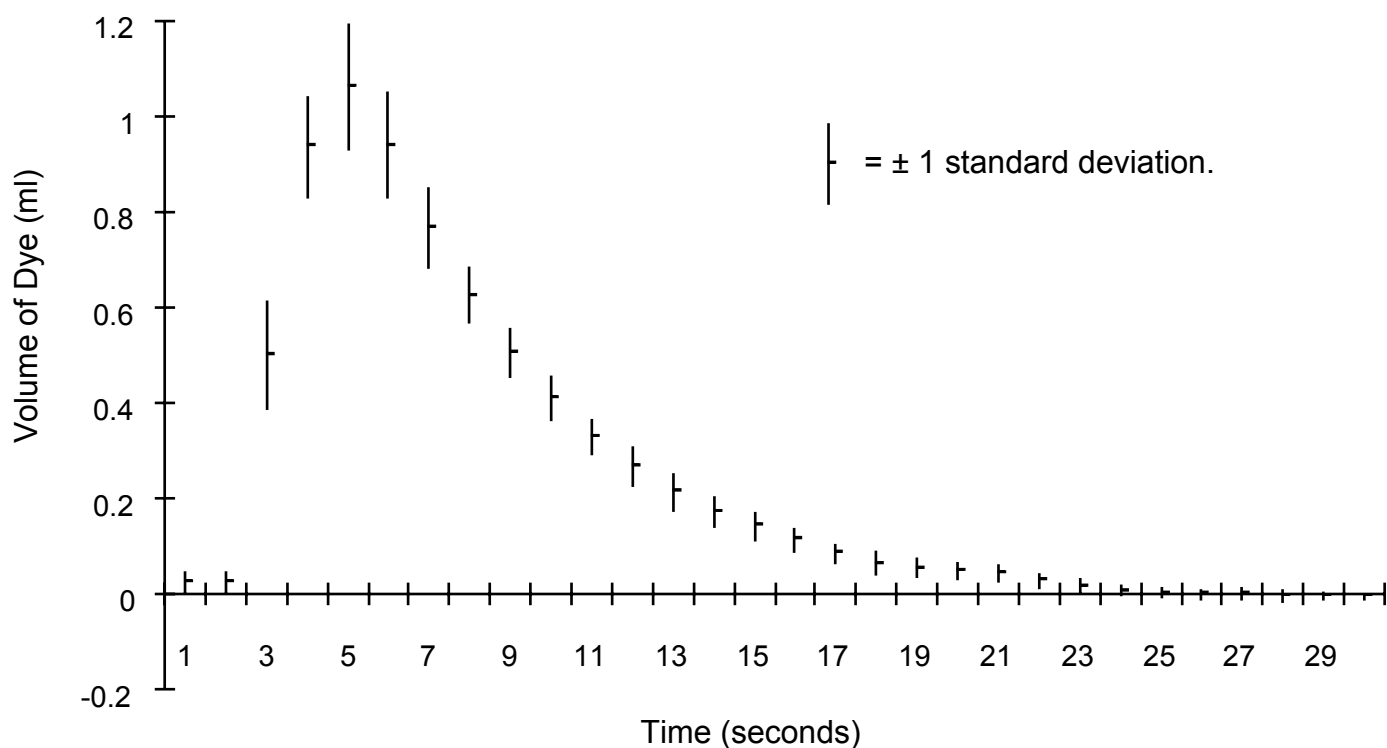


Figure 5.2. The mean and standard deviation of ten clearance curves, for the same pumping chamber, at the same flow and pumping rate.

Figure 5.3. Process for converting a video frame of dye, inside a pumping chamber, to a colour map of dye concentration along each line of site through the pumping chamber.

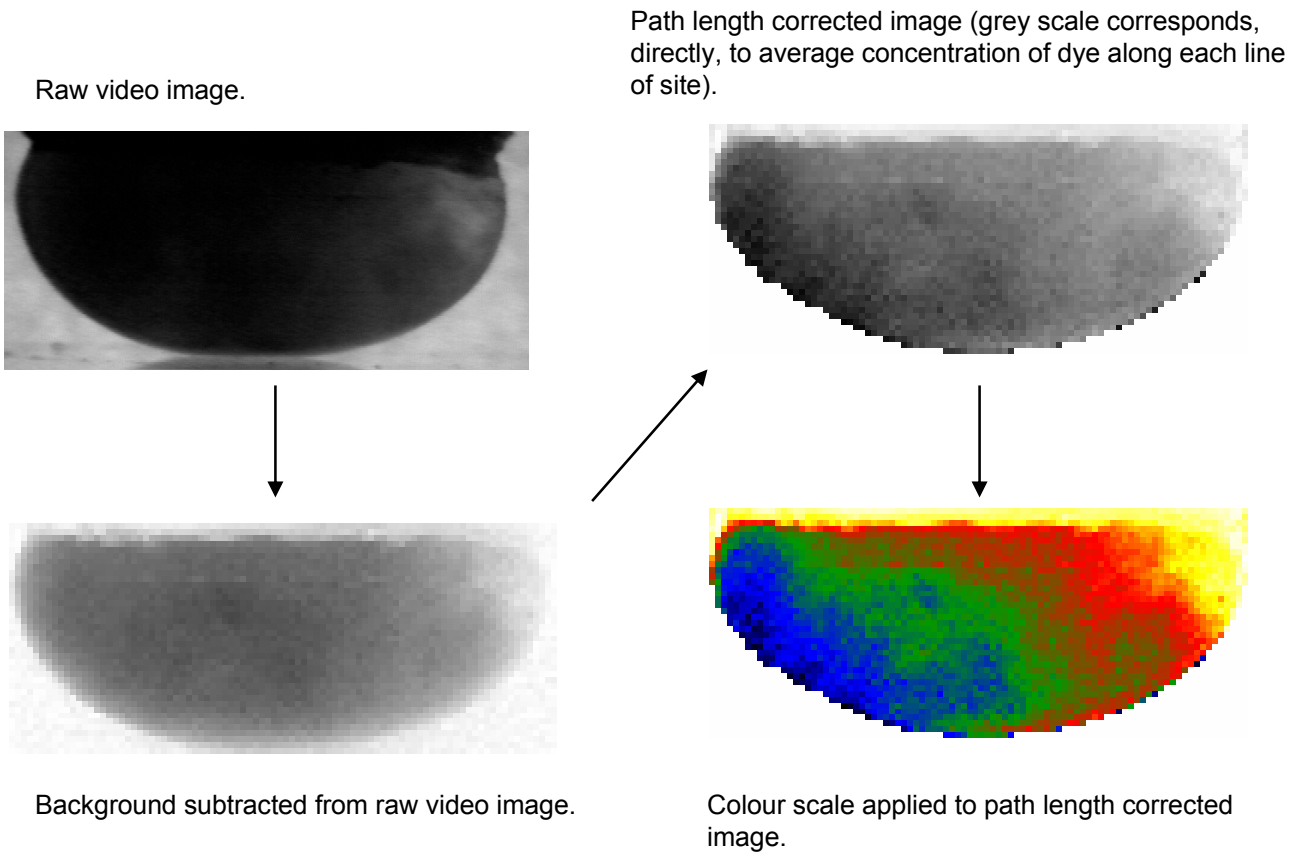


Figure 5.4. Path lengths as a grey scale image, with a linear scale from white (grey value of 255) to black (grey value of 0) corresponding to a scale of 0mm to 56mm path length.

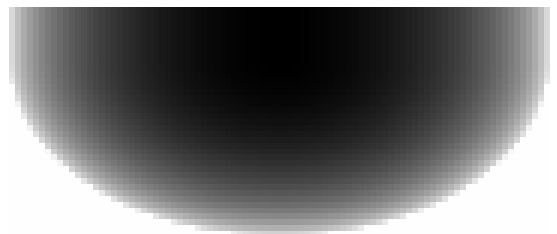
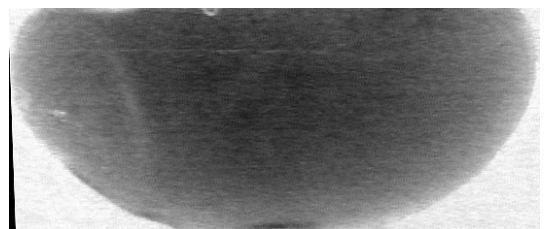


Figure 5.5. A typical calibration image after the background effects have been subtracted. 0.9 ml of dye, uniformly concentrated, present in a ventricle.



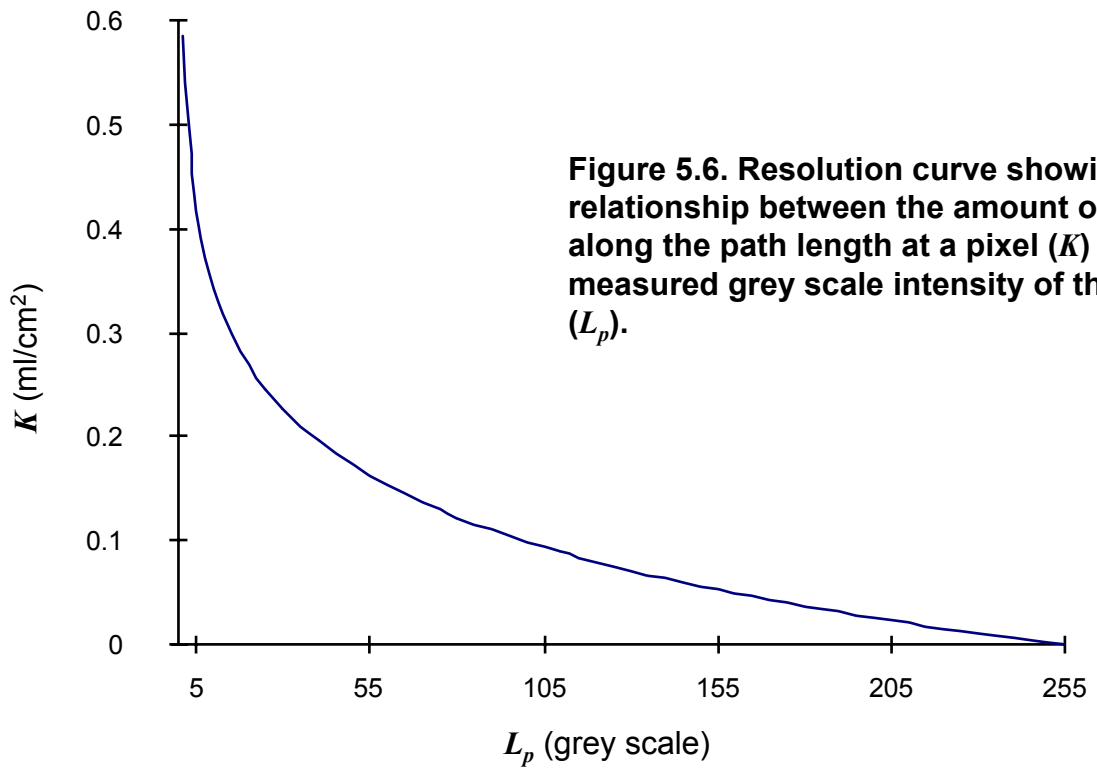
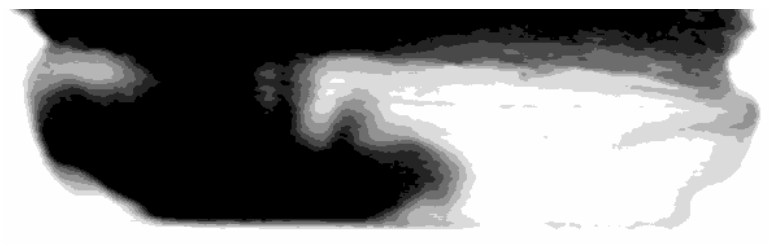


Figure 5.6. Resolution curve showing the relationship between the amount of dye along the path length at a pixel (K) and the measured grey scale intensity of the pixel (L_p).

Raw video image.



Figure 5.7. Enhancement of a raw video image. The inflow jet is visualized with dye.



Enhanced image.

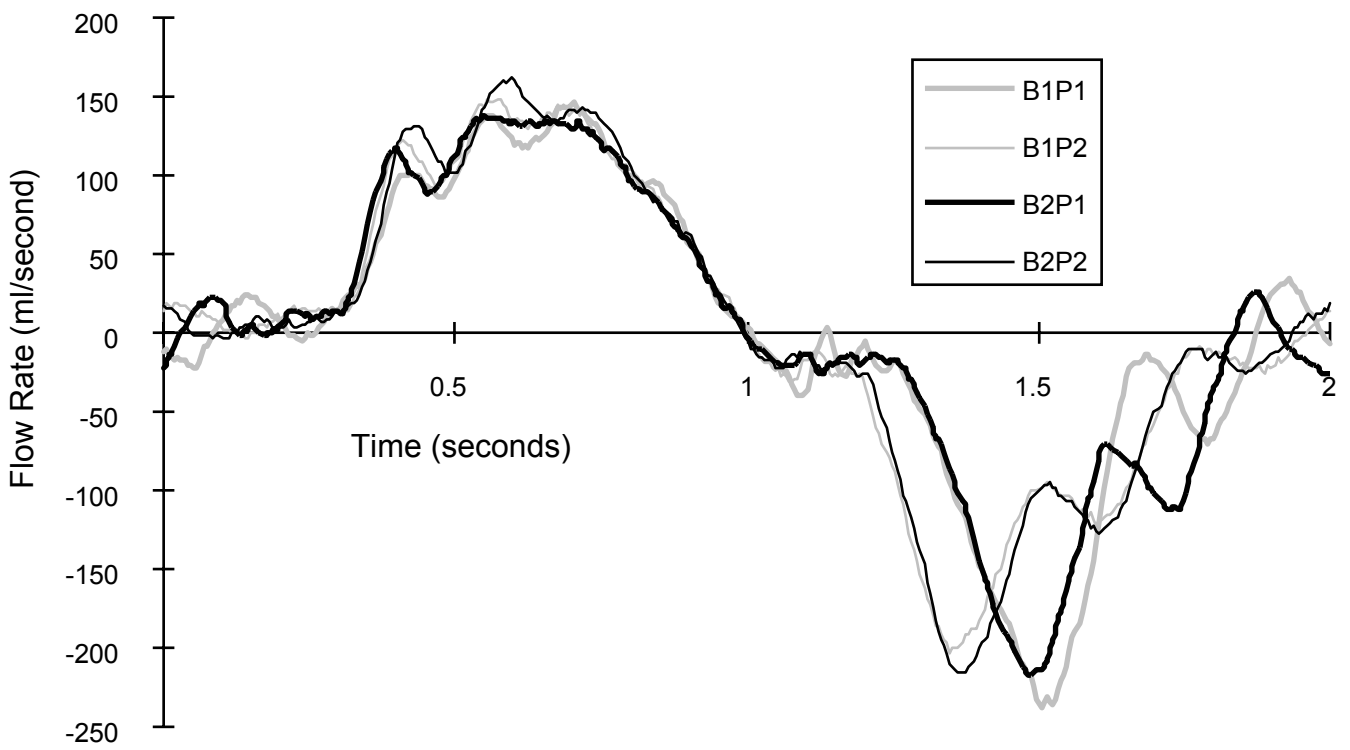


Figure 5.8. Resultant flow curves for the four designs at a flow rate of 2.1 litres/minute. Outflow is positive and inflow negative.

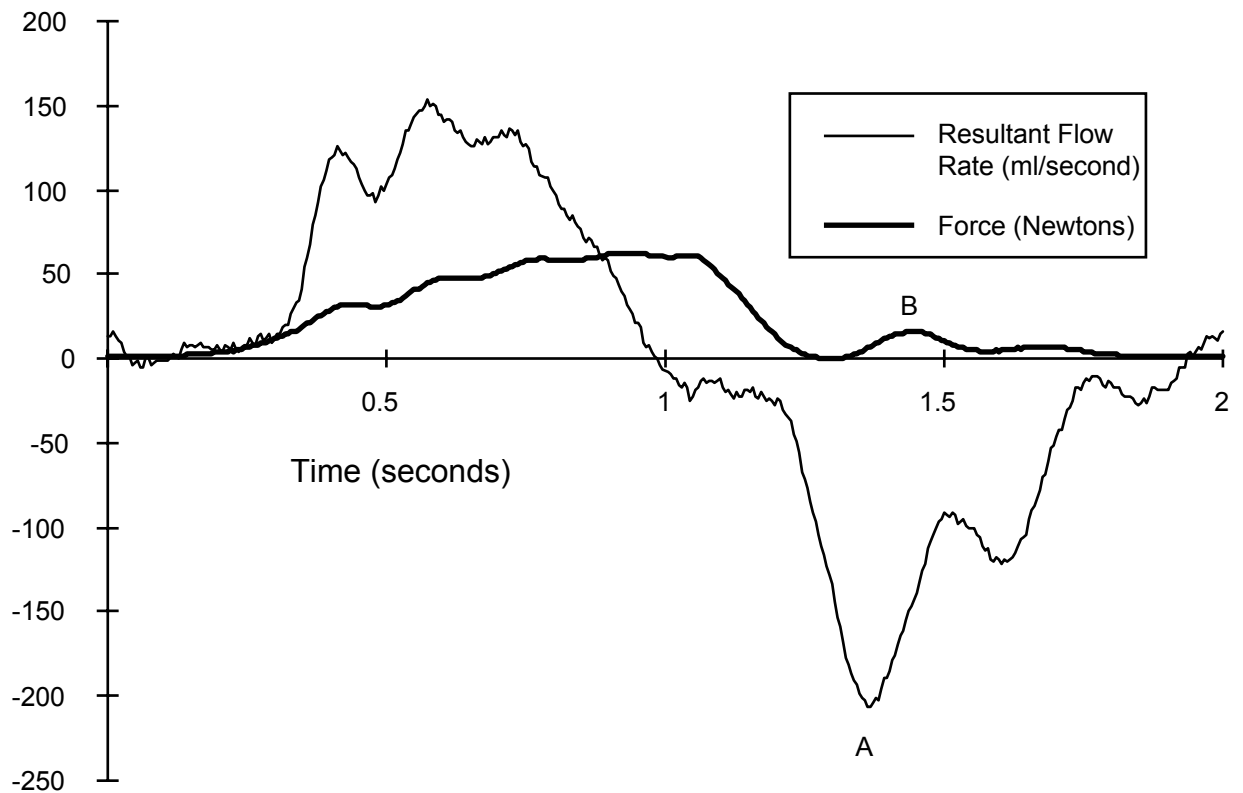


Figure 5.9. Comparison of force and flow curves for B2P2, flow rate of 2.0 litres/minute at 30bpm.

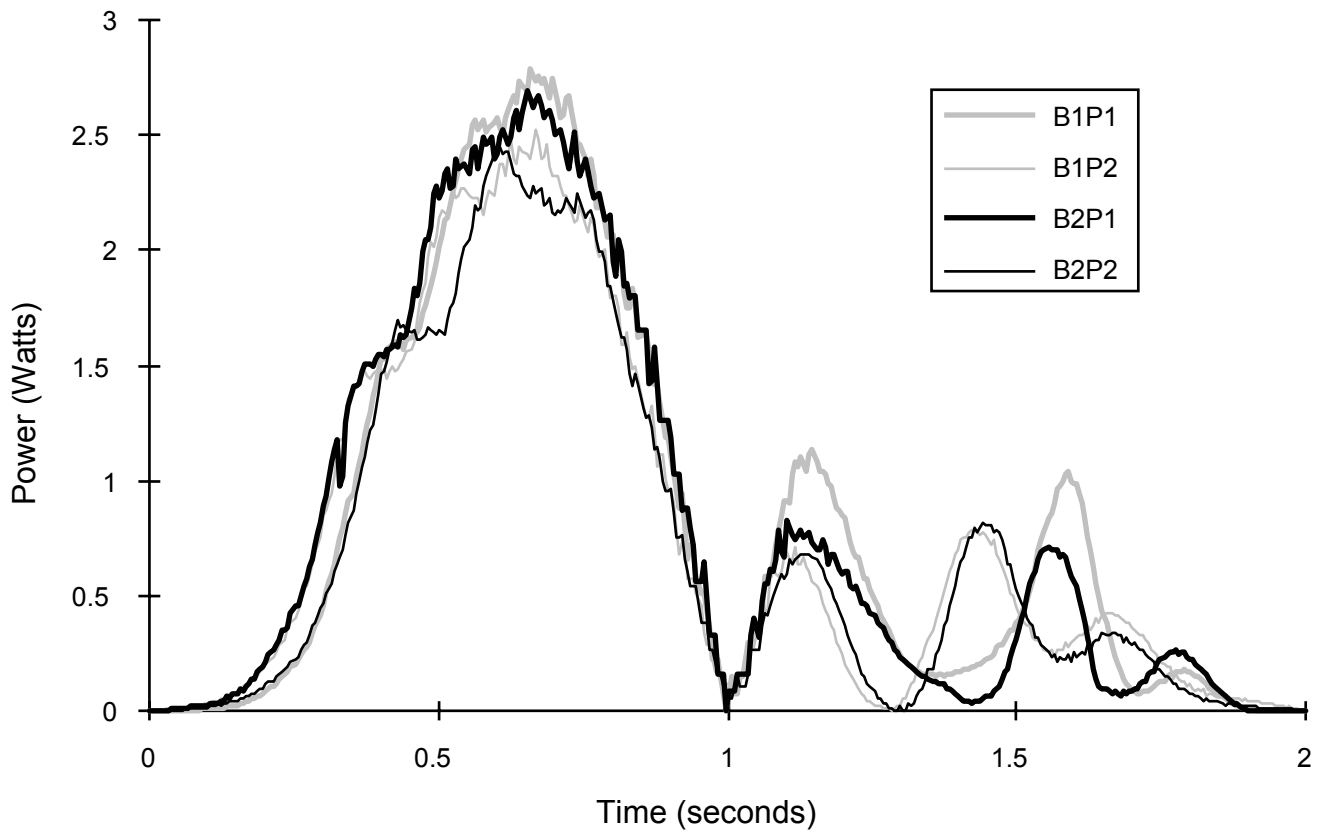


Figure 5.10. Power curves for the four designs at a flow rate of 2.0 litres/minute, pumping at 30bpm. The curves from 0 to 1 seconds represent power expended in pumping fluid by compressing an artificial ventricle, while from 1 to 2 seconds represents power imparted to the compression plate by in-flowing fluid and back pressure.

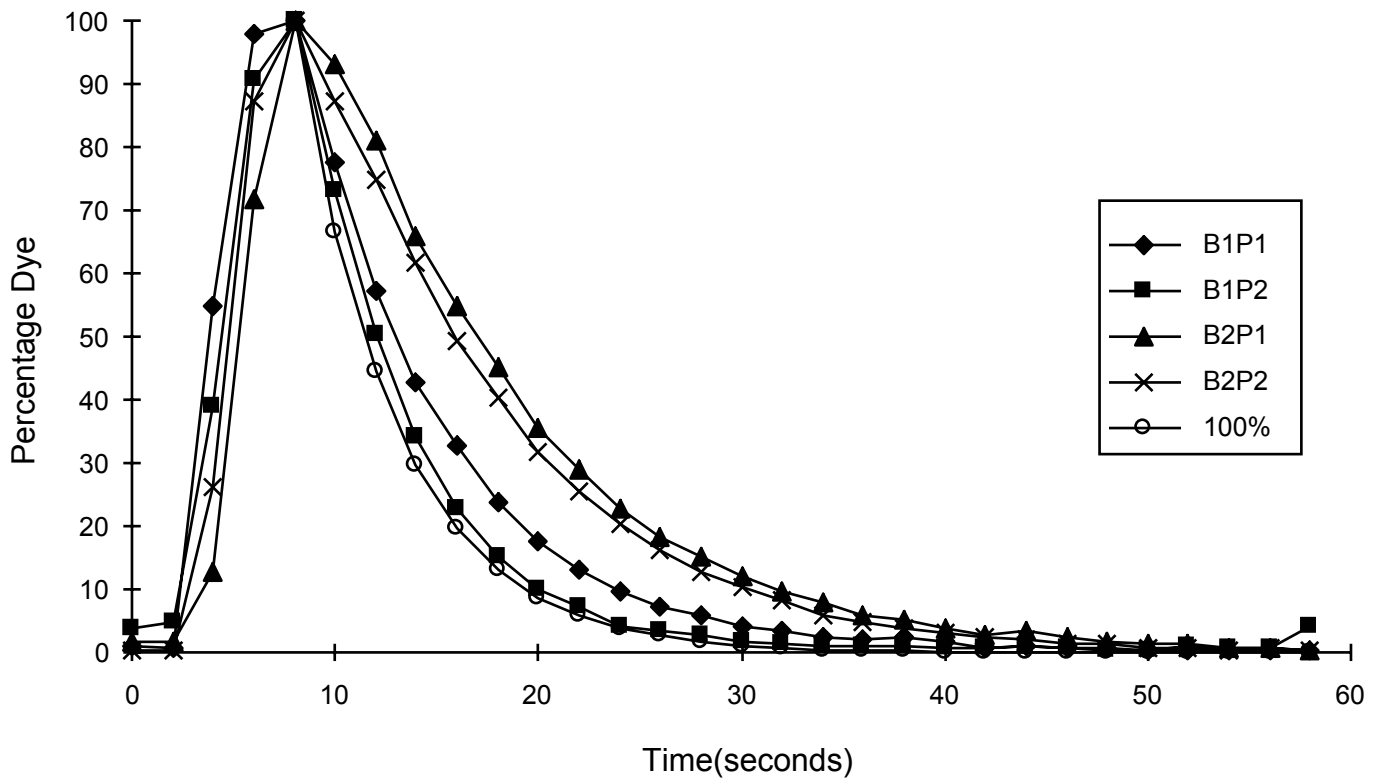


Figure 5.11. Clearance curves for the 4 geometries at a flow rate of 1.0 litres/minute and a 30 bpm pumping rate. The characteristic quick filling of the pumping chambers is evident, followed by a decreasing exponential emptying.

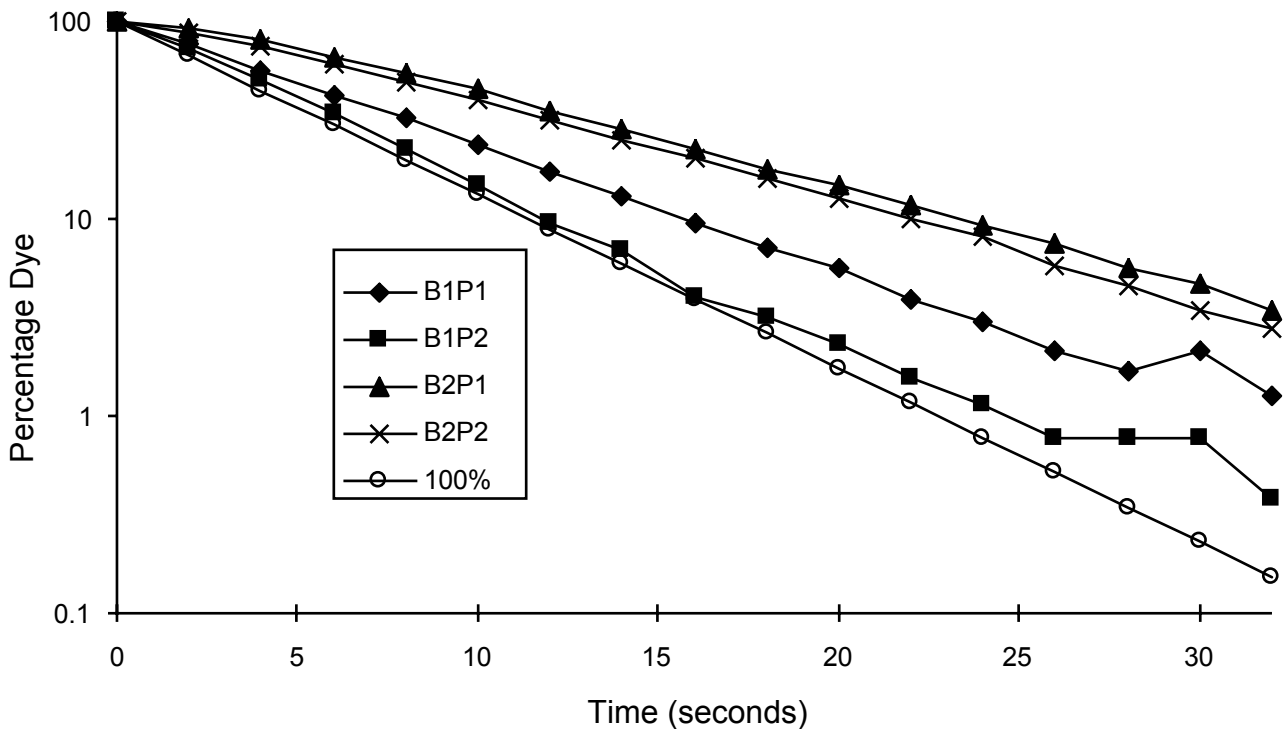


Figure 5.12. Clearance curves for the 4 geometries at a flow rate of 1.0 litres/minute and a 30 bpm pumping rate.

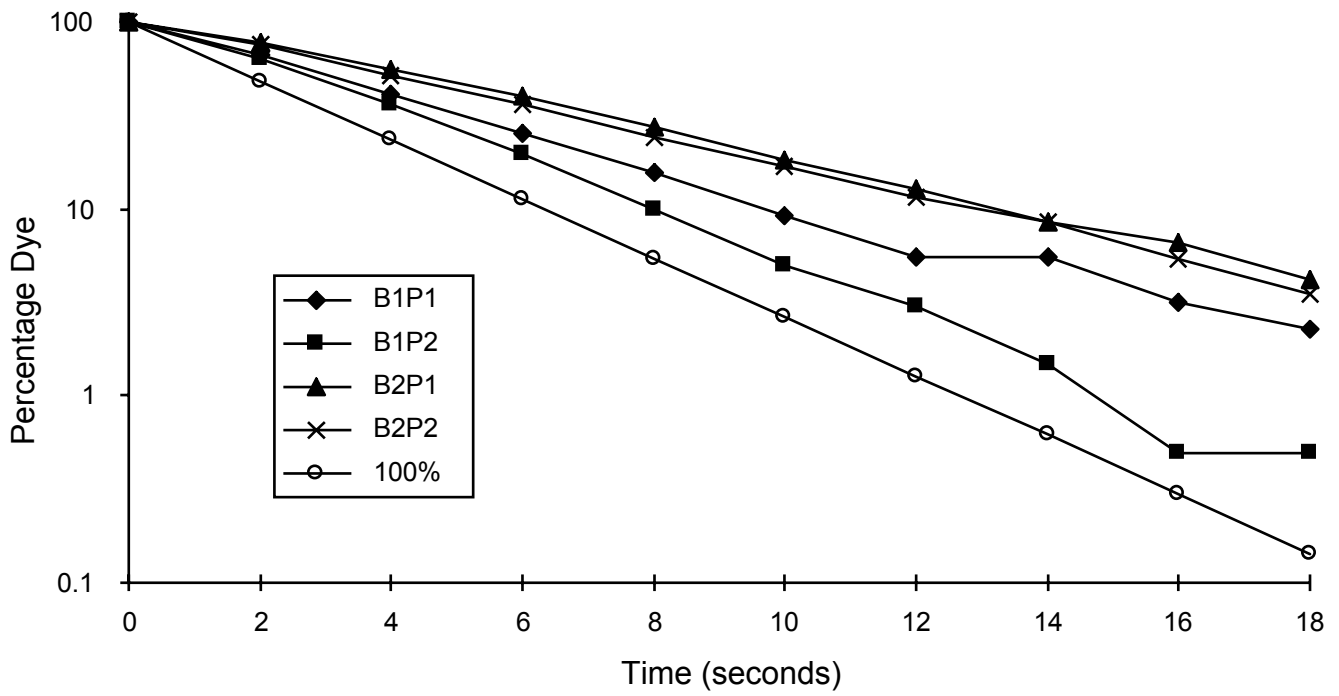


Figure 5.13. Clearance curves for the 4 geometries at a flow rate of 1.55 litres/minute and a 30 bpm pumping rate.

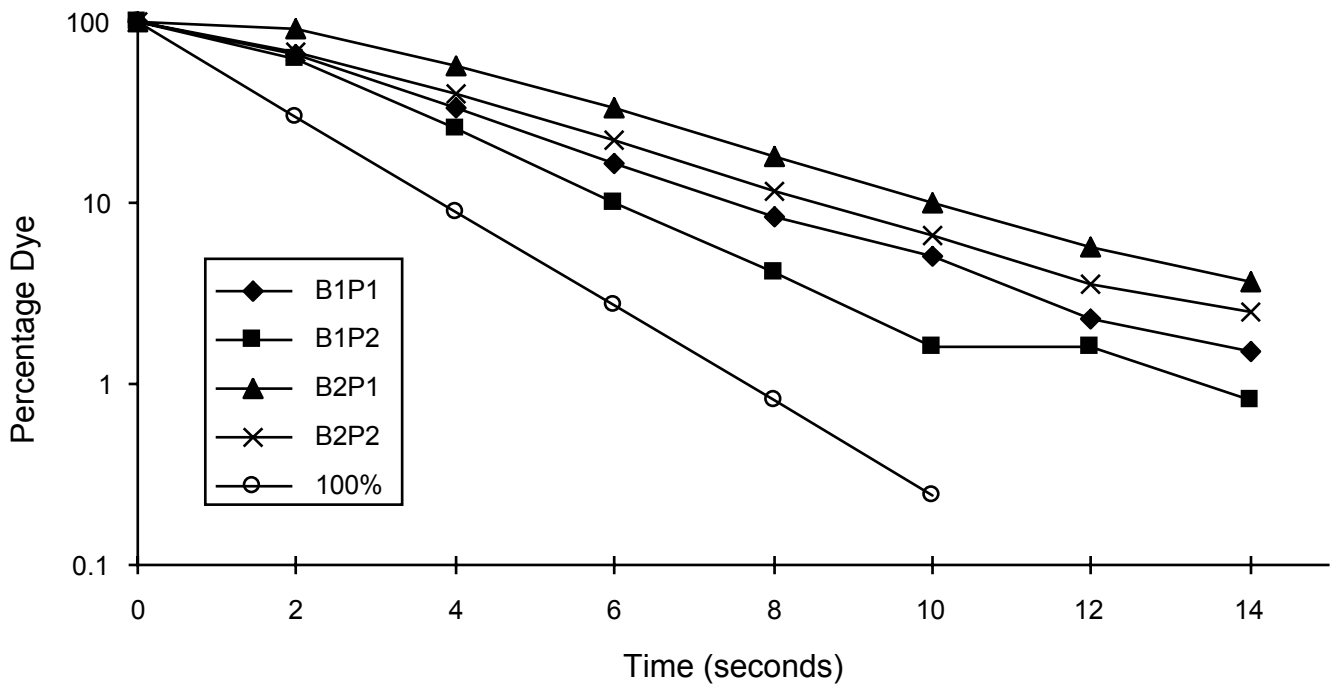


Figure 5.14. Clearance curves, on a log scale, for the 4 geometries at a flow rate of 2.1 litres/minute and a 30 bpm pumping rate.

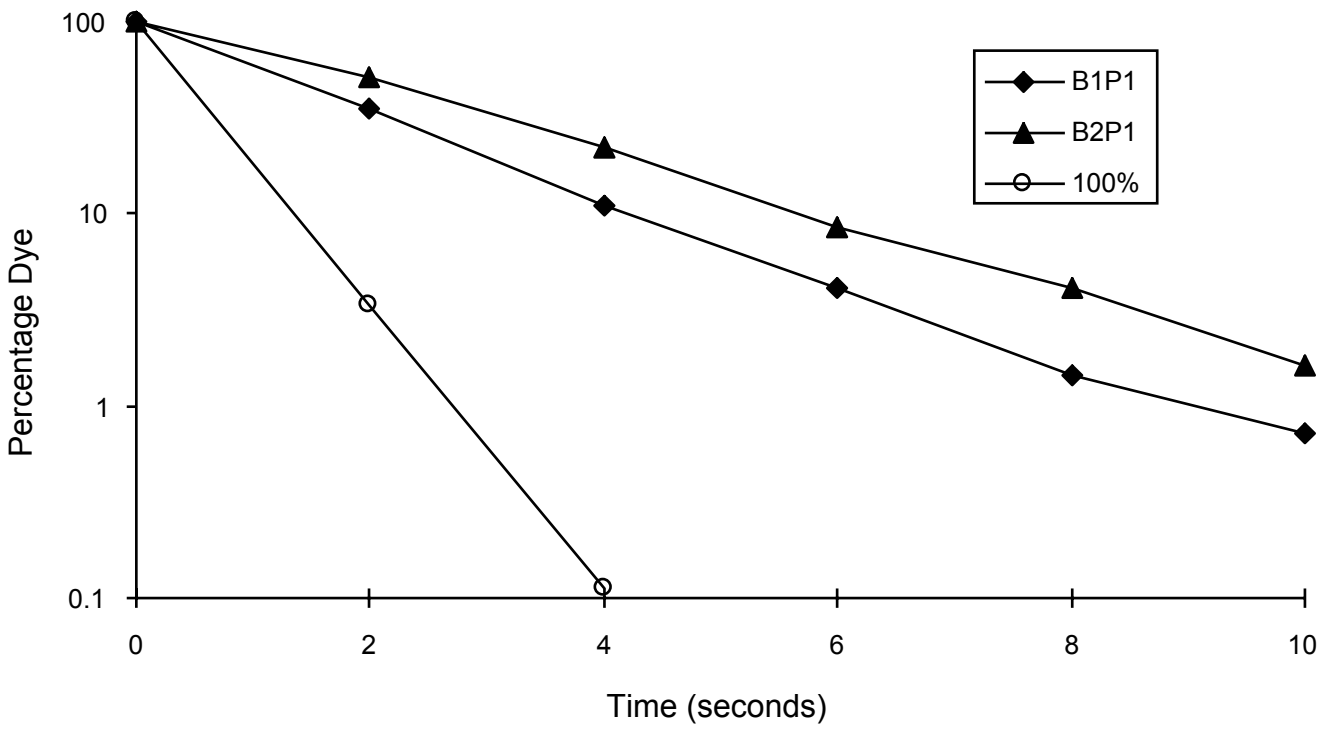


Figure 5.15. Clearance curves for the two P1 geometries at a flow rate of 2.9 litres/minute and a 30 bpm pumping rate.

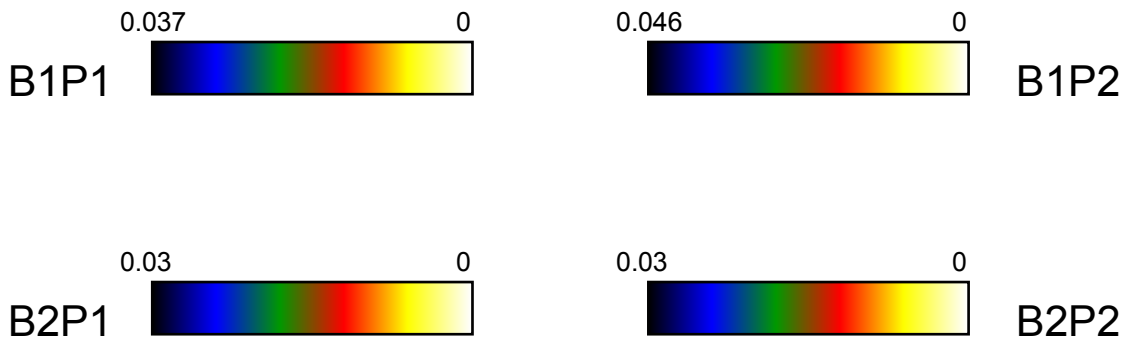
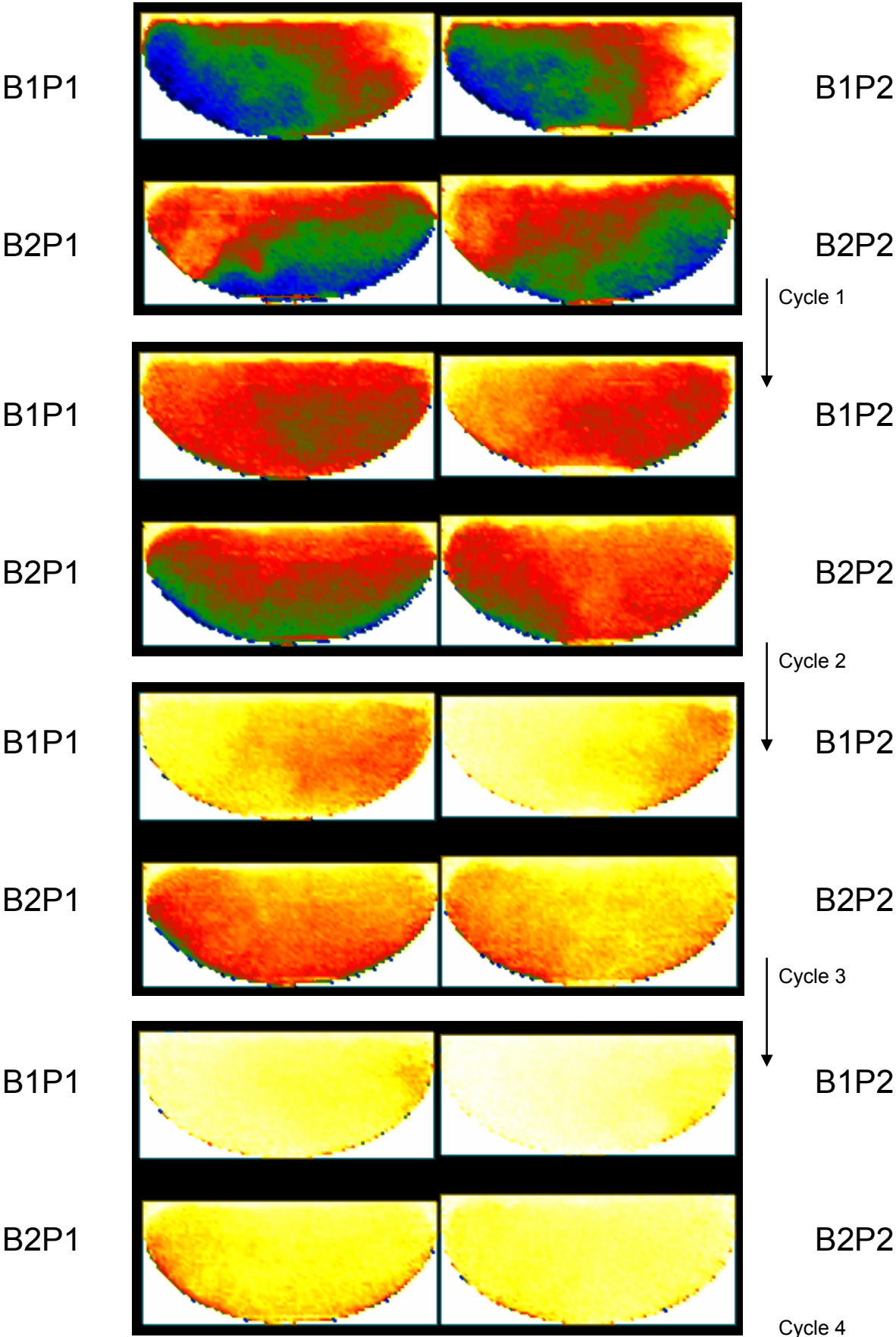


Figure 5.16a. Linear scales of dye concentration (ml of dye / cm³) against colour for the quantitative images for each pumping chamber geometry.

Figure 5.16b. Images of dye concentration, at the instant of maximum pumping chamber volume, over consecutive cycles..



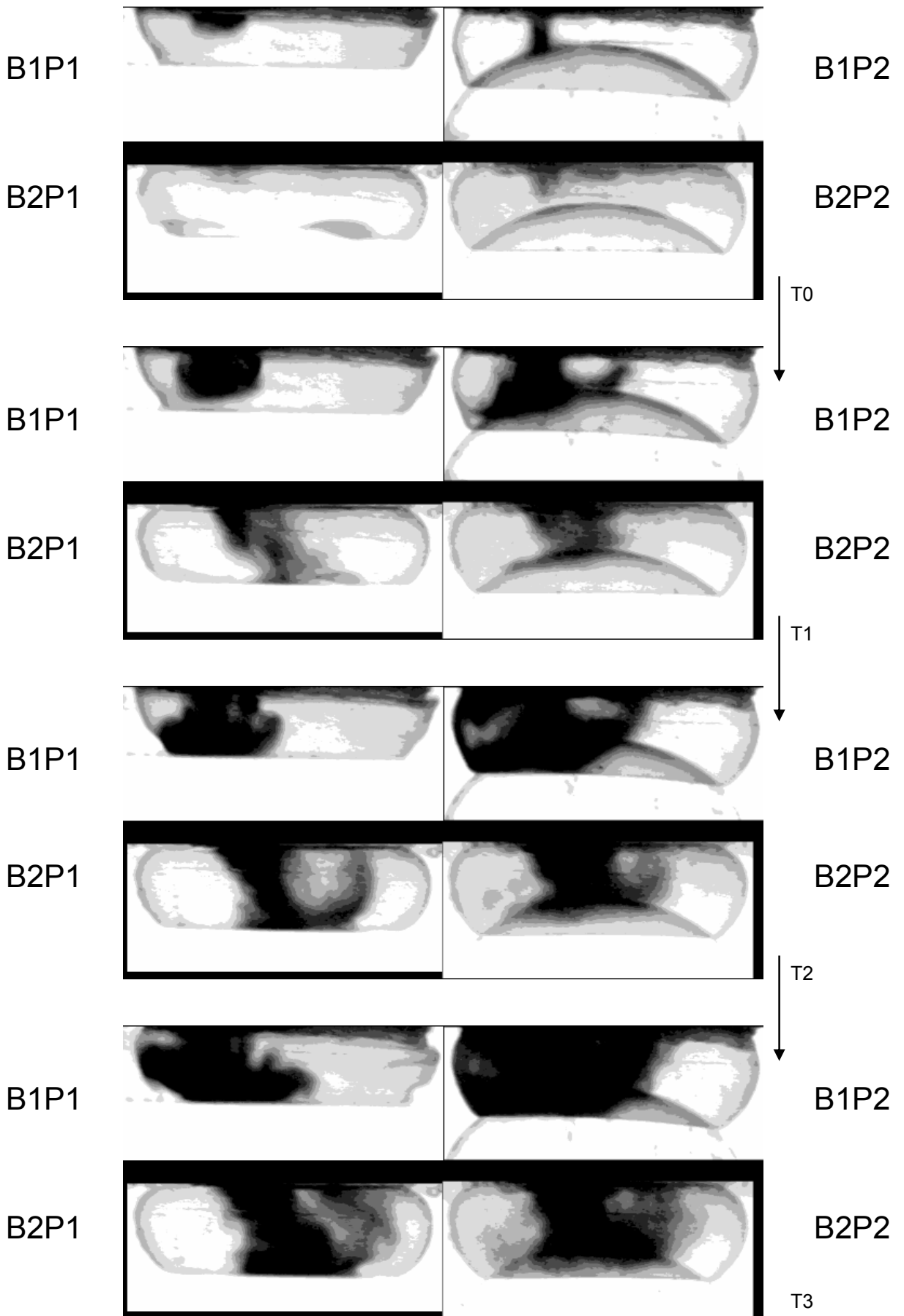


Figure 5.17. Consecutive video images (40 msec exposure) of a dye bolus entering each pumping chamber geometry.

Figure 5.18a. Conveyor belt (Mode a) and 100% mixing (Mode b) clearance curves at 50% ejection fraction.

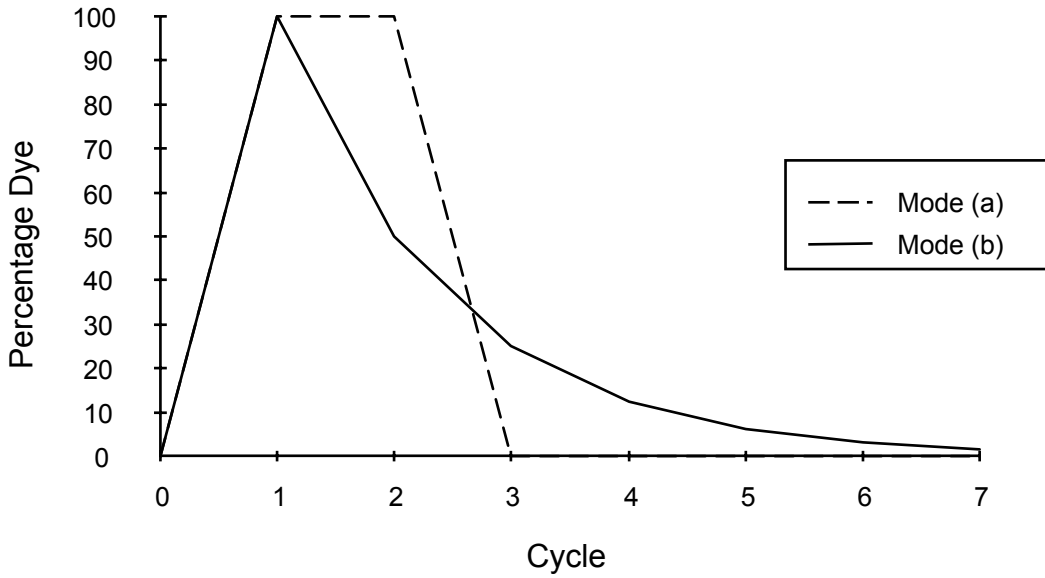


Figure 5.18b. Schematic of the artificial ventricle showing the regions within which apparent ejection fraction is calculated. The %standard deviation, from the mean, of each region's apparent ejection fraction is shown, below the region number (n=5).

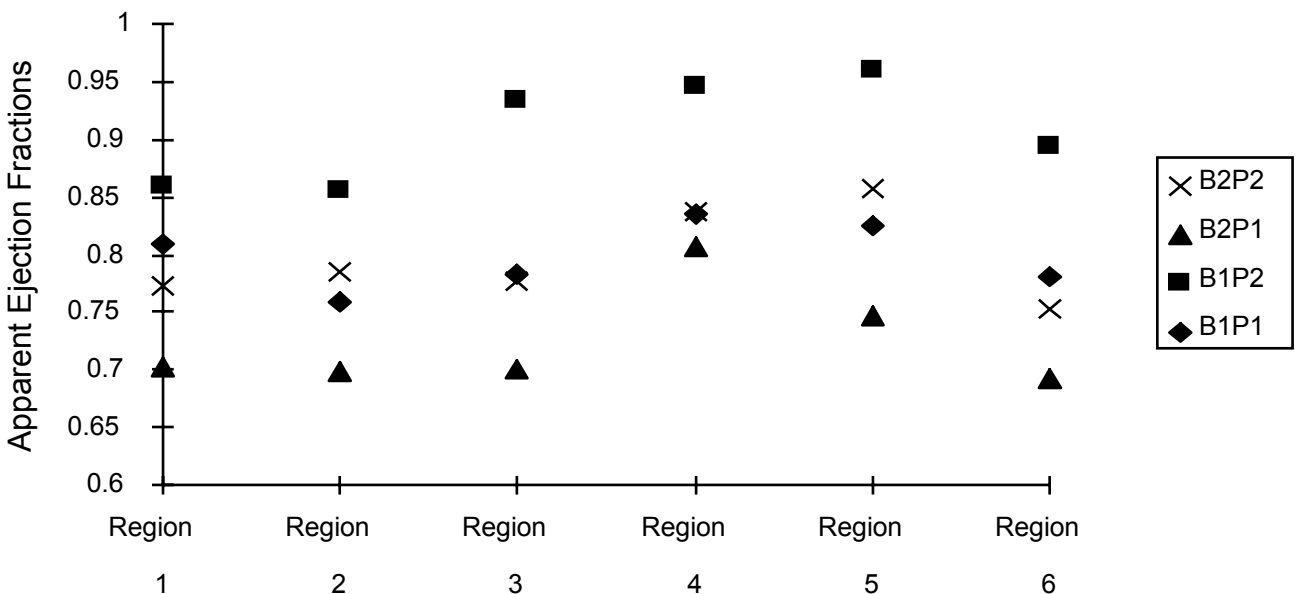
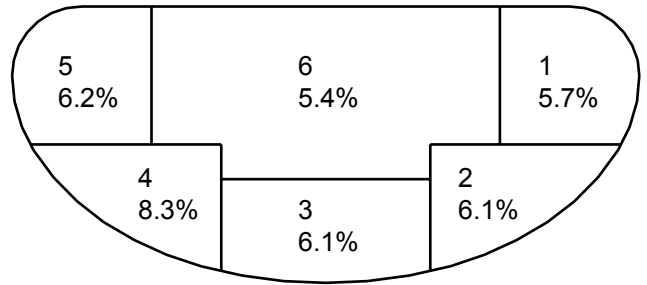


Figure 5.18c. Apparent ejection fractions for each design in six regions, at 2.1 litres/minute. The regions are defined and labeled in the schematic of figure 13b.

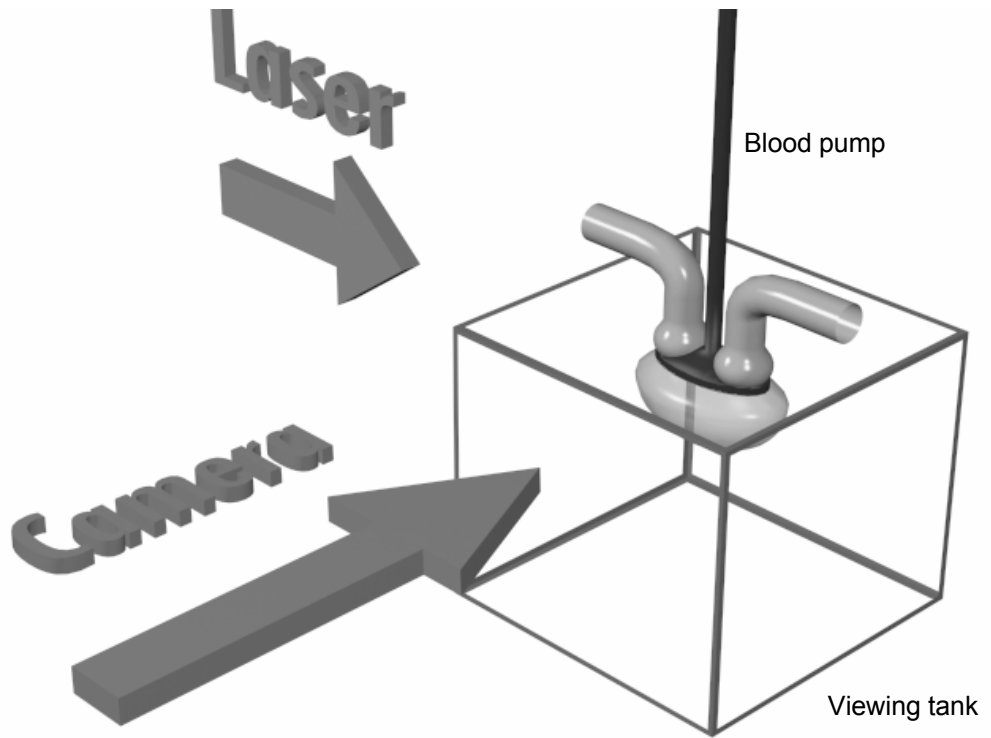
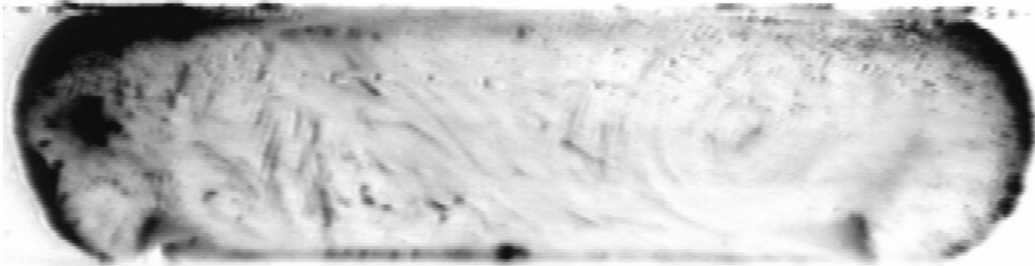


Figure 6.1. Three dimensional image of a proto-type blood pump suspended inside a viewing tank. Laser light is incident perpendicular to the orientation of the camera.

Fluka particles



Fluorescent particles

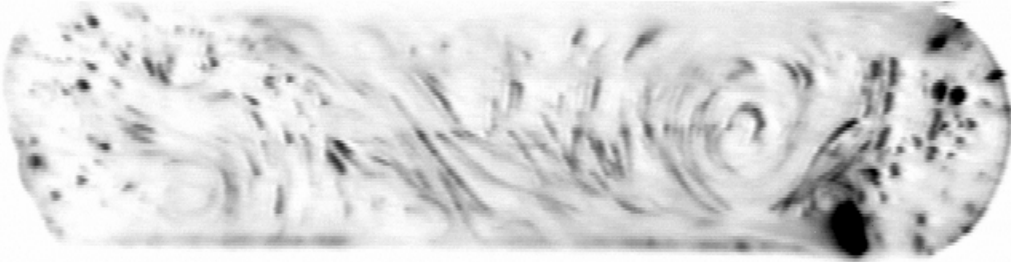
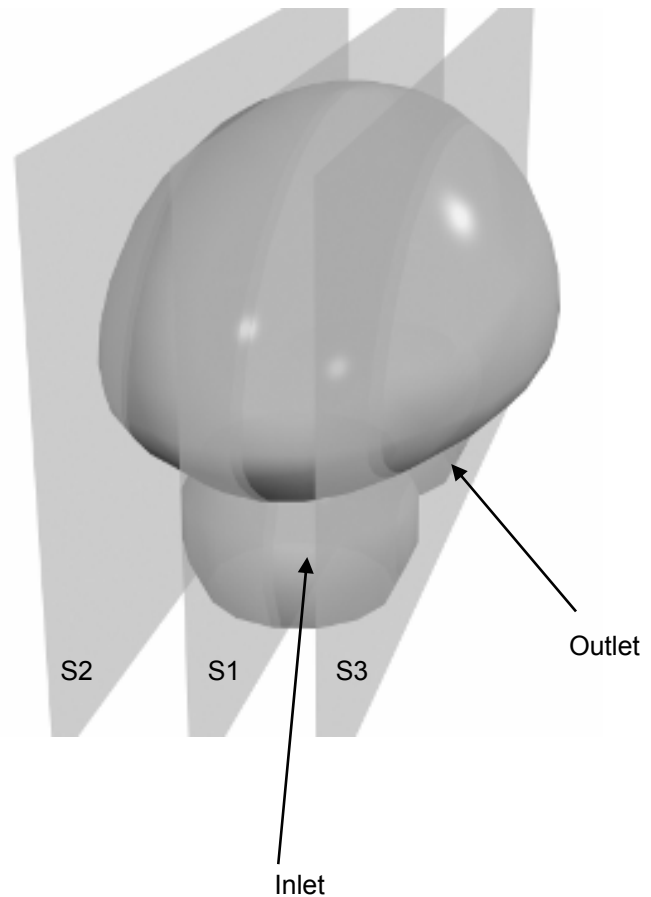
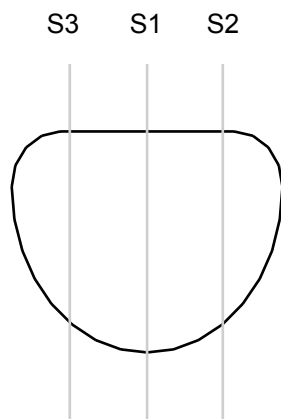


Figure 6.3. Fluid flow inside B2P1 visualized with polystyrene (above) and fluorescent (below) tracer particles, at a flow rate of 2.1 l/min at 30bpm. The fluorescent particles were made in the laboratory. The image grey scales have been reversed, so particle streaks are black rather than white.

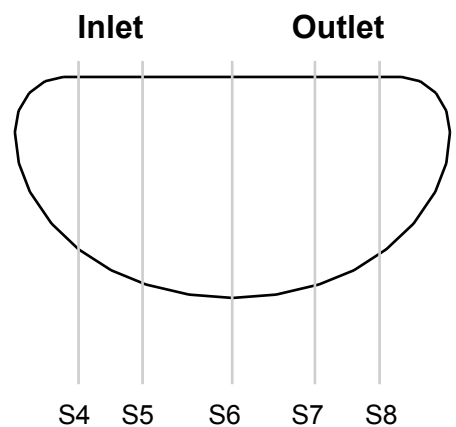
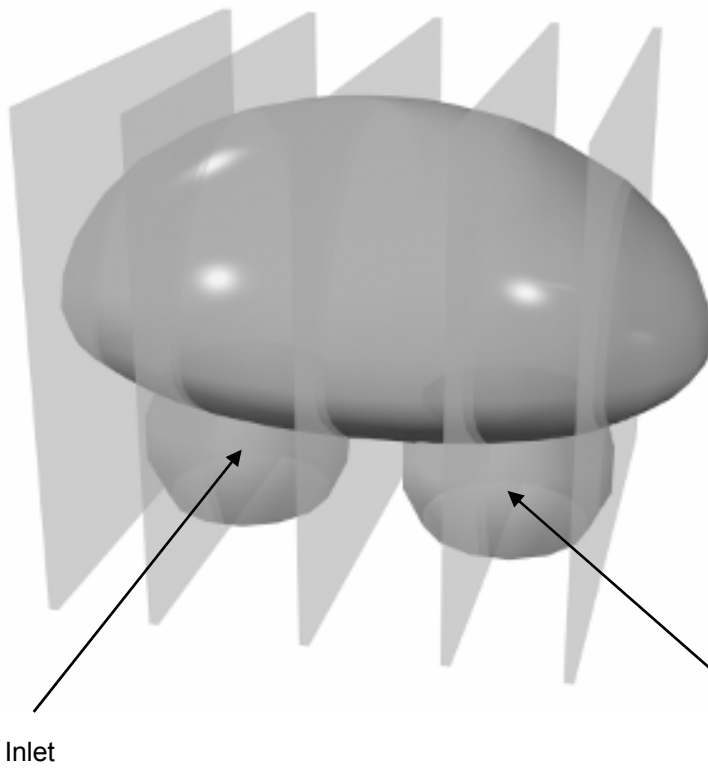
Figure 6.4. The schematics of two views of the ventricles show the positions of the sections (S1, 2.. 8) as viewed in figures 6.6, 6.7, 6.8 and 6.9. (a) The 3 two-dimensional sections in which fluid flow is studied parallel to the long axis of the ventricle, selected with laser light sheets S1, S2 and S3. (b) The 5 two-dimensional sections in which fluid flow is studied, selected with laser light sheets S4, S5, S6, S7 and S8.

(a)



(b)

S4 S5 S6 S7 S8



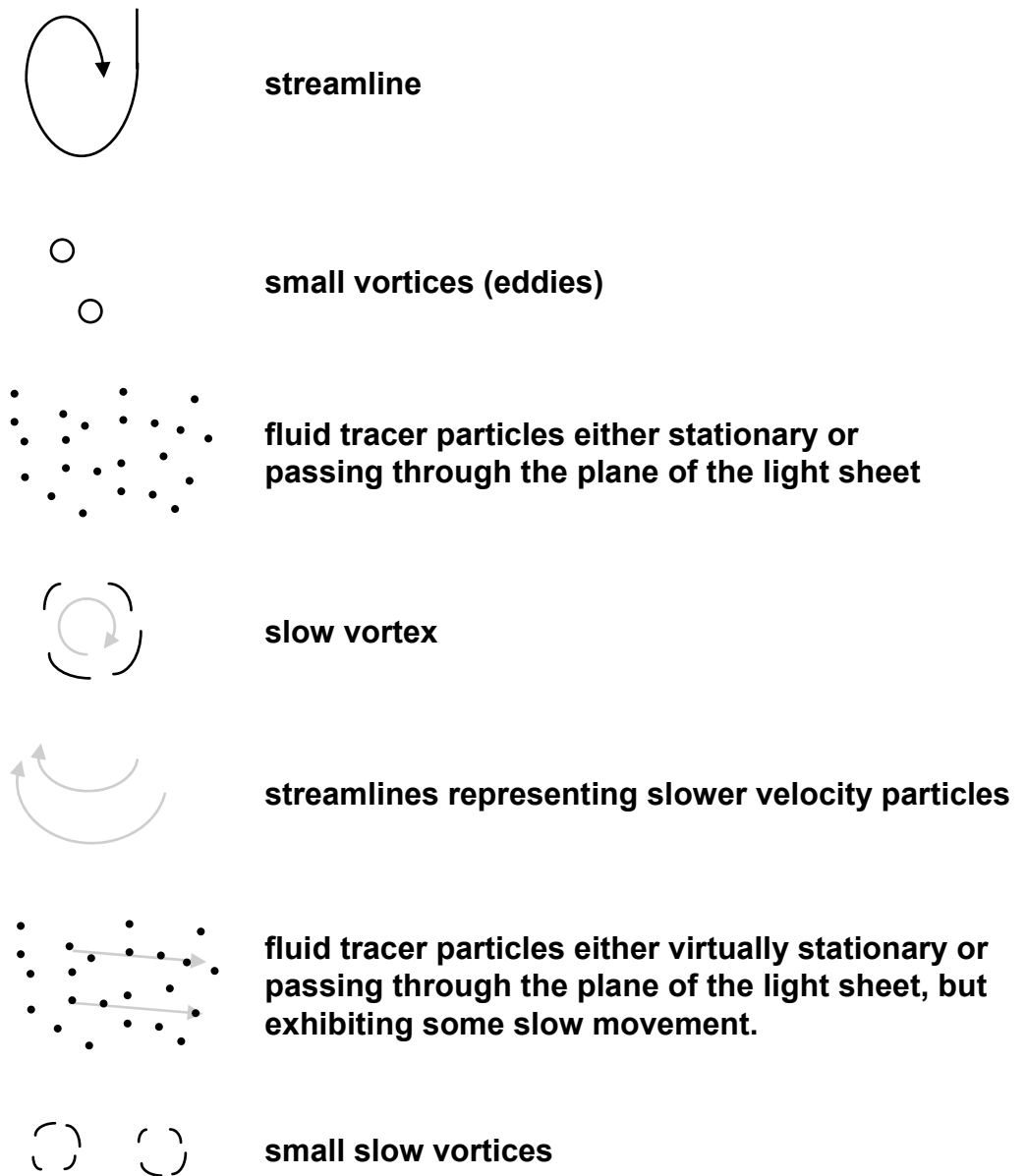


Figure 6.5. Key to flow pattern symbols used for figures 6.6, 6.7, 6.8 and 6.9.

Figure 6.6. Fluid flow in B1P1 (a) at frame 10, (b) at frame 16, (c) at frame 24 and (d) at frame 40.

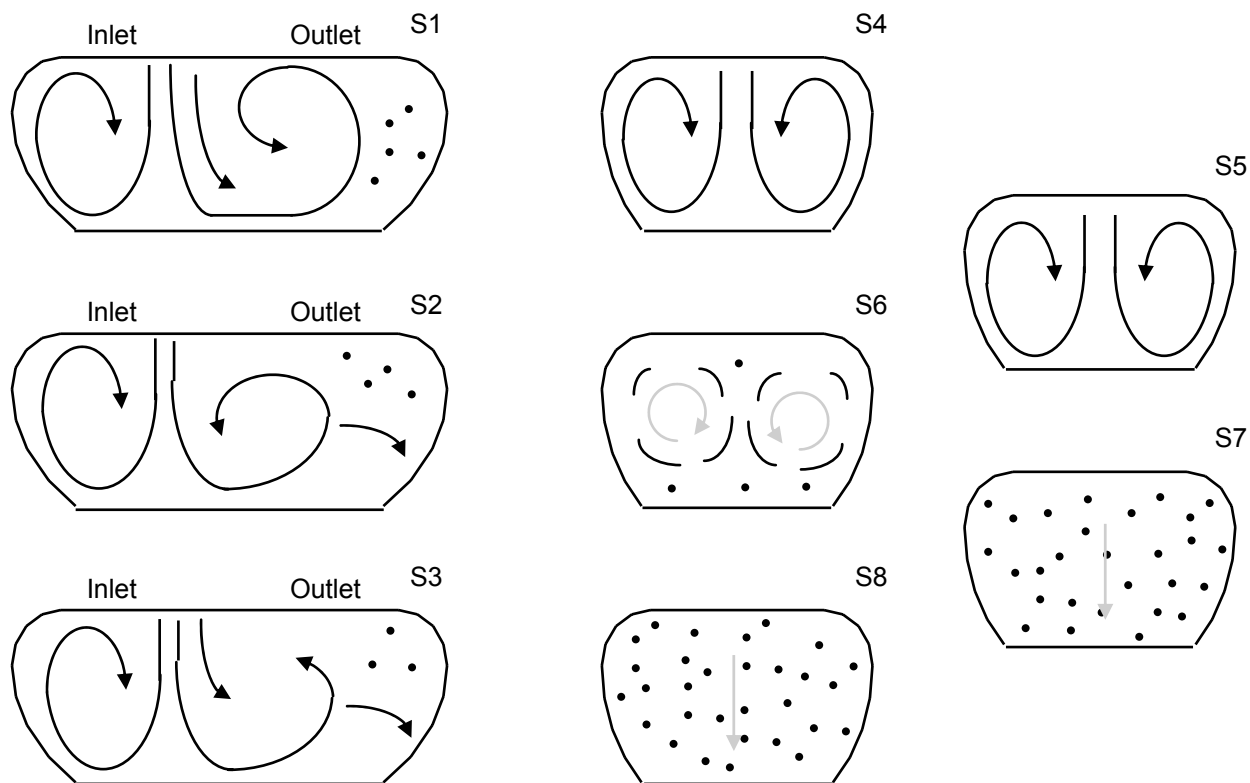


Figure 6.6a.

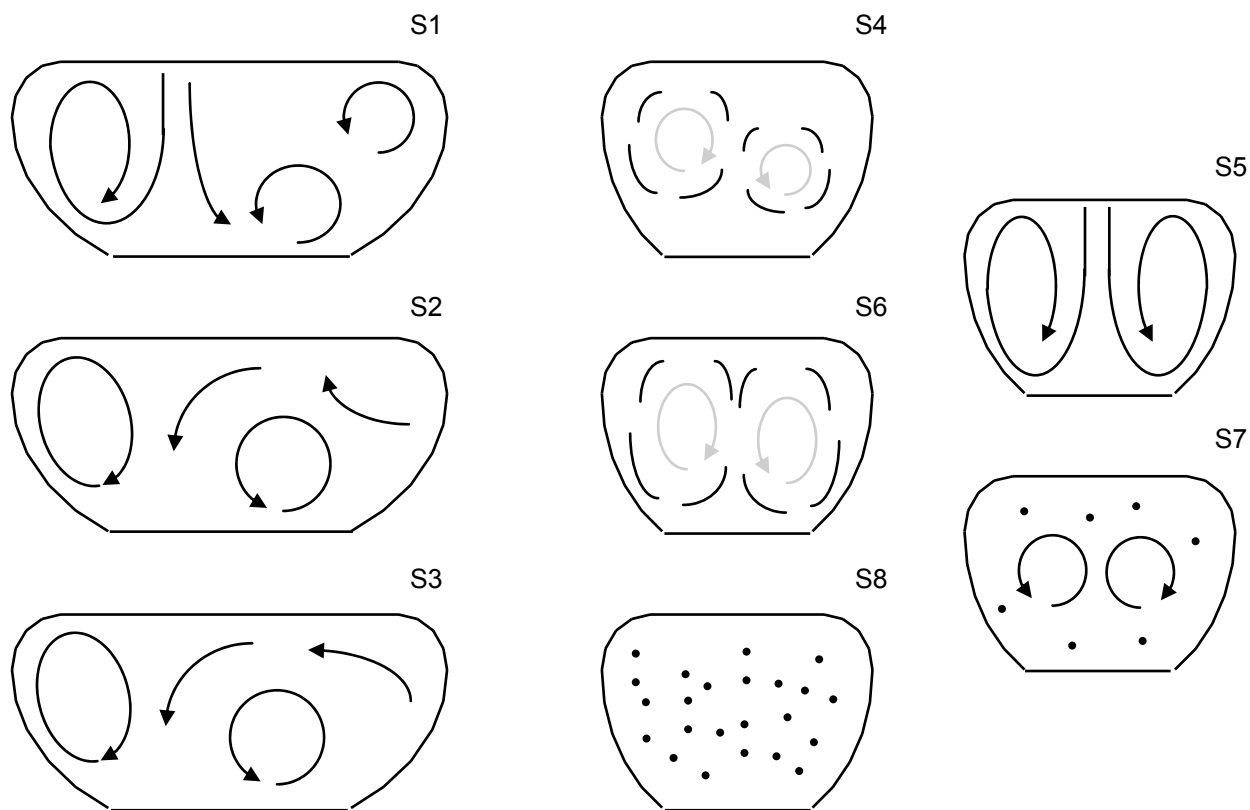


Figure 6.6b.

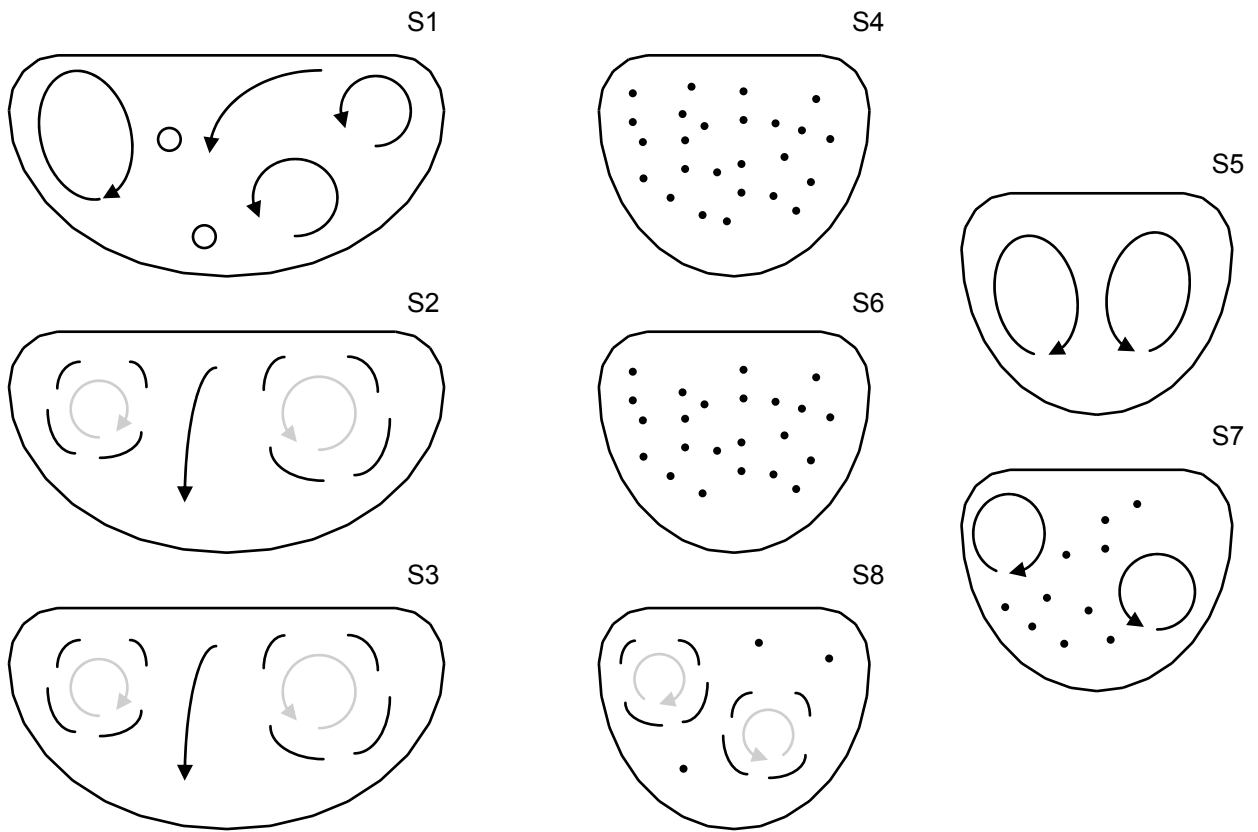


Figure 6.6c.

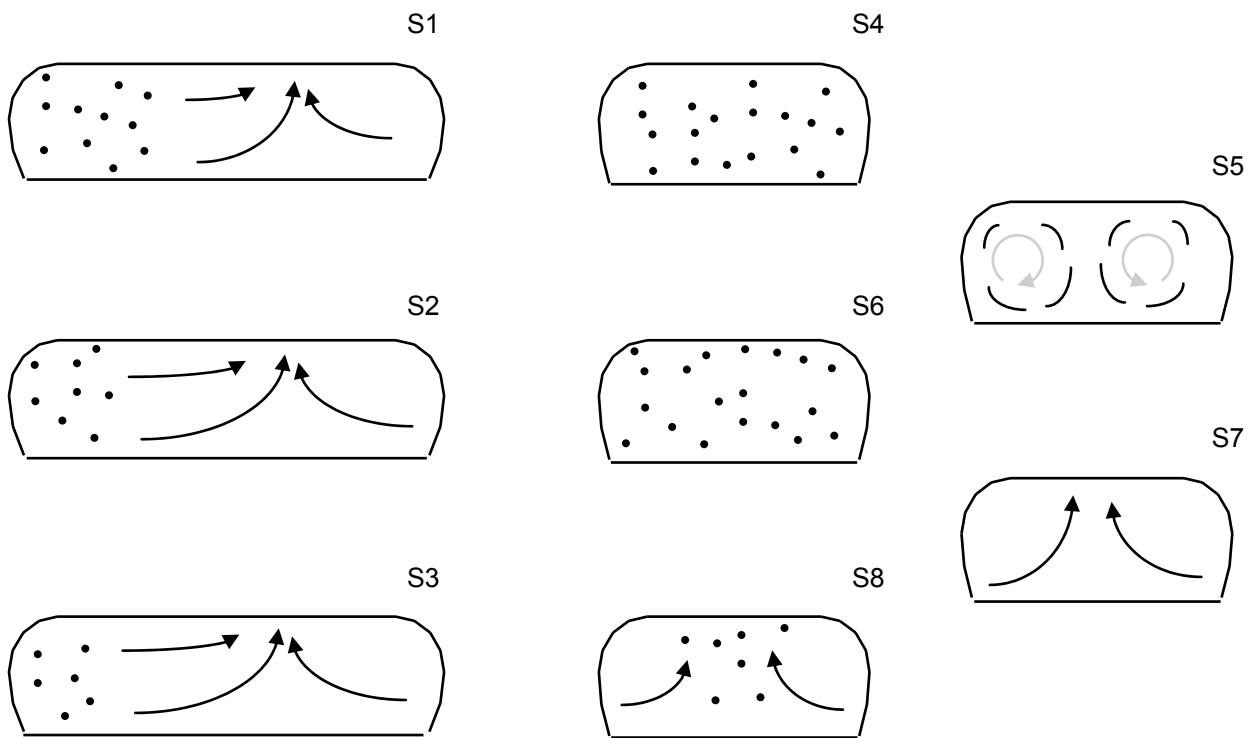


Figure 6.6d.

Figure 6.7. Fluid flow in B1P2 (a) at frame 10, (b) at frame 16, (c) at frame 24 and (d) at frame 40.

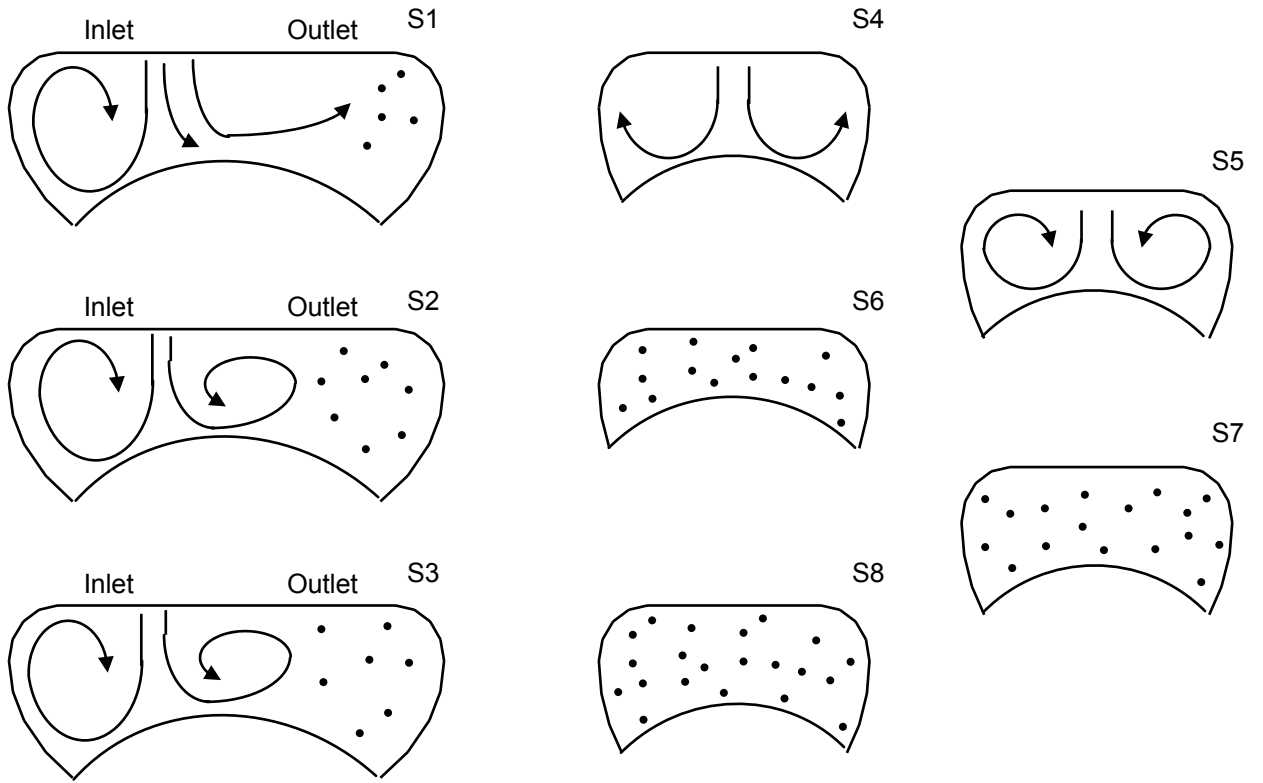


Figure 6.7a.

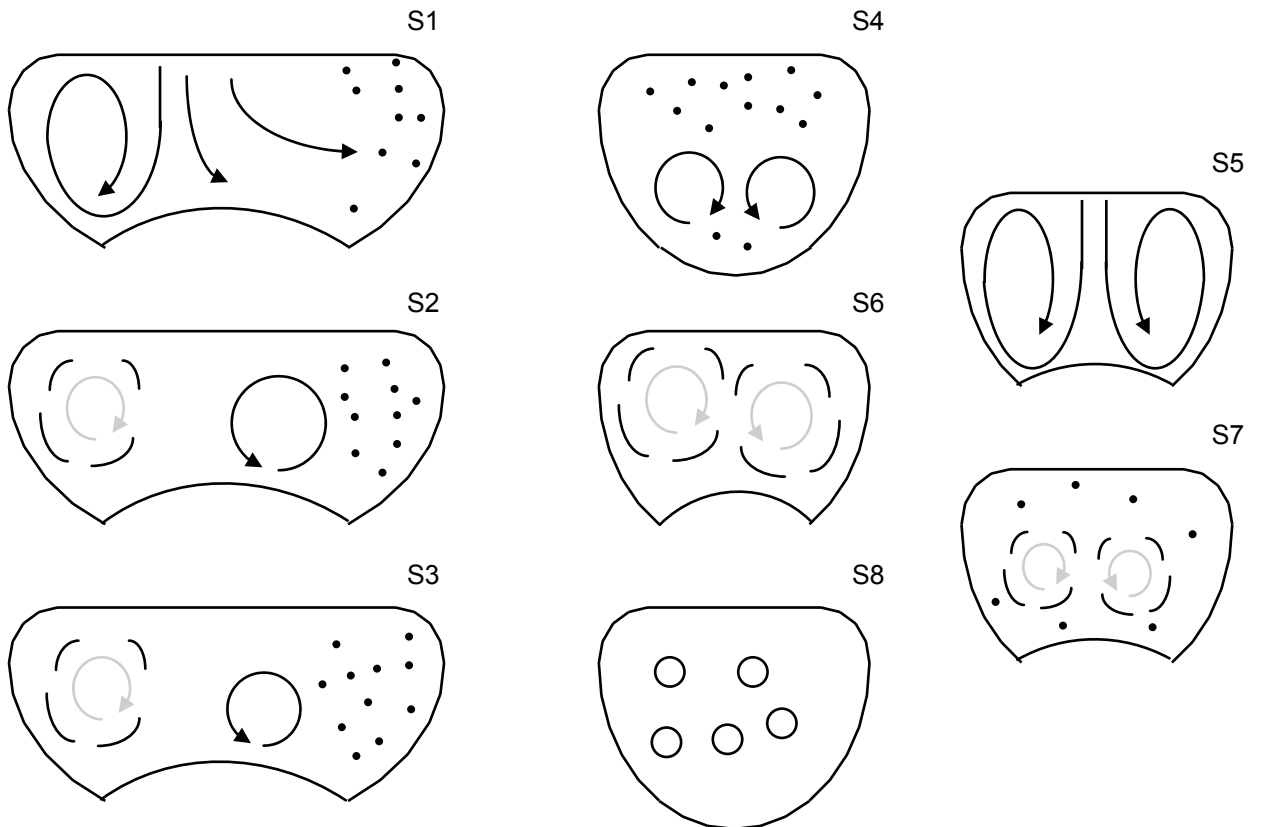


Figure 6.7b.

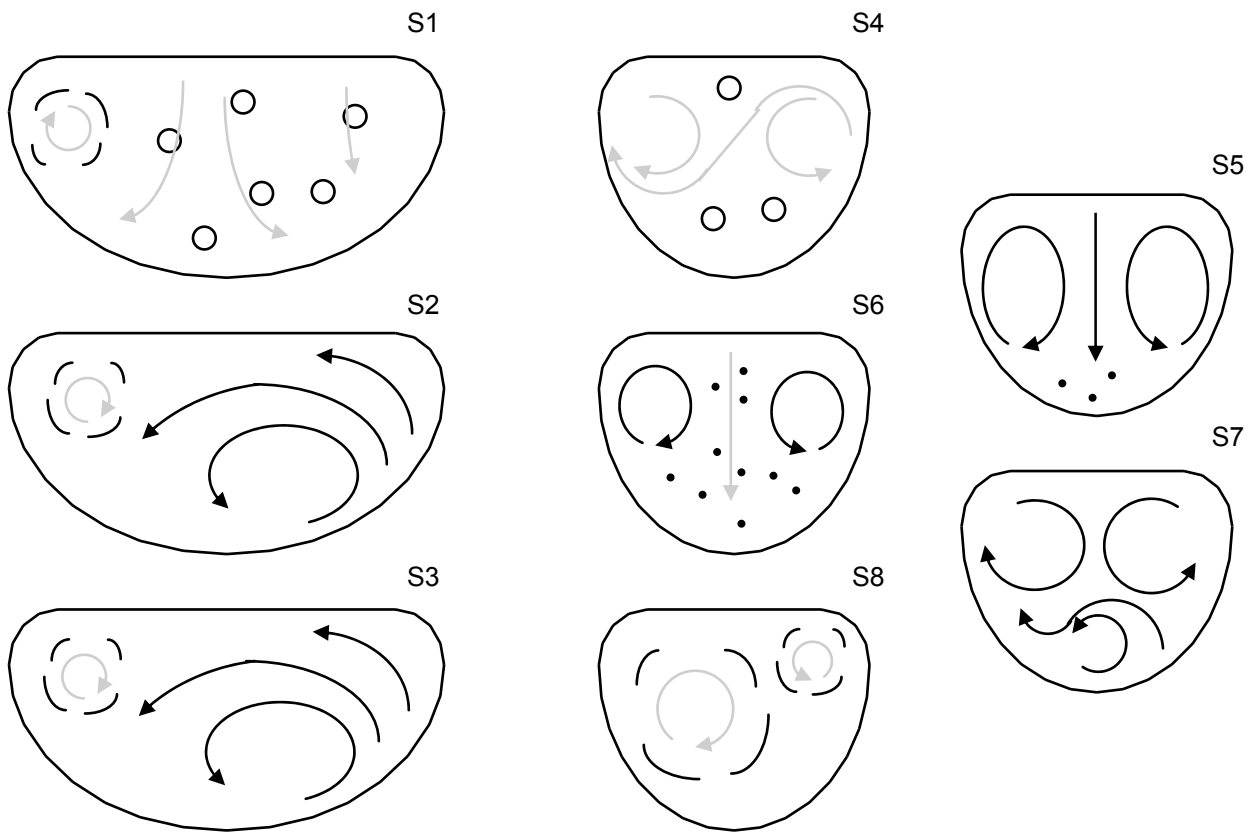


Figure 6.7c.

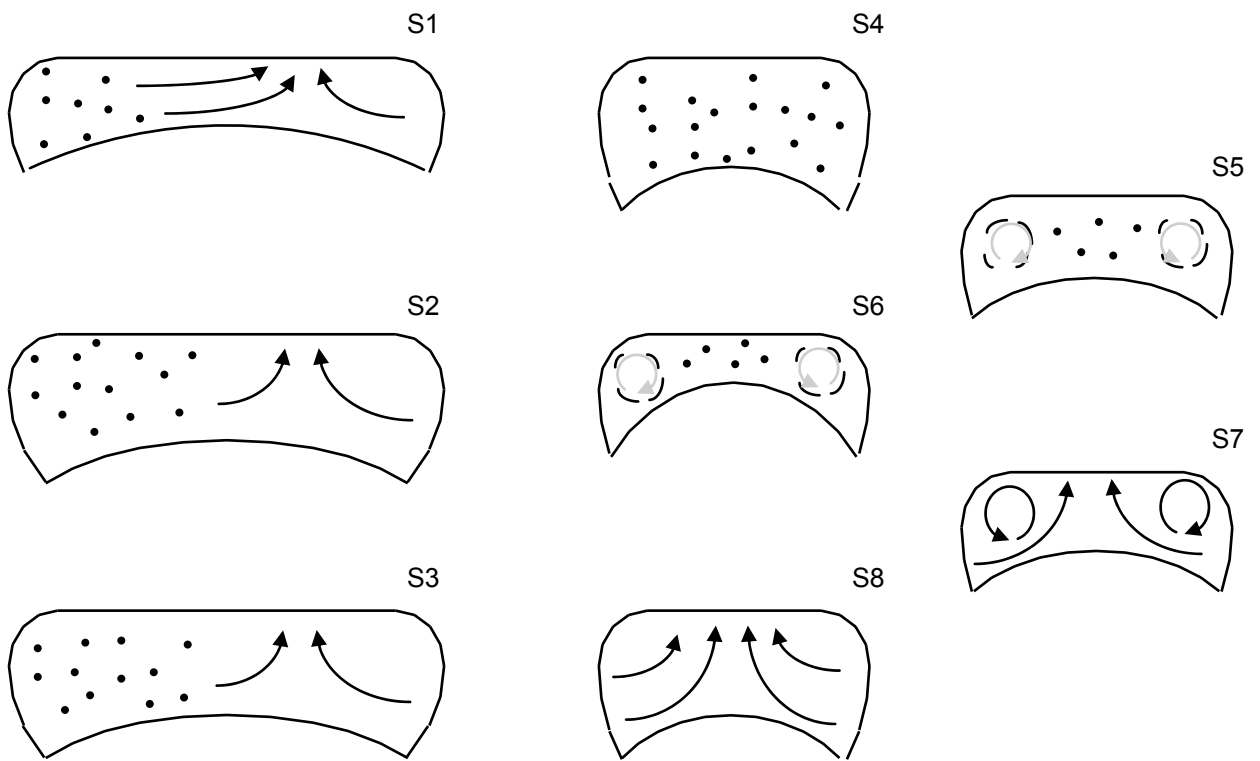


Figure 6.7d.

Figure 6.8. Fluid flow in B2P1 (a) at frame 10, (b) at frame 16, (c) at frame 24 and (d) at frame 40.

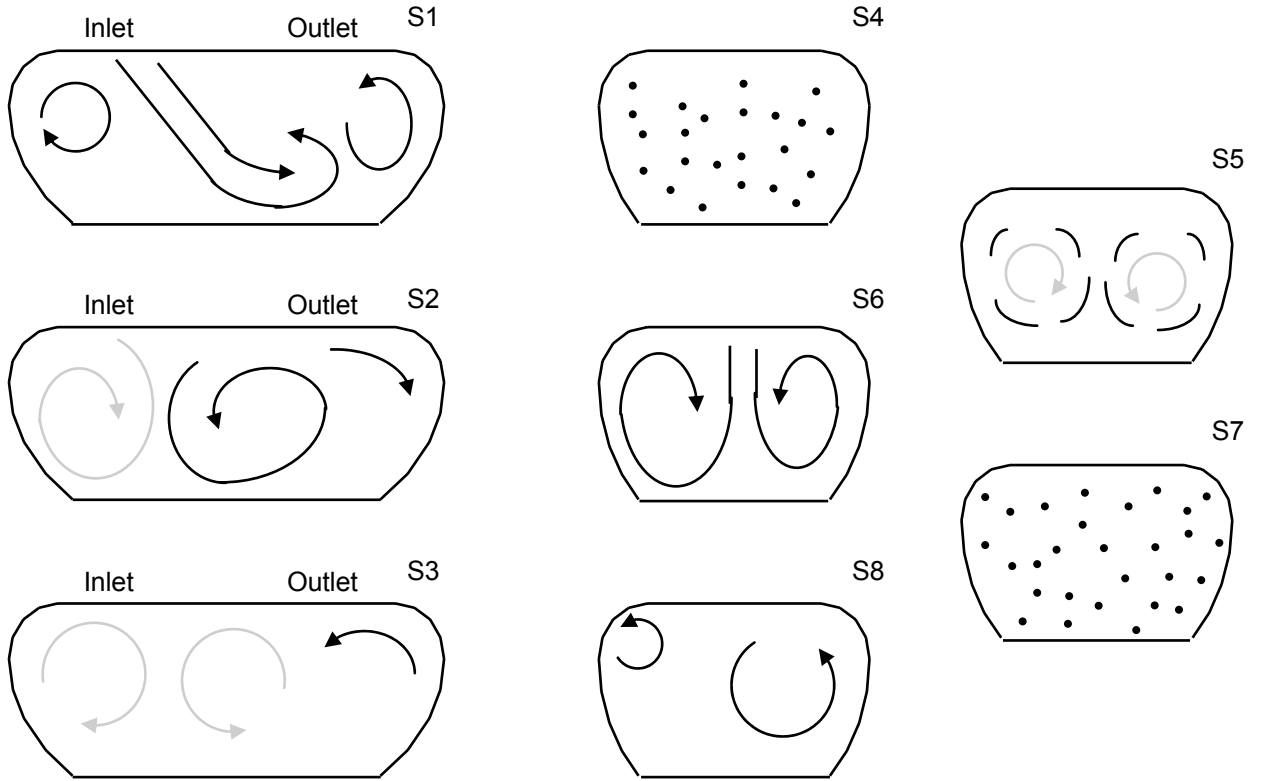


Figure 6.8a.

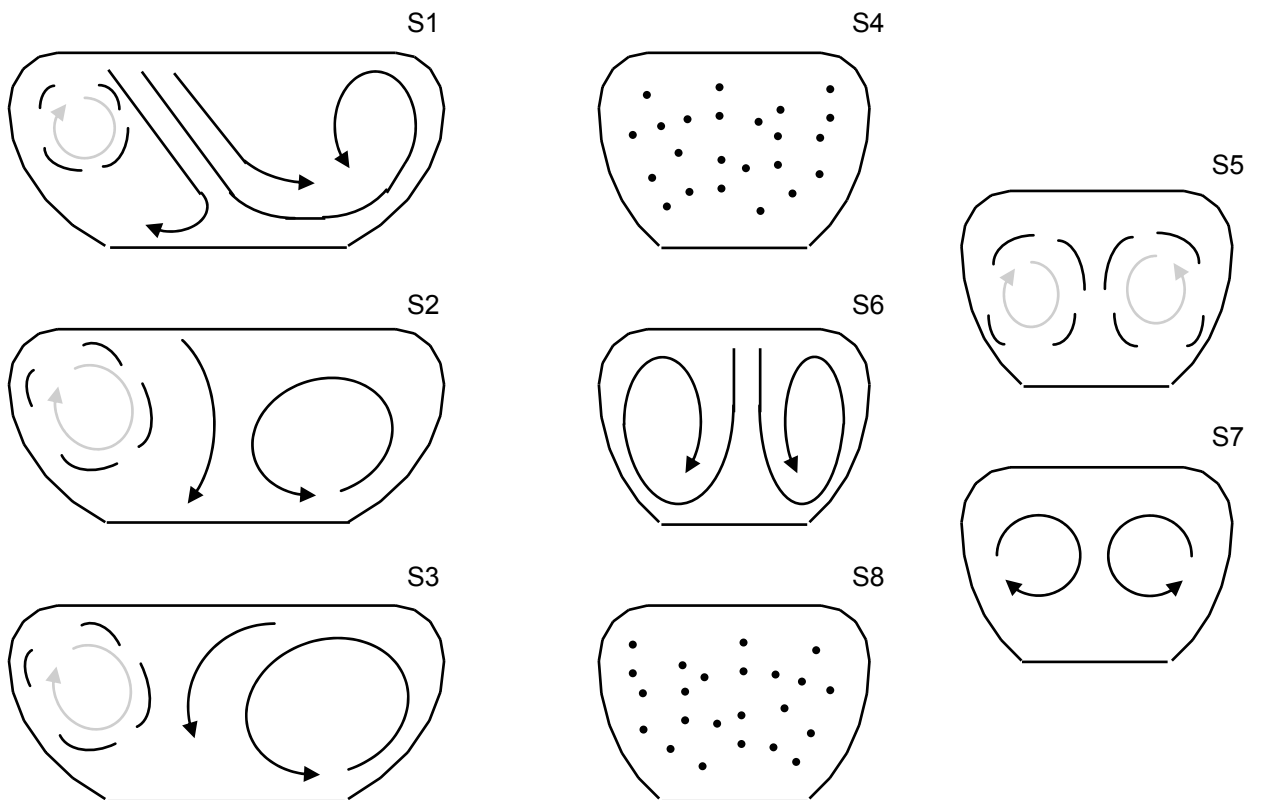


Figure 6.8b.

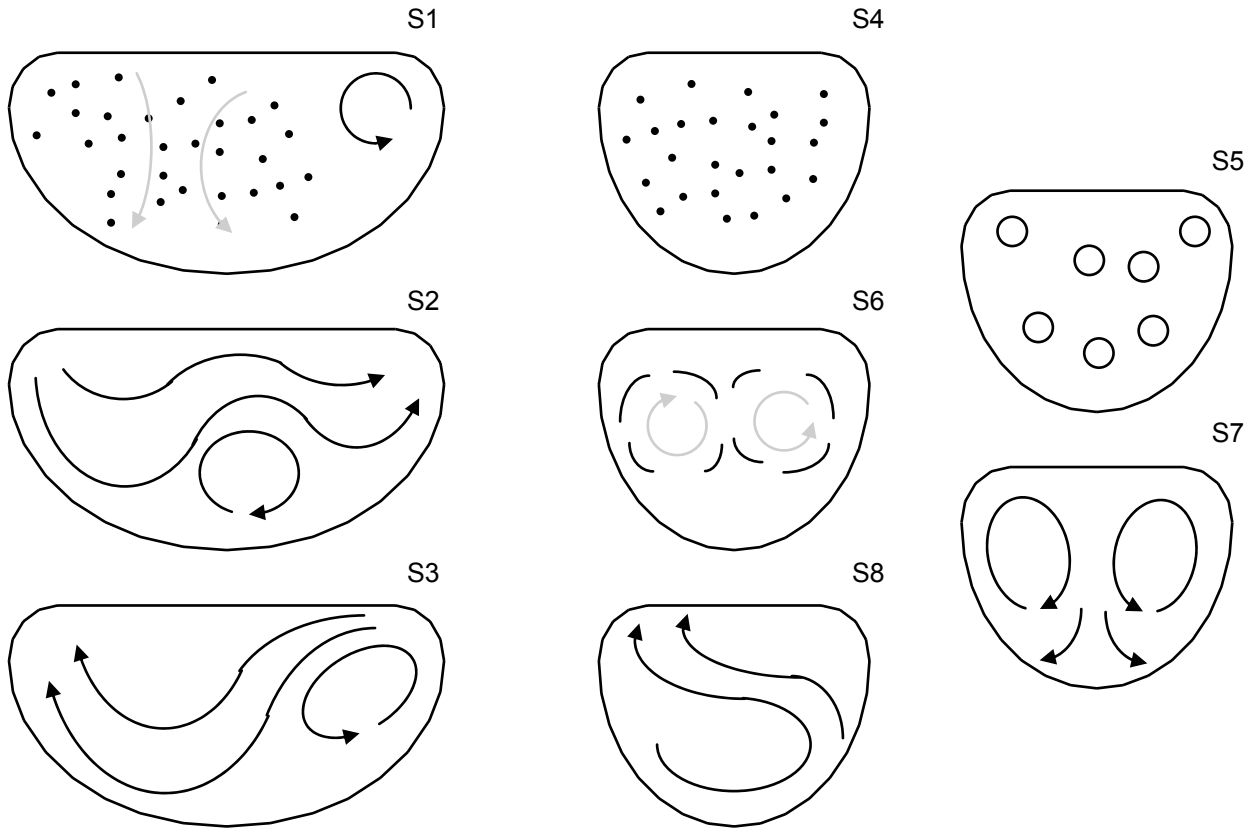


Figure 6.8c.

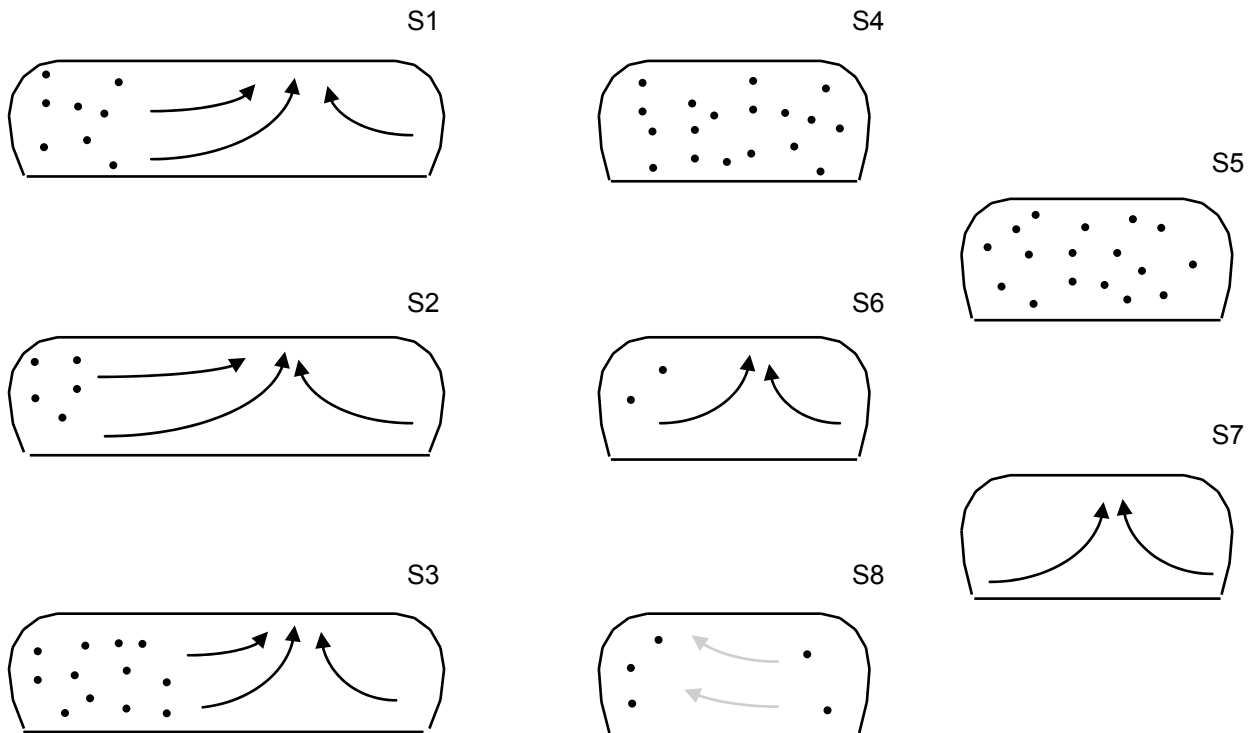


Figure 6.8d.

Figure 6.9. Fluid flow in B2P2 (a) at frame 10, (b) at frame 16, (c) at frame 24 and (d) at frame 40.

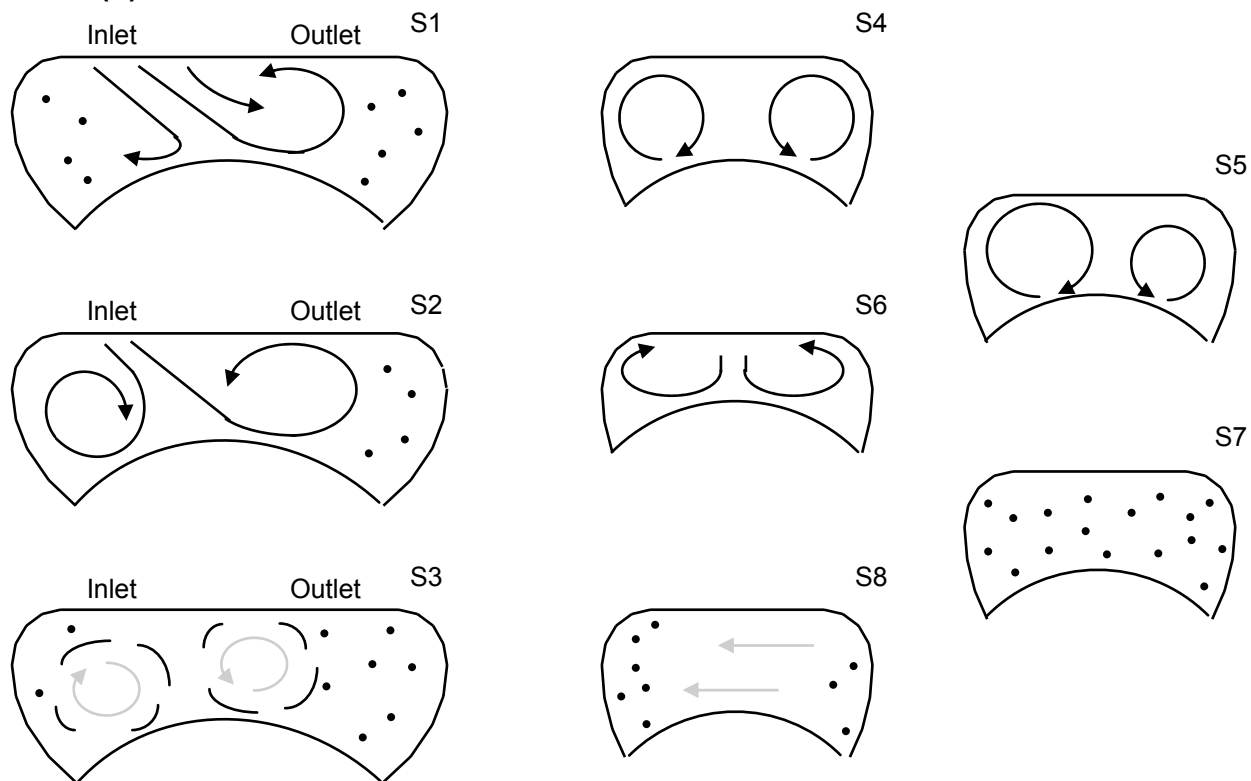


Figure 6.9a.

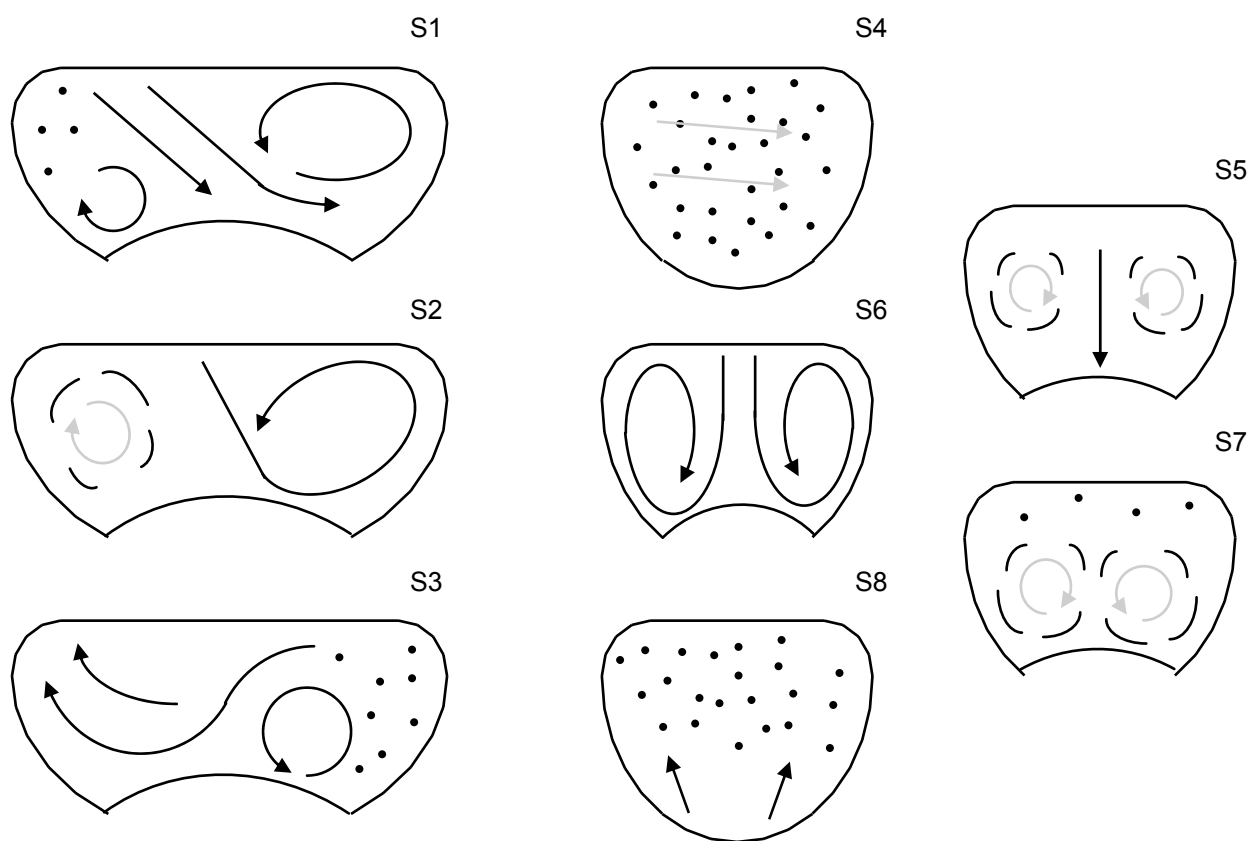


Figure 6.9b.

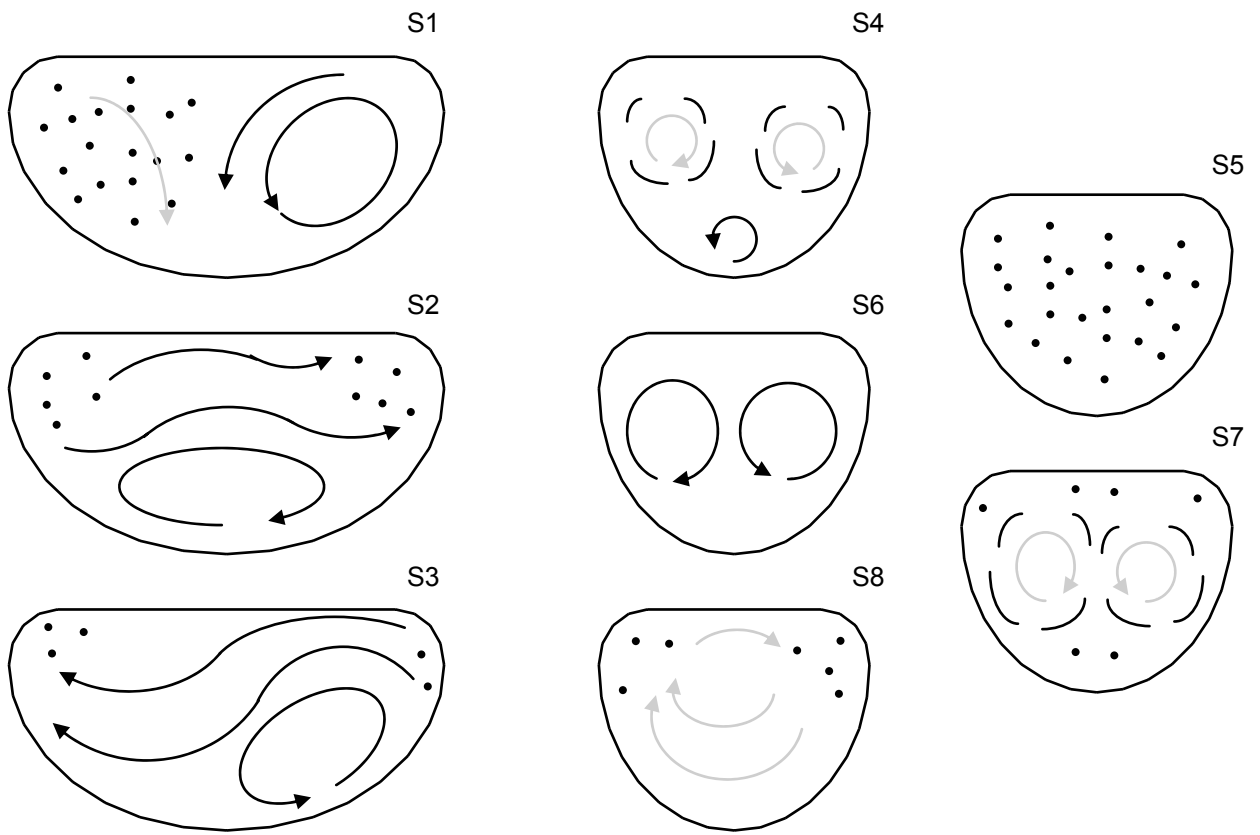


Figure 6.9c.

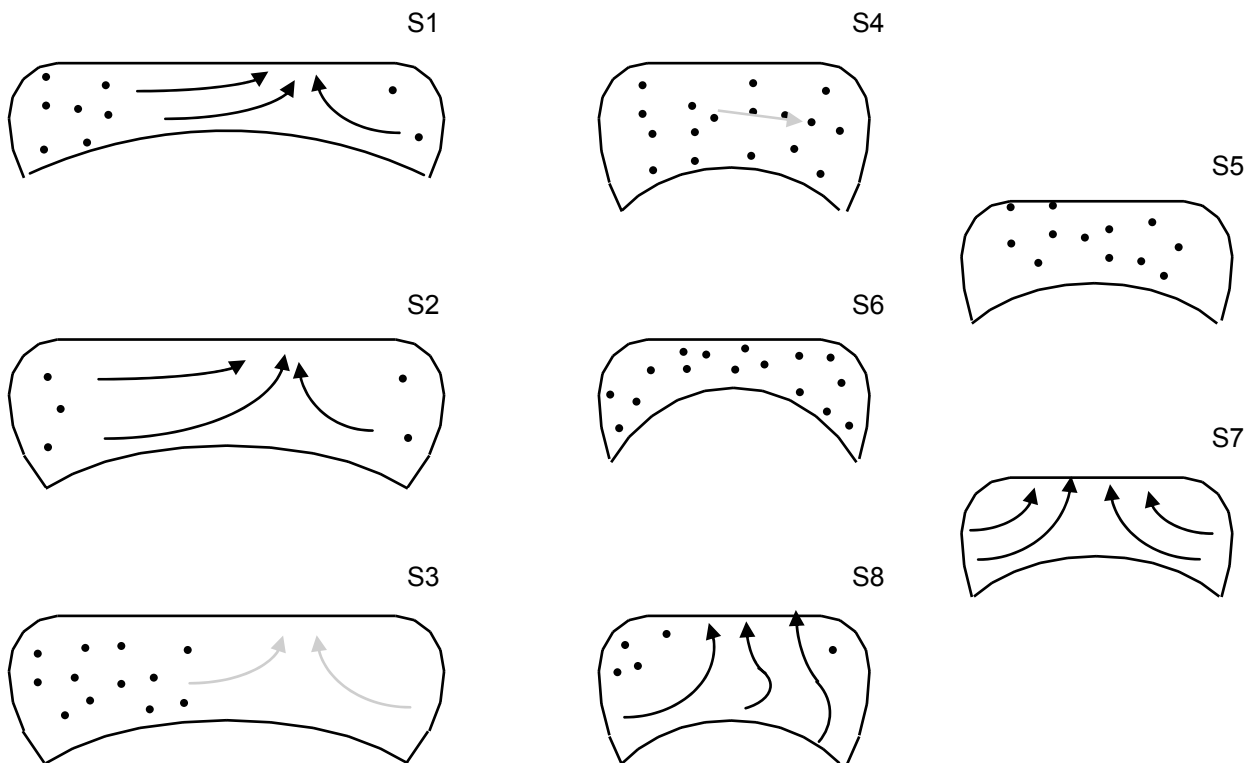


Figure 6.9d.

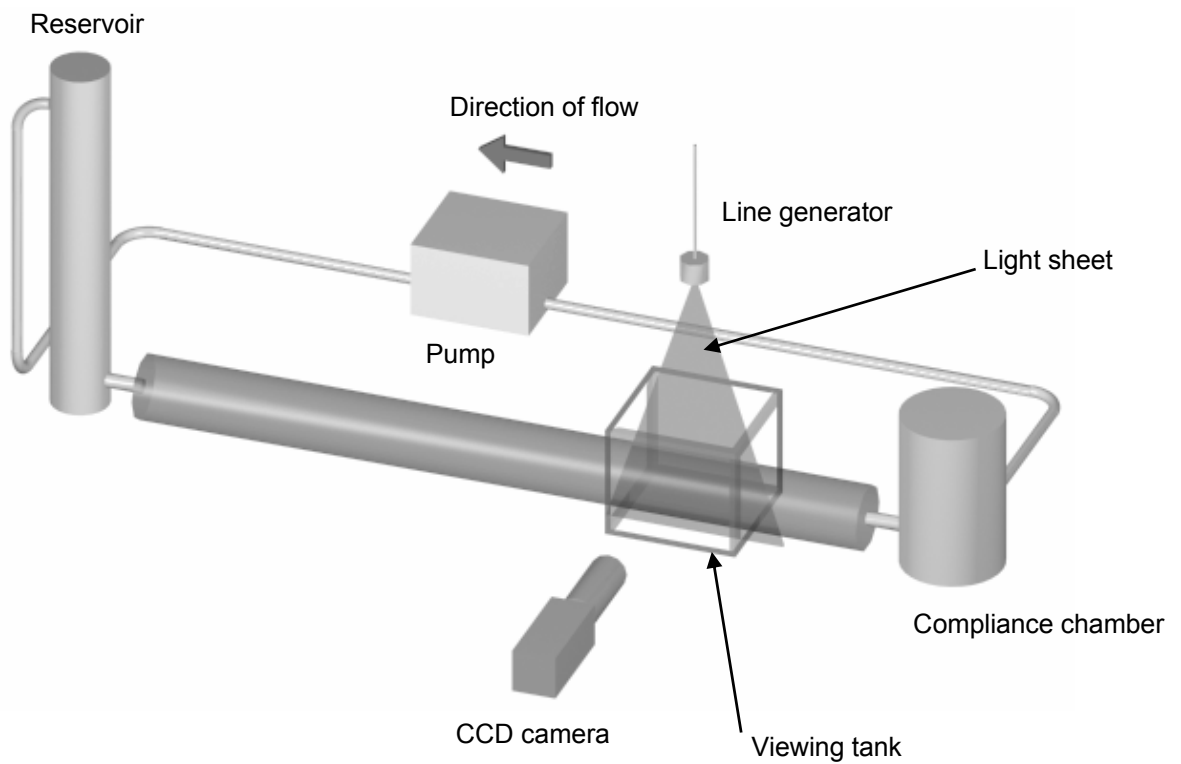


Figure 7.1. Rendered solid model of the experimental flow circuit for producing developed laminar flow in a cylindrical pipe, and capturing illuminated fluid tracer particles on video.

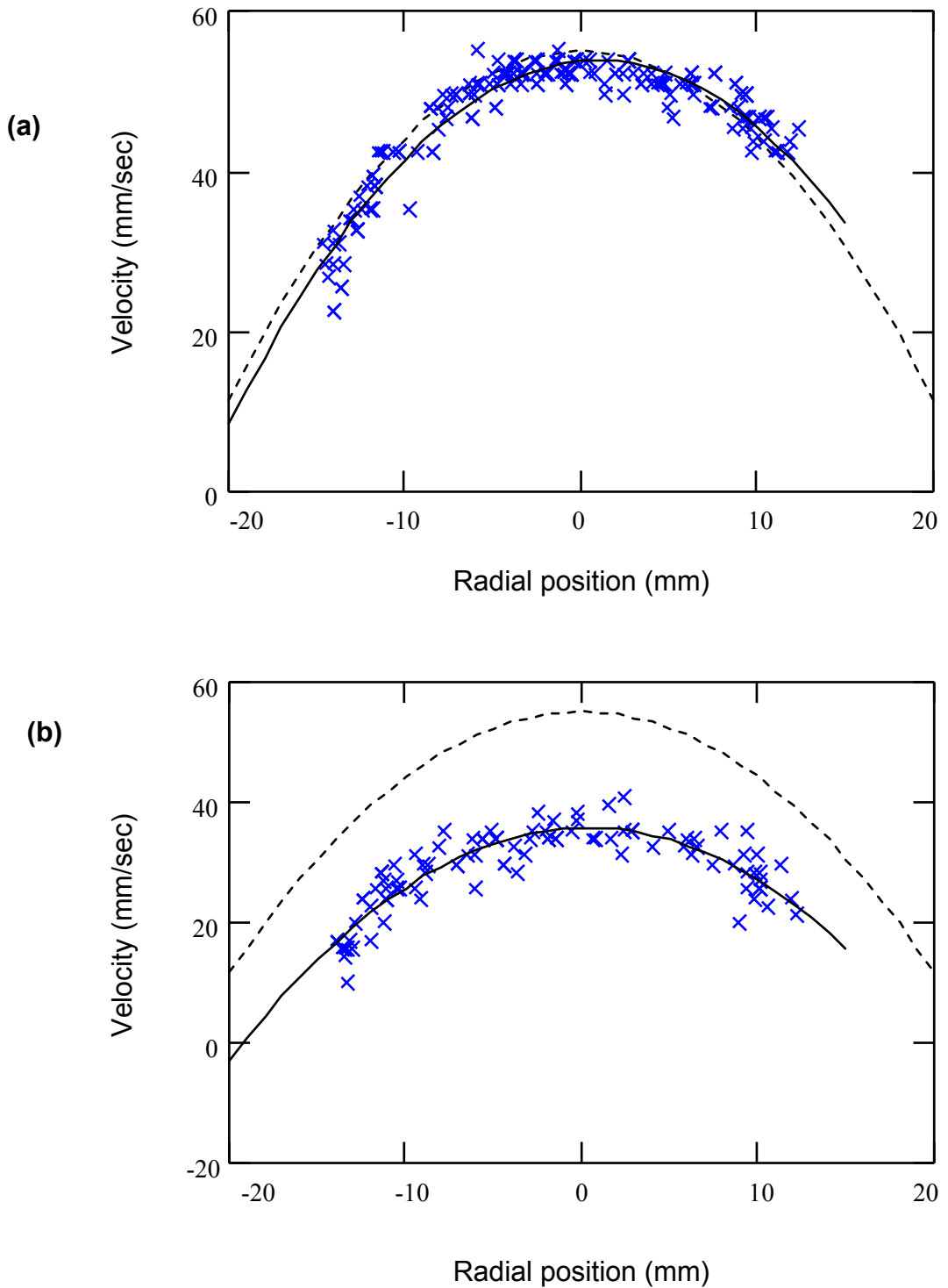


Figure 7.2. The steady, developed, velocity profile in a pipe calculated by fitting a quadratic function to velocity measurements made by measuring (a) the distance between dots and (b) the length of streaks.

- × Data points.
- Quadratic fitted to data points.
- - - Velocity profile calculated from equation 7.1.

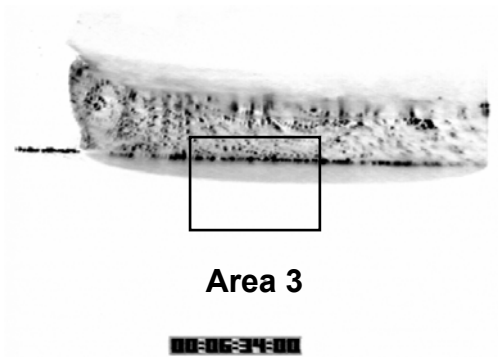
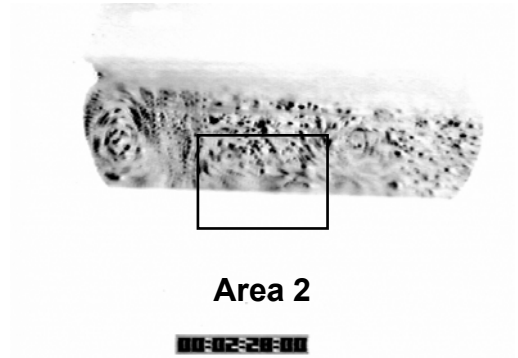
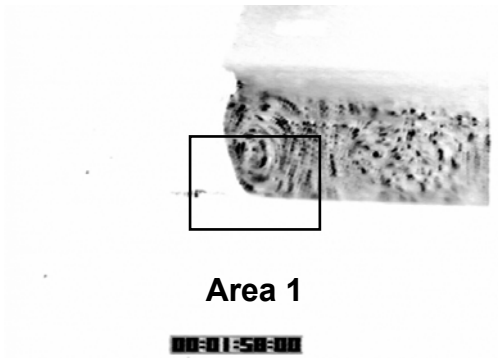


Figure 7.3. Images of particles in design B1P1 in section S1. The light sheet has been pulsed to show particle paths as dots. The black rectangles are the areas in which fluid shear stresses have been measured more accurately by zooming the camera in on them.

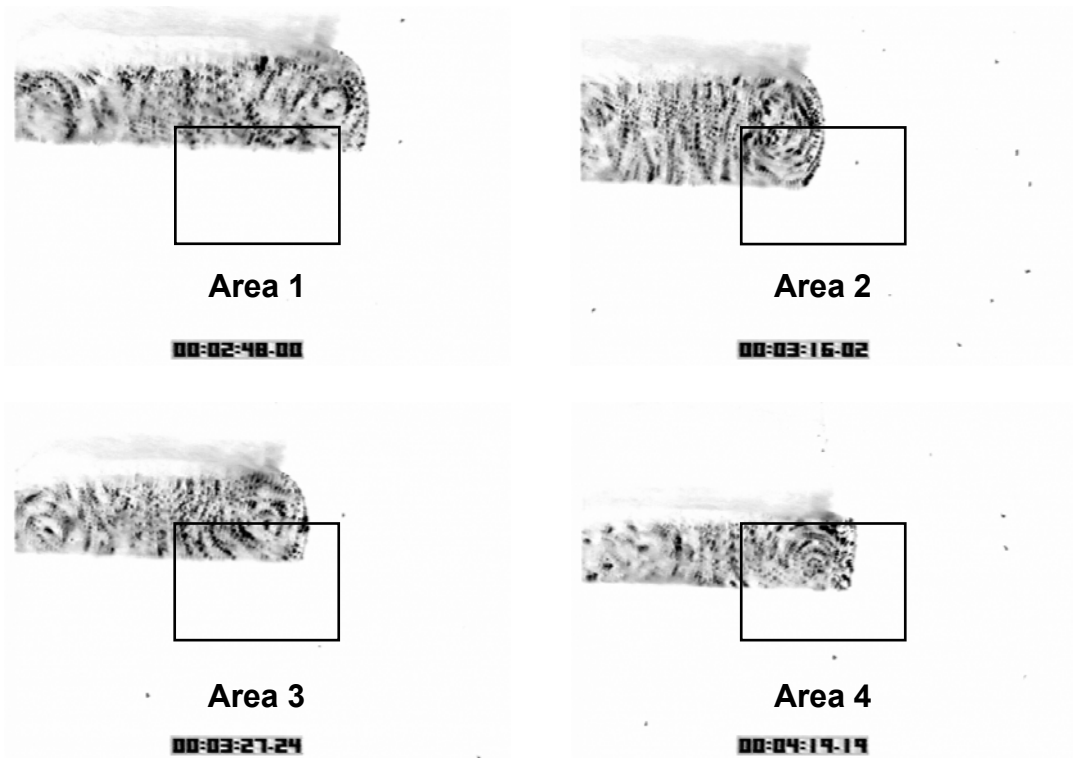


Figure 7.4. Images of particles in design B1P1 in section S5. The light sheet has been pulsed to show particle paths as dots. The black rectangles are the areas in which fluid shear stresses have been measured more accurately by zooming the camera in on them.

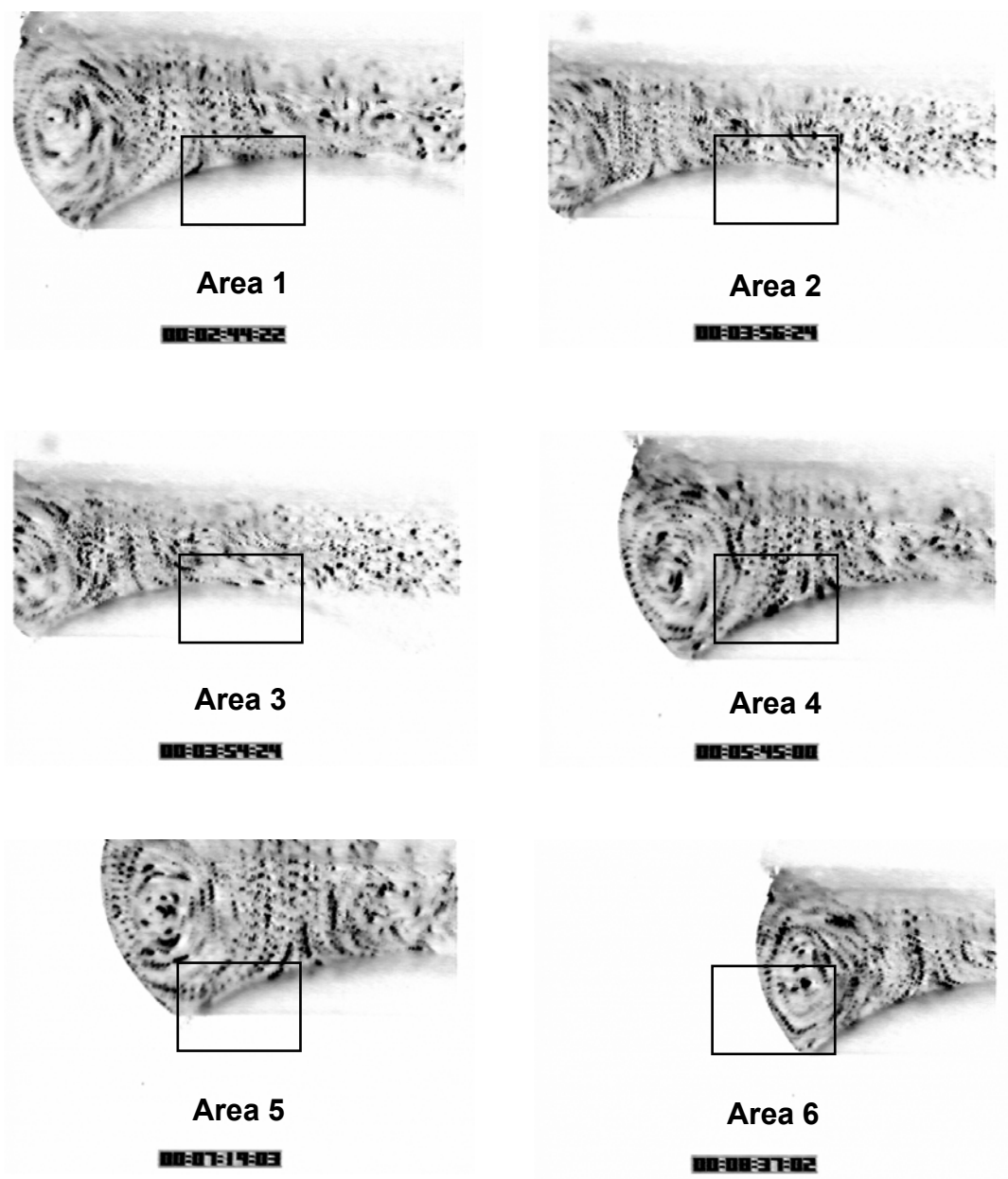


Figure 7.5. Images of particles in design B1P2 in section S1. The light sheet has been pulsed to show particle paths as dots. The black rectangles are the areas in which fluid shear stresses have been measured more accurately by zooming the camera in on them.

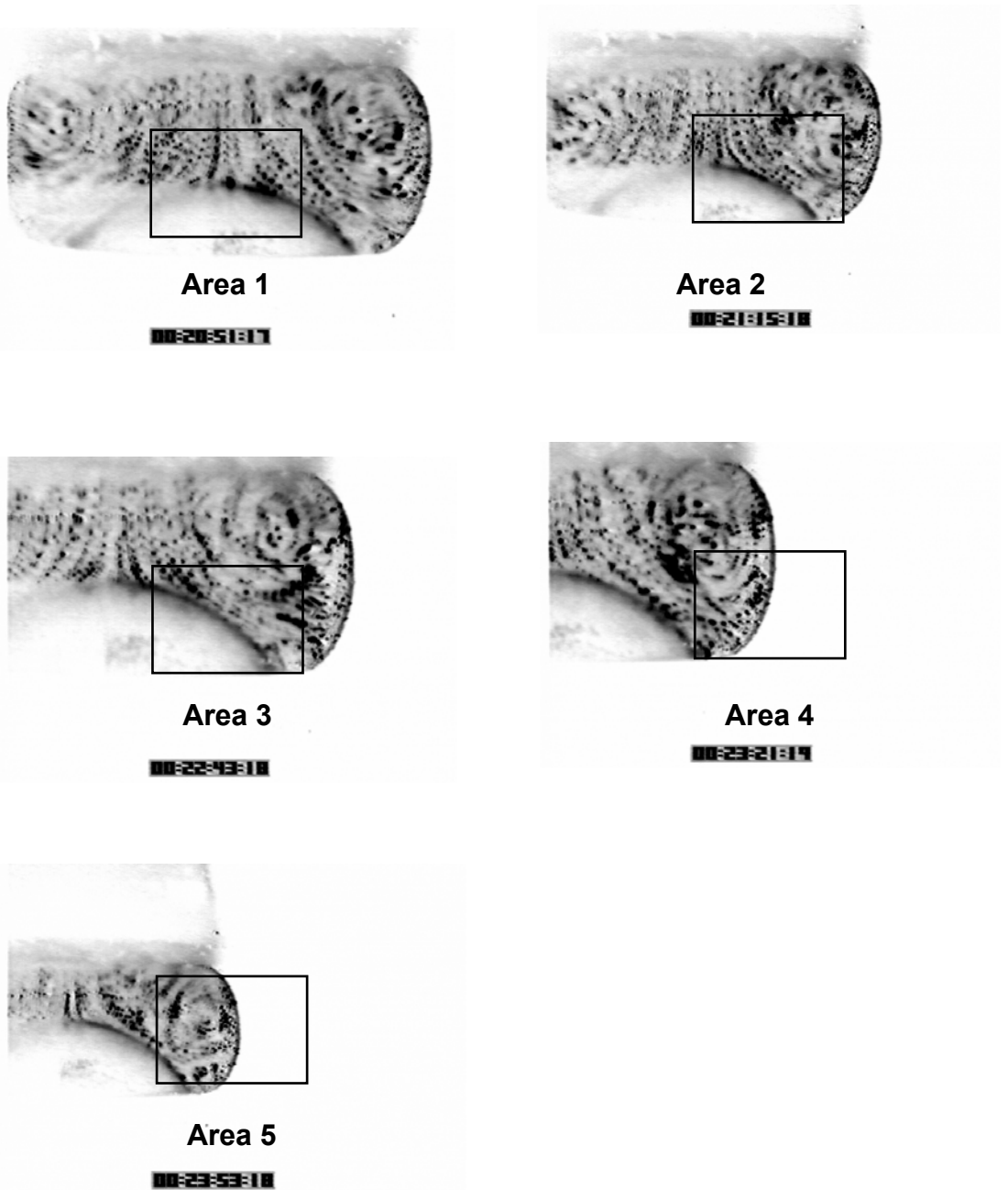


Figure 7.6. Images of particles in design B1P2 in section S5. The light sheet has been pulsed to show particle paths as dots. The black rectangles are the areas in which fluid shear stresses have been measured more accurately by zooming the camera in on them.

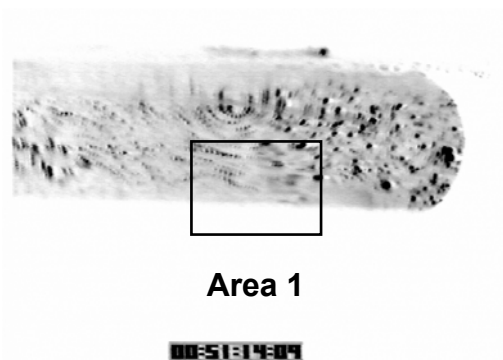
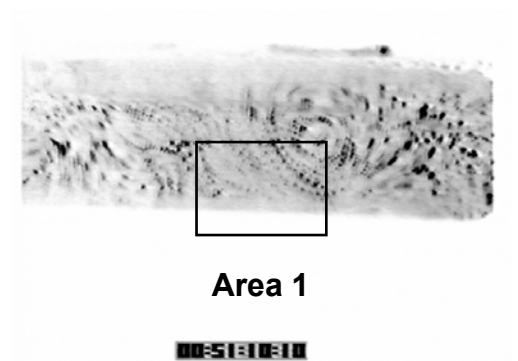
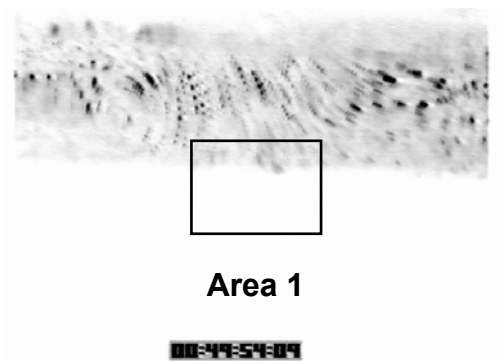
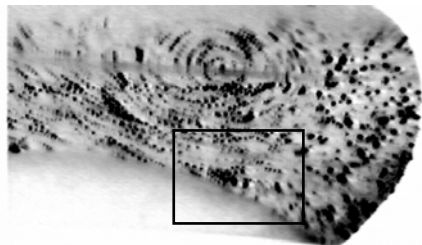
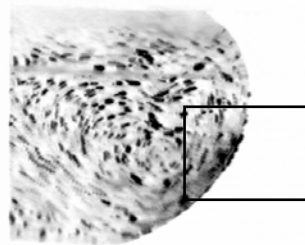


Figure 7.7. Images of particles in design B2P1 in section S1. The light sheet has been pulsed to show particle paths as dots. The black rectangles are the areas in which fluid shear stresses have been measured more accurately by zooming the camera in on them.



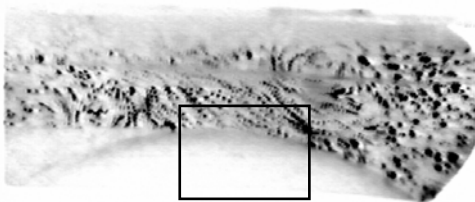
Area 1

00:08:01:11



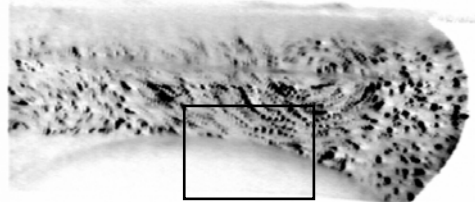
Area 2

00:08:49:17



Area 3

00:09:41:00



Area 4

00:11:25:05

Figure 7.8. Images of particles in design B2P2 in section S1. The light sheet has been pulsed to show particle paths as dots. The black rectangles are the areas in which fluid shear stresses have been measured more accurately by zooming the camera in on them.

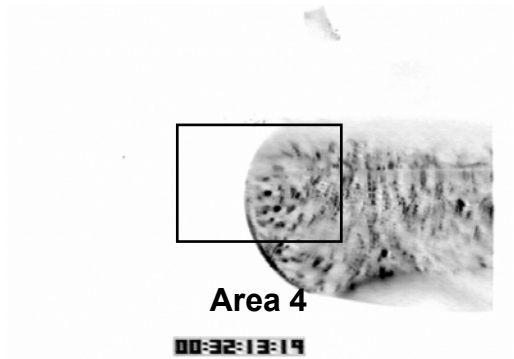
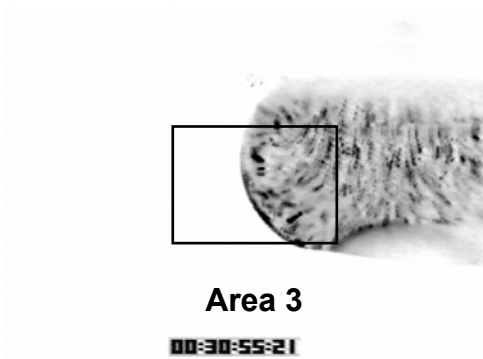
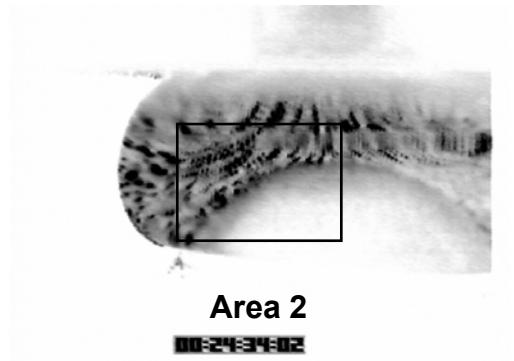
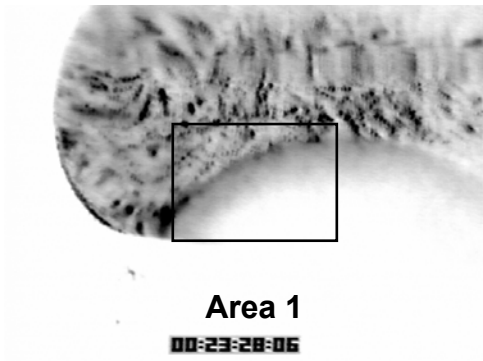


Figure 7.9. Images of particles in design B2P2 in section S5. The light sheet has been pulsed to show particle paths as dots. The black rectangles are the areas in which fluid shear stresses have been measured more accurately by zooming the camera in on them.

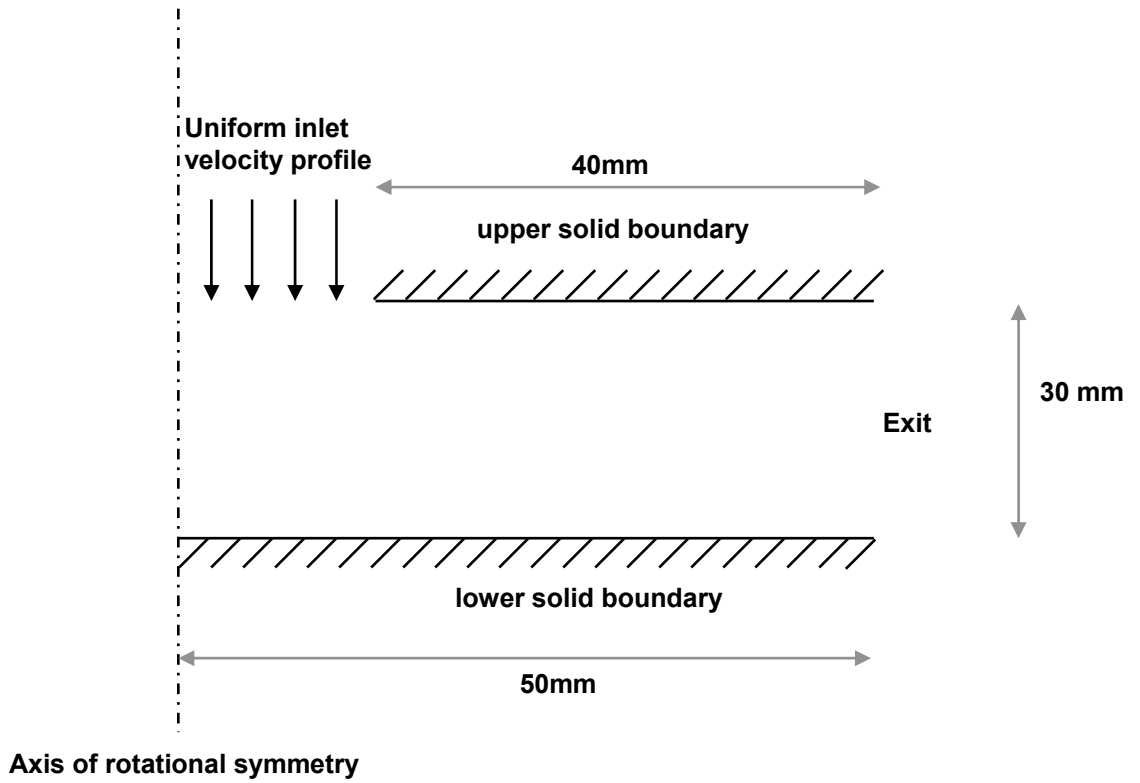


Figure 7.10. Schematic of the numerical fluid model of a submerged jet impacting a plate.

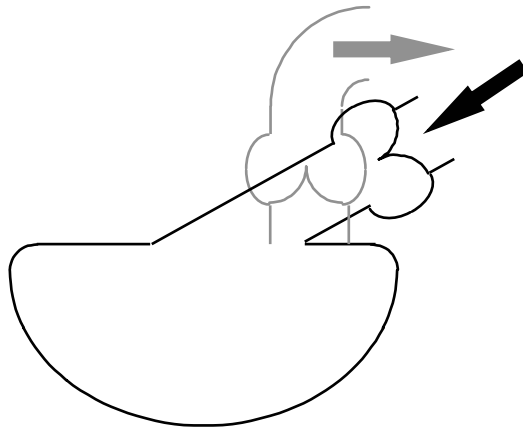


Figure 8.1. A potentially improved inlet/outlet pipe configuration for the proposed skeletal muscle powered VAD. The light grey outlet pipe is behind the inlet pipe.

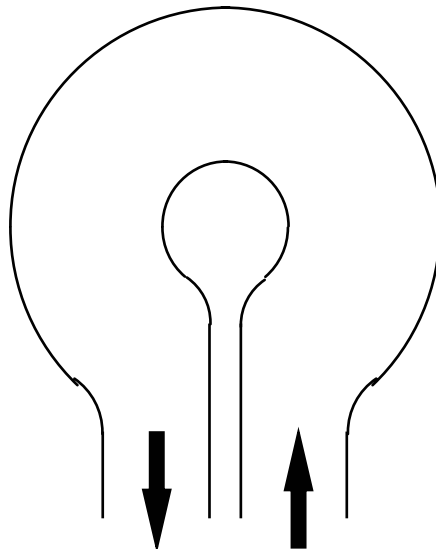


Figure 8.2. Curved tube type pumping chamber.

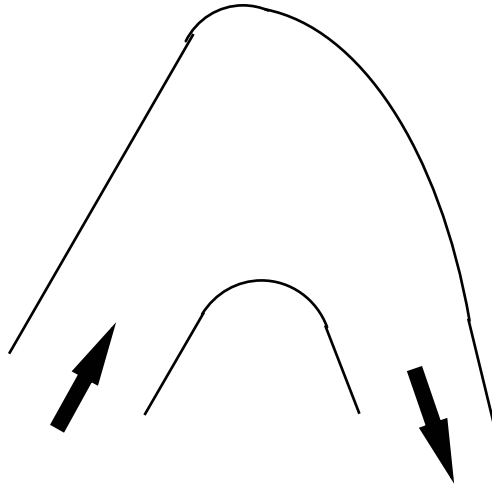


Figure 8.3. A pumping chamber based upon the shape of the natural ventricle in a human heart.